CELLULAR MECHANISMS UNDERLYING CORTICAL SPREADING DEPRESSION

by

Ning Zhou

B.Sc., Peking University, 2002

A THESIS SUBMITTED IN PARTIAL FULFILLMENT OF
THE REQUIREMENTS FOR THE DEGREE OF

DOCTOR OF PHILOSOPHY

in

The Faculty of Graduate Studies
(Neuroscience)

The University of British Columbia
(Vancouver)

June, 2010

ABSTRACT

Cortical spreading depression (SD) is a slowly propagating wave of brain cell depolarization that manifests in several neurological conditions, including migraine with aura, ischemia and brain trauma. The unique pattern of SD propagation suggests that it arises from an unusual form of intercellular communication. To advance our understanding of SD, we used two-photon imaging, intrinsic optical imaging, electrophysiological recording, and amperometric glutamate biosensor measurement to study the mechanisms underlying SD propagation in acute isolated brain slices.

In Chapter 2 we examined and compared the neuronal versus astrocytic changes in cellular processes which are fundamental to both cell types including cell volume, pH and metabolism during SD propagation. We found that SD was correlated in neurons with robust yet transient increased volume, intracellular acidification and mitochondrial depolarization. Our data indicated that a propagating large conductance during SD generated neuronal depolarization, which led to both calcium influx triggering metabolic changes and H^+ entry. Notably, astrocytes did not exhibit changes in cell volume, pH or mitochondrial membrane potentials associated with SD but they did show alterations induced by changing external [K^+]. This suggests that astrocytes are not the primary contributor to SD propagation but are instead activated passively by extracellular potassium accumulation.

In Chapter 3 we used enzyme based glutamate electrodes to show that NMDA receptors likely at presynaptic sites, trigger SD by evoking glutamate release via vesicular exocytosis, independent of action potentials and voltage gated calcium channels. Both SD- and NMDA-induced vesicular exocytosis of glutamate are triggered by efflux of calcium from mitochondria via the mitochondrial Na^+/Ca^{2+} exchanger. Through this mechanism NMDAR stimulation evokes a vicious cycle of glutamate-induced glutamate release. Diffusion of glutamate to more distant

NMDARs will generate a slowly propagating regenerative glutamate release to cause widespread neuronal depolarization.

These data offer support for the hypothesis that neuronal signaling pathways play a crucial role in propagation of SD and the following pathophysiological responses. Particularly, a novel form of NMDAR-dependent regenerative glutamate release is responsible for the cellular mechanisms that promote SD progression. In addition, this research may provide insight into possible clinical targets for treatment of SD-related neurological disorders.

TABLE OF CONTENTS

ABSTRACT ..... **ii**

TABLE OF CONTENTS ..... **iv**

LIST OF TABLES ..... **vii**

LIST OF FIGURES ..... **viii**

ABBREVIATIONS ..... **x**

ACKNOWLEDGEMENTS ..... **xi**

DEDICATION ..... **xii**

CO-AUTHORSHIP STATEMENT ..... **xiii**

1. INTRODUCTION **1**

1.1. Historical Overview 2

1.2. Experimental Models of SD 6

1.3. Pathophysiological Responses of Brain Tissue to SD 8

1.3.1. Sustained extracellular potential shifts and ion fluxes *8*

1.3.2. Tissue pH changes *15*

1.3.3. Extracellular space volume changes *16*

1.3.4. Intrinsic optical signals *17*

1.3.5. Cerebral blood flow and metabolic changes *20*

1.4. Mechanisms of SD 22

1.4.1. Involvement of Na^+ channels *22*

1.4.2. Involvement of Ca^{2+} channels *23*

1.4.3. Involvement of K^+ channels *24*

1.4.4. Involvement of glutamate and glutamate receptors *25*

1.4.5. Astrocytic calcium signaling and gap junctions *29*

1.5. SD and Neurological Disorders 31

1.5.1. Migraine *31*

1.5.1.1. SD and migraine aura *31*

1.5.1.2. Spreading oligemia in migraine patients *32*

1.5.1.3. Familial hemiplegic migraine *33*

1.5.1.4. Studies in FHM1 knock-in animal models *37*

1.5.2. Ischemia *38*

1.5.2.1. Comparison of normoxic SD and anoxic depolarization *39*

1.5.2.2. Peri-infarct depolarization *42*

1.6. Rationale, Hypothesis and Objectives 44

1.7. References 47

2. TRANSIENT SWELLING, ACIDIFICATION AND MITOCHONDIRAL DEPOLARIZATION OCCURS IN NEURONS BUT NOT ASTROCYTES DURING SPREADING DEPRESSION 69

2.1. Introduction 69

2.2. Materials and Methods 71

2.2.1. Neocortical slice preparation and induction of SD 71

2.2.2. Two-photon imaging and analysis 72

2.2.3. Electrophysiology 77

2.2.4. Statistical analysis 78

2.3. Results 78

2.3.1. Imaging cortical SD with IOS 78

2.3.2. The IOS at single-cell resolution was temporally correlated with electrophysiological signals during SD 82

2.3.3. Neuronal and astrocytic volume changes evoked by SD 87

2.3.4. Neuronal versus astrocytic intracellular pH changes during SD 90

2.3.5. Mitochondrial membrane potential changes during SD 93

2.4. Discussion 101

2.4.1. IOS and KCl induction of SD 102

2.4.2. Contribution of neurons versus astrocytes to the interstitial volume changes 103

2.4.3. Intracellular pH changes 104

2.4.4. $\Delta\psi_m$ changes during SD 105

2.5. References 107

3. A NOVEL FORM OF REGENERATIVE GLUTAMATE RELEASE BY NMDA RECEPTORS CAUSES SPREADING DEPRESSION 111

3.1. Introduction 111

3.2. Methods 113

3.2.1. Slice preparation 113

3.2.2. Induction of SD 114

3.2.3. Recording SD propagation 114

3.2.4. Glutamate measurement 115

3.2.5. Electrophysiology 116

3.2.6. Drugs 117

3.2.7. Data analysis 117

3.3. Results 118

3.3.1. Glutamate is released in SD without AP and VGCC *118*
3.3.2. SD glutamate is released by vesicular exocytosis *125*
3.3.3. SD glutamate release is dependent upon NMDAR *130*
3.3.4. Activation of NMDAR triggers glutamate release in the absence of AP and VGCC *133*
3.3.5. SD glutamate release involves activation of NCXmito in the absence of Ca^{2+} entry *134*
3.3.6. Activation of NMDAR induced glutamate release is dependent on NCX_{mito} activity *137*
3.4. Discussion 140
3.5. References 143
4. CONCLUDING CHAPTER 148
4.1. Summary of Findings 148
4.2. Mechanisms of SD Initiation 149
4.3. Mechanisms of SD Propagation 151
4.3.1. Contribution of astrocytes *154*
4.3.2. Contribution of potassium *154*
4.3.3. Pre- and post-synaptic NMDARs *155*
4.3.4. Mitochondrial Na^{+}/Ca^{2+} exchanger *156*
4.4. Future Directions 156
4.5. References 160
APPENDIX: ETHICS BOARD CERTIFICATES 163

LIST OF TABLES

Table 1.1. Effects of NMDA receptor antagonists on spreading depression 27

Table 1.2. A comparison between spreading oligemia of regional cerebral blood flow during migraine aura in man and Leão's cortical spreading depression in animals 33

Table 1.3. Comparison of normoxic SD and hypoxic SD-like depolarization 41

LIST OF FIGURES

Figure 1.1. Leão's original illustration of spreading depression..... 3

Figure 1.2. Extracellular potential shift and whole-cell current recorded during SD from a pyramidal neuron in CA1 of a hippocampal slice 10

Figure 1.3. Changes of interstitial ion concentrations and local electrical potential (Ve) during SD……..13

Figure. 1.4. Schematic representation of Sporadic Hemiplegic Migraine (SHM) and FHM mutations in FHM gene-encoded proteins..... 35

Figure 2.1. Imaging BCECF by two-photon microscopy 74

Figure 2.2. Imaging of spreading depression in cortex 80

Figure 2.3. The rapid rate of change of IOS was coincident with the depolarizing currents and field potentials of SD 83

Figure 2.4. Time course of whole-cell current (top trace), IOS (bottom) and changes in the IOS (middle) during SD in a representative astrocyte 85

Figure 2.5. Transient volume increases in neurons but not astrocytes during SD 88

Figure 2.6. Imaging intracellular pH changes show neurons display a transient acidification during SD……...91

Figure 2.7. IOS and pH_i changes during SD induced by local injection of high KCl..... 94

Figure 2.8. Neuronal mitochondrial changes during SD..... 96

Figure 2.9. Astrocytic mitochondrial changes were not associated with SD 99

Figure 3.1. IOS changes are coincident with extracellular potential changes and glutamate transients during SD..... 119

Figure 3.2. SD-associated glutamate release is independent of action potentials and VGCCs121

Figure 3.3. TTX and Cd^{2+} completely block synaptic transmission in hippocampal slices.... 123

Figure 3.4. Input-output relationship of fEPSP after incubation of bafilomycin. 126

Figure 3.5. Bafilomycin inhibits both the glutamate release and waveforms of SD showing that SD requires TTX and Cd^{2+}-insensitive vesicular release..... 128

Figure 3.6. SD glutamate release in TTX and Cd^{2+} requires activation of NMDARs..... 131

Figure 3.7. SD glutamate release in 0 $[Ca^{2+}]_o$, TTX and Cd^{2+} is blocked by inhibitors of NCX_{mito}……135

Figure 3.8. Diagram of SD model involving NMDA-evoked glutamate release..... 138

Figure 4.1. Conceptual diagram of positive feedback involving glutamate release during SD progression…… ……..152

Figure 4.2. Schematic drawing of the enzyme-based glutamate sensor tip. 157

ABBREVIATIONS

α -NS^- – α-Naphthalenesulfonate

AMPA – α-amino-3-hydroxyl-5-Methyl-4-isoxazole-Propionic Acid

AsF_6^- – Hexafluoroarsenate

CSD – Cortical Spreading Depression

DC – Direct Current

EAAT – Excitatory Amino Acid Transporter

ECoG – Electrocorticographic

FHM – Familial Hemiplegic Migraine

GABA – γ-Aminobutyric Acid

IOS – Intrinsic Optical Signal

I_{SD} – Spreading Depression Associated Whole-Cell Current

MA – Migraine with Aura

NCX_{mito} – Mitochondrial Na^+/Ca^{2+} Exchanger

NMDAR – N-methyl-D-aspartic Acid Receptor

pH_i – Intracellular pH

pH_o – Extracellular pH

SD – Spreading Depression

SHM - Sporadic Hemiplegic Migraine

siRNA – Small Interfering RNA

TMA – Tetramethylammonium

TEA – Tetraethylammonium

TTX – Tetrodotoxin

VGCC – Voltage-Gated Calcium Channel

VGSC – Voltage-Gated Sodium Channel

VSOAC – Volume-Sensitive Organic Anion Channels

ΔV_i – Intracellular Potential Shift

ΔV_o – DC-coupled Extracellular Potential Shift

Ψ_m – Mitochondrial Membrane Potential

ACKNOWLEDGEMENTS

First and foremost I offer my sincerest gratitude to my supervisor, Dr. Brian MacVicar, who gives me an opportunity to work in his research group and supports me throughout my graduate study. Without his continuous support and assistance it would not have been possible to finish this dissertation. I cannot find any words that would describe how much his guidance, advice, patience and friendliness have meant to me. His knowledge, passion and belief of science have inspired me to look upon him as a role model for my future endeavours.

I am very thankful to my committee members including Dr. Yu Tian Wang and Dr. Lynn Raymond, who gave important comments on the whole project.

I would like to thank all the members of the MacVicar lab. Dr. Grant Gordon of his support of my science and his help with my writing. Ms. Denise Feighan for her help with all the endless preliminary experiments and proofreading. Mr. Ravi Rungta for his idea and hard work on the glutamate project. Dr. Dustin Hines, Dr. Chao Tai, Dr. Choi and Ms. Jingfei Zhang for their friendship and all the laughter they brought to me. Finally, thanks to my parents for their selfless help in my life.

DEDICATION

To Dongchuan

for his love, encouragement and tolerance

CO-AUTHORSHIP STATEMENT

I was involved in the original conception and planning of all of the experiments involved with this thesis. I also participated in all of the experimental procedures needed to conduct the research. For chapter 2, I conducted all the imaging and electrophysiology experiments. G.J.R. Gordon assisted with BCECF spectra measurement. D. Feighan assisted with IOS imaging. For chapter 3, R.L. Rungta conducted extracellular recording experiments in hippocampus, and D. Feighan assisted with IOS imaging experiments. I prepared all of the figures for, and co-wrote both manuscripts in conjunction with Dr. Brian MacVicar, with assistance from Dr. G.J.R. Gordon.

1. INTRODUCTION

The biophysical mechanism underlying spreading depression (SD) has intrigued researchers since its first discovery by A.A.P. Leão more than 60 years ago (Leão, 1944b). SD is a slowly propagating wave of neuronal and glial depolarization that leads to a transient depression of synaptic activities (Somjen, 2001). SD is a highly reproducible response that occurs in the gray matter of central nervous system. It can be triggered by various stimuli in the normal brain tissue and appears to be harmless; however, recurrent SD might lead to irreversible cell damage (Hossmann, 1996). Several recent studies in humans have demonstrated that SD-like phenomena can occur under pathological conditions, such as stroke and trauma, and may have important impact on the neurological status and outcome in the human brain (Strong et al., 2002; Fabricius et al., 2006; Dreier et al., 2009). The critical role of SD in migraine with aura has been established by studies in both human and animal models (Pietrobon and Striessnig, 2003). Advances in animal studies using transgenic, electrophysiology and imaging approaches have helped us understand more about mechanisms of SD regarding its initiation, propagation and relationship to neurological disorders. However, despite significant progress, several important questions remain largely unknown. In particular, there is controversy in the literature as to which cell types and what signaling pathways mediate the propagation of SD wave. Understanding the cellular mechanism of SD progression will provide us broader knowledge of both neurophysiology of central nervous system and the pathogenesis of SD-related disorders like migraine, stroke and brain trauma.

1.1. Historical Overview

Spreading depression (SD for short) was first described in 1943 by Aristides Leão, who published a paper entitled "Spreading depression of activity in the cerebral cortex," subsequently known as "Leão's spreading depression" (Leão, 1944b). The original aim of Leão's study was to induce cortical epileptic activities by electrical stimulation of rabbit cortical surface. In his experiments, the skull of rabbits was opened under anesthesia and a row of chlorided silver wire electrodes was arranged in contact with the cortical surface (Leão, 1944b). Of these electrodes, one pair served for stimulation and the others, connected in six staggered pairs, for bipolar recording of the electrocorticogram at increasing distance from the stimulated points (Figure 1.1). Surprisingly, Leão found an unexpected and contradictory result following the stimulation: "the activity at the nearest pair of recording electrodes did not increase, but ceased almost entirely" (Leão, 1944b). The distinctive feature of this response was a marked, enduring depression of the spontaneous electrical activity of the cortex; and this depression spread out slowly, in all directions, from the region that was stimulated to more and more distant parts of the cerebral cortex. Therefore it was termed "spreading depression". The traveling rate of SD is slow compared to other neuronal activities: when started from near the occipital pole it might take more than 5 minutes to reach the occipital pole in rabbit cortex (Leão, 1944b). In the same study, Leão also revealed that SD is accompanied by a large, slow, negative voltage variation, the feature of which was further studied in his next paper published in 1947. The voltage variation showed a first negativity of 7 to 15 mV followed by a smaller positive phase (Leão, 1947). The complete variation lasted about 4 to 6 minutes. As the negativity increased, the spontaneous electrical activity of the same region began to decrease, and the pial arteries to dilate (Leão, 1947). This observation was further described in other brain areas, such as hippocampus

Figure 1.1. Leão's original illustration of spreading depression. The traces show the electrocorticography (ECoG) recorded from the exposed surface of the brain of a rabbit anesthetized with Dial. *Inset* in *F* shows the positions of the electrodes; S, stimulating electrodes, *1-7*, recording electrodes. *A-L* show "push-pull" (balanced input) recordings from pairs of surface electrodes, as marked in *A*. Between *A* and *B* the cortex was stimulated by "tetanic" stimulation from an inductor coil; the times elapsed since the end of stimulation are noted at the bottom of panels. The ECoG becomes isoelectric in successive pairs of electrodes as the depression spreads over the surface. Seven minutes elapsed between *K* and *L*; *L* shows complete recovery of ECoG activity. Figure adapted from Leão, J Neurophyiology, 1944, 7: 357-390 and Somjen, Physiological Reviews, 2001, 81(3): 1065-96.

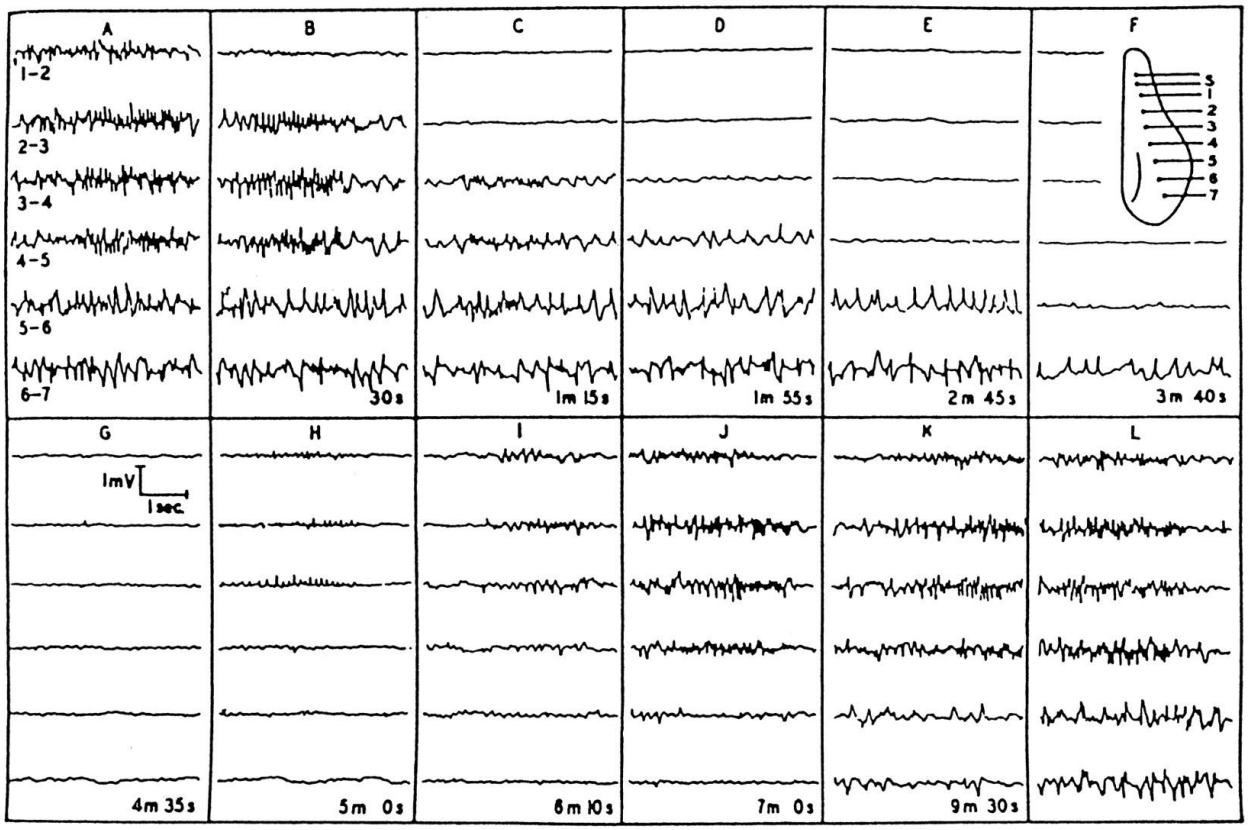
A
B
C
D
E
F
1-2
2-3
3-4
4-5
5-6
6-7
30s
1m 15s
1m 55s
2m 45s
3m 40s
S
1
2
3
4
5
6
7
G
H
I
J
K
L
1mV
1sec.
4m 35s
5m 0s
6m 10s
7m 0s
9m 30s

(Monakhov et al., 1962), striatum (Weiss and Fifkova, 1963), cerebellum (Fifkova et al., 1961; Nicholson and Kraig, 1975), and also in isolated retina (Gouras, 1958; Martins-Ferreira and de Castro, 1966). Leão discovered all the major features of SD in the following few years, which are that "1) CSD occurs only in certain conditions that render the tissue susceptible to it; 2) the speed of the spread is in the order of 3 mm/minute, and the profound depression lasts for 1-3 minutes at all sites; 3) the spread is self-sustained; 4) although all intrinsic and evoked neuronal activity is depressed, abnormal activity may occur locally in the course of CSD; 5) CSD is followed by an absolute refractory period of at least 1 minute at all sites." (Leão, 1987)

The significance of SD in neurological disorders was revealed shortly after its discovery in 1940s. In 1941, Lashley analyzed the progression of his own visual aura of migraine, and proposed that the scintillation-scotoma during migraine aura resulted from a region of depressed neural activity in the visual cerebral cortex (Lashley, 1941). He calculated that the neural disturbance spread across the cortex at about 3 mm/min. In 1945, Leão and Morrison suggested that SD could be involved in the pathophysiology of migraine, since the propagation rate of scotoma was similar to SD (Leão, 1945). The relationship between Lashley's findings and SD was pointed out by Milner (Milner, 1958) and Basser (Basser, 1969), and was supported by Lauritzen's studies that the spreading oligemia observed in migraine is similar to that associated with SD (Olesen et al., 1981; Lauritzen et al., 1982). Although this idea was questioned because EEG recordings from human brain surgery rarely show SD, recent human studies have provided strong evidence for the existence of SD-like activities during migraine aura with both fMRI and magnetoencephalography techniques (Bowyer et al., 2001; Hadjikhani et al., 2001). In addition, SD has also been recorded from injured or ischemic human brain with electrocorticographic approaches (Strong et al., 2002; Dreier et al., 2006).

Leão's finding of SD has intrigued many scientists to study the mechanisms underlying this interesting phenomenon. Grafstein (Grafstein, 1956) first raised the potassium theory as the interpretation of the mechanism underlying SD propagation: the intense neuronal activity preceding depression results in the liberation of K^+ into the interstitial spaces in sufficient quantity to depolarize adjacent cells. These cells are in turn forced to intense activity and liberate more K^+, so that the cycle is repeated. The second interpretation of SD was raised by Van Harreveld (Van Harreveld, 1958), who proposed that SD was mediated by a similar cycle that a substance is released from cells into interstitial fluid but that was based on a different compound – glutamate. He was the first to point out that glutamate triggers SD, and his theory was further supported by Lauritzen's study that SD was triggered by topical application of glutamate receptor agonists (Lauritzen et al., 1988). The role of NMDA type ionotropic glutamate receptors (NMDAR) was supported by a large body of studies from mid-1980s showing the blocking effect by NMDA receptor antagonists (see section 1.4.4). Another theory of SD proposed that SD propagation was mediated not by the release of certain substances but instead by the intercellular transfer of a signal through the opening of either interneuronal (Herreras et al., 1994) or glial gap junctions (Martins-Ferreira et al., 2000). It is worthy to note that there are still unsolved problems existing in all of these theories. The basic mechanism of SD initiation and propagation still remains largely unknown.

1.2. Experimental Models of SD

The occurrence of SD has been reported in various regions of the central nervous system, including neocortex, hippocampus (Herreras and Somjen, 1993a), corpus striatum (Bures et al., 1968), cerebellum (Case et al., 2002), thalamus, caudate (Trachtenberg et al., 1970), tectum

(Guedes et al., 2005), olfactory bulb (Amemori et al., 1987), brainstem (Richter et al., 2008), spinal cord (Gorji et al., 2004), and also retina (Martins-Ferreira and de Castro, 1966). Cortical SD has been shown to occur in mature brains of all mammalian species studied including human. SD can be initiated by various stimuli in both *in vivo* and *in vitro* systems. In the *in vivo* system, the brain is typically surgically exposed using a small craniotomy in the anesthetized rat. The *in vitro* studies of SD have involved isolated brain slab, brain slices, and retina.

It has been pointed out (Somjen, 2001) that the initiation of SD, which can be triggered by various stimuli, might be caused by a mechanism different from its propagation. According to this hypothesis, SD is ignited when a small region of brain tissue is hyperexcited, and thus the neuronal excitability exceeds a certain threshold to trigger a chain of events that lead to further depolarization. There are various strategies to achieve this, mainly including electrical, mechanical, KCl and other chemical stimulation. Electrical stimulation, like brief tetanus stimuli or DC stimuli, was used in the first observations of SD in the rabbit cortex by Leão (Leão, 1944b) and was widely used in later studies in both *in vivo* (Back et al., 1996) and *in vitro* systems (Snow et al., 1983). Mechanical stimuli can evoke SD in the *in vivo* systems, for instance, by stroking of the brain surface with a blunt or sharp instrument (Fabricius et al., 1995), by lightly tapping the cortex (Leão, 1944b), or by dropping a weight onto the brain as a brain injury model (Nilsson et al., 1993). However, the most adopted and the most reliable method to induce SD is focal application of high KCl. Microdialysis (Herreras and Somjen, 1993b), a droplet onto the cortex (Reuter et al., 1998), or a surgical sponge saturated of KCl on the intact surface of the dura mater (Eikermann-Haerter et al., 2009b) are widely used in the *in vivo* systems. Puff ejection of high KCl from a glass pipette (Czeh et al., 1993; Tong and Chesler, 1999) or bath application of KCl (Anderson and Andrew, 2002) can effectively induce SD in brain slices. Elevation of extracellular K^+ concentration has been observed to accompany SD and this might

greatly contribute to SD generation by depolarizing membrane potentials and inducing neuronal discharges (see section 1.4.3). In addition, SD can be triggered by several types of chemicals. Focal application of glutamate or other glutamate receptor agonists is effective (Lauritzen et al., 1988), however other studies report it is less reliable than the high KCl application (Obrenovitch et al., 1996). The Na^+/K^+-ATPase inhibitor ouabain has been used in brain slices and this effect is possibly due to the increase of extracellular K^+ (Basarsky et al., 1998; Dietz et al., 2008). However, ouabain-induced SD is more reminiscent of ischemic depolarization, since they share similar features including malfunction of the Na^+/K^+-ATPase and consequent irreversible damages, such as cellular swelling (Balestrino et al., 1999). Finally, endothelin-1 has been found to be a potent inducer of SD *in vivo* but not in brain slices (Dreier et al., 2007). It is still unclear how endothelin-1 triggers SD, the mechanism of which probably involves an early rise in $[K^+]_o$ or a local necrotic cell response (Goadsby et al., 1996; Kleeberg et al., 2004; Dreier et al., 2007).

1.3. Pathophysiological Responses of Brain Tissue to SD

SD is accompanied by several types of tissue and cellular responses, such as sustained and profound potential shift, tissue pH changes, extracellular space shrinkage, and light transmittance changes of the tissue. Some of these responses are characteristic of SD, and may contribute to the pathogenesis that is induced by recurrent SD under certain neurological conditions.

1.3.1. Sustained extracellular potential shifts and ion fluxes

The most striking feature characterizing SD is a profound DC-coupled extracellular potential shift that can reach an amplitude of -5 to -15 mV at the wave front. This extracellular potential

shift (ΔV_o) reaches its maximal value in about 0.5 to 1 minute and lasts several minutes, and so it is also termed the slow potential shift of SD (Leão, 1947). Extracellular recordings demonstrate that the ΔV_o begins with a first slight positive shift that is sometimes not observed, followed by a brief (2-3 seconds) burst of high frequency population spikes that herald the arrival of the propagating SD wave (Figure 1.2A) (Czeh et al., 1992; Herreras et al., 1994). The brief population spikes have also been observed as increased spontaneous neuronal activities (Grafstein, 1956). The onset of SD is normally characterized by the large negative sustained potential shift consist of two phases: a negative ΔV_o phase that rapidly reaches a peak, is followed by either a less negative plateau or a subsequent slower shift to the second negative maximum (Herreras and Somjen, 1993b). The transient relatively positive "hump" or "notch" between the two negative phases is described as an "inverted saddle shape", which has been recorded from retina (do Carmo and Martins-Ferreira, 1984), neocortex (Hansen and Lauritzen, 1984), cerebellar cortex (Nicholson, 1984), and most commonly from stratum radiatum of CA1 region of the hippocampus (Herreras and Somjen, 1993b). Current source density analysis in this region has revealed that apical dendrites of pyramidal neurons are involved in the generation of the voltage shift (Wadman et al., 1992; Kunkler et al., 2005). Although SD can be triggered by different stimuli, the ΔV_o itself has all-or-none character: once initiated, its electrical properties are uniform and are independent of the triggering stimulus (Somjen, 2001).

Figure 1.2. Extracellular potential shift and whole-cell current recorded during SD from a pyramidal neuron in CA1 of a hippocampal slice. (A) V_o, extracellular potential recorded near the cell; I_h, holding current recorded by whole-cell recording with a holding potential (V_h) of -71 mV. The vertical transients intersecting the I_h trace are due to ramp voltage tests probing the voltage-dependent responses. During the time marked by the horizontal two-headed arrow, high K^+ solution was applied to the slice in the CA3 region; SD propagated from CA3 to the recording site in CA1. Note the population spikes occurred at the beginning of the negative V_o. (B) current-voltage (*I-V*) curves derived from ramp voltage tests of the same cell. The cell was first hyperpolarized for 20 ms to −110 mV and then depolarized by linear ramp over 300 ms to −10 mV. The top *I-V* plot is from before high K^+ administration, the bottom plot during the maximal SD-related increase of I_h. The control record shows current spikes presumably generated outside the clamped region, in axon (Na^+ mediated) and dendrites (Ca^{2+} mediated); these disappeared during SD, and the steeper slope of the *I-V* curve indicates greatly increased input conductance. K^+ currents were largely eliminated by the Cs^+ in the pipette. Figure adapted from Czeh et al, Brain Research, 1993, 632(1-2): 195-208.

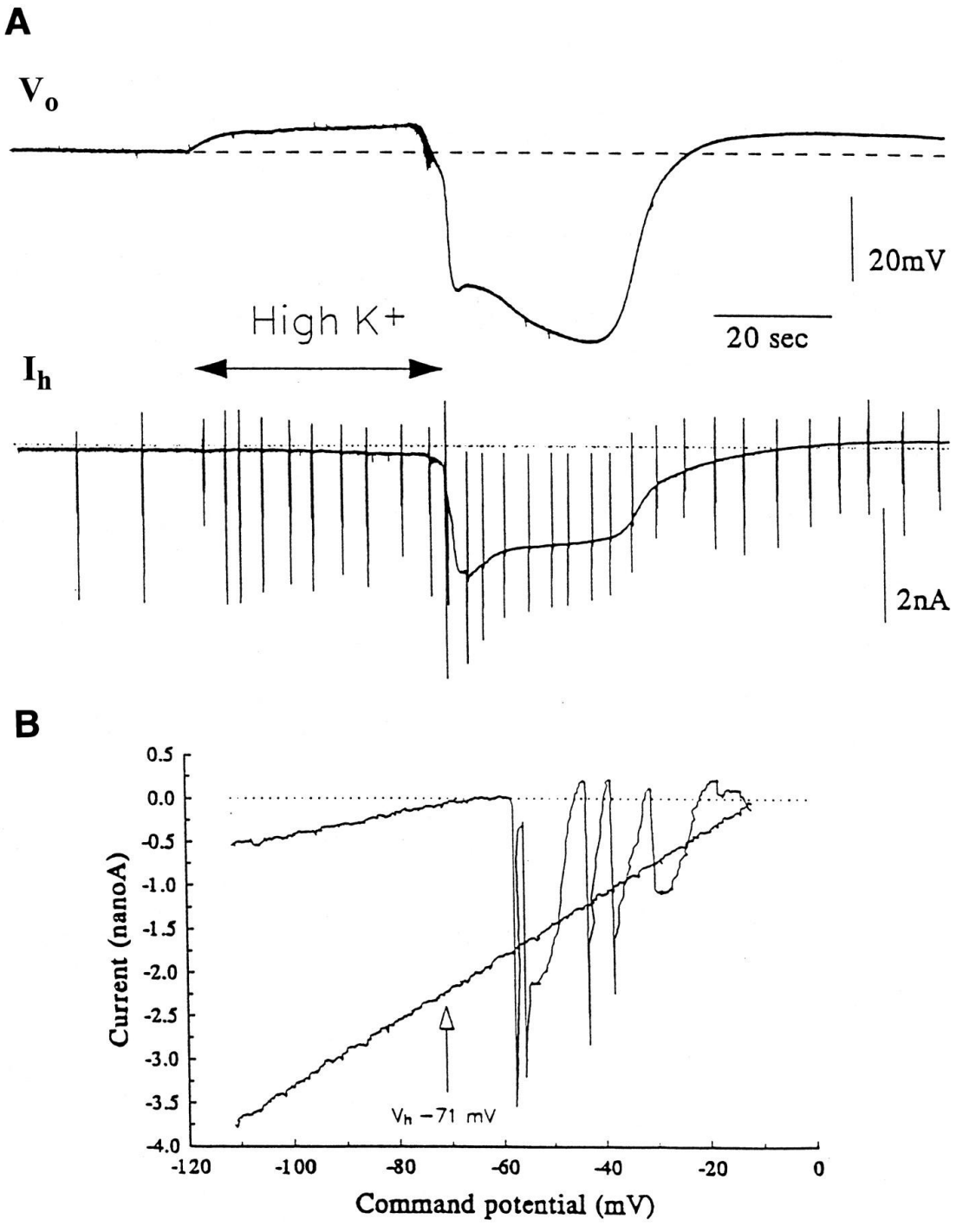
A
V_o
20mV
High K+
20 sec
I_h
2nA
B
Current (nanoA)
0.5
0.0
-0.5
-1.0
-1.5
-2.0
-2.5
-3.0
-3.5
-4.0
V_h −71 mV
-120
-100
-80
-60
-40
-20
0
Command potential (mV)

Intracellular recordings during SD have shown that neurons undergo profound depolarization, and the intracellular potential (ΔV_i) of neurons can approach zero (Collewijn and Harreveld, 1966; Snow et al., 1983). Even though the ΔV_i and ΔV_o share a similar time course, the trajectories of the two are not parallel. Compared with ΔV_o, ΔV_i exhibits an earlier maximal value and then sagged more slowly without the second phase maximum (Snow et al., 1983). Whole-cell voltage clamp recordings reveal that the ΔV_o is associated with a large inward membrane current termed I_{SD} (Figure 1.2B). When SD is evoked by focal high KCl application, there is a gradual and slight increase of the membrane current, followed by the abrupt large I_{SD} that indicates the arrival of the SD wave (Czeh et al., 1993). During the progress of I_{SD}, the voltage-gated Ca^{2+} and Na^+ currents gradually disappear possibly due to the inactivation of these channels by the membrane depolarization, and this also manifests the observation of the silencing period of neuronal electrical activities. The I_{SD} can reach a mean maximum of about 1.75 nA, and the average reversal potential of the membrane current is close to 0 mV, indicating a mixed ion conductance (Czeh et al., 1993).

Understanding the nature of ion conductance will add another piece of knowledge to the puzzle of ΔV_o and I_{SD}. By measuring extracellular ion concentrations, it has been shown that the ΔV_o and I_{SD} are mediated by large fluxes of several ions, including K^+, Na^+, Ca^{2+} and Cl^- (Figure 1.3). The $[K^+]_o$ rapidly rises when ΔV_o starts its first phase and can reach levels as high as 60-80 mM, suggesting K^+ outflow into the extracellular space (Vyskocil et al., 1972; Hansen and Zeuthen, 1981). At the same time $[Na^+]_o$ and $[Cl^-]_o$ levels decrease to approximately 50 mM as these ions enter cells (Kraig and Nicholson, 1978; Hansen and Zeuthen, 1981; do Carmo and Martins-Ferreira, 1984; Nicholson, 1984), and these changes are resistant to TTX (Tobiasz and Nicholson, 1982). Ca^{2+} enters the cells after the outward movement of K^+, resulting in a net decrease in $[Ca^{2+}]_o$ from 1.2-1.5 mM to about 0.1 mM (Hansen and Zeuthen, 1981). Cations are not

Figure 1.3. Changes of interstitial ion concentrations and local electrical potential (Ve) during SD. (a) Changes of interstitial concentration of Ca^{2+} and K^+ during SD. (b) Changes of interstitial concentration of Na^+ and Cl^- during SD. (c) The change of the electrical potential and interstitial concentration of Na^+, K^+, Ca^{2+}, and Cl^- during the initial phase of a SD. Note the initial simultaneous changes of $[K^+]_e$ and V_e, and that Na^+ and Ca^{2+} decreases abruptly when $[K^+]_e$ has already increased up to about 10 mM. Figure adapted from Hansen et al, Acta Physiologica Scandinavica, 1981, 113(4): 437-435.

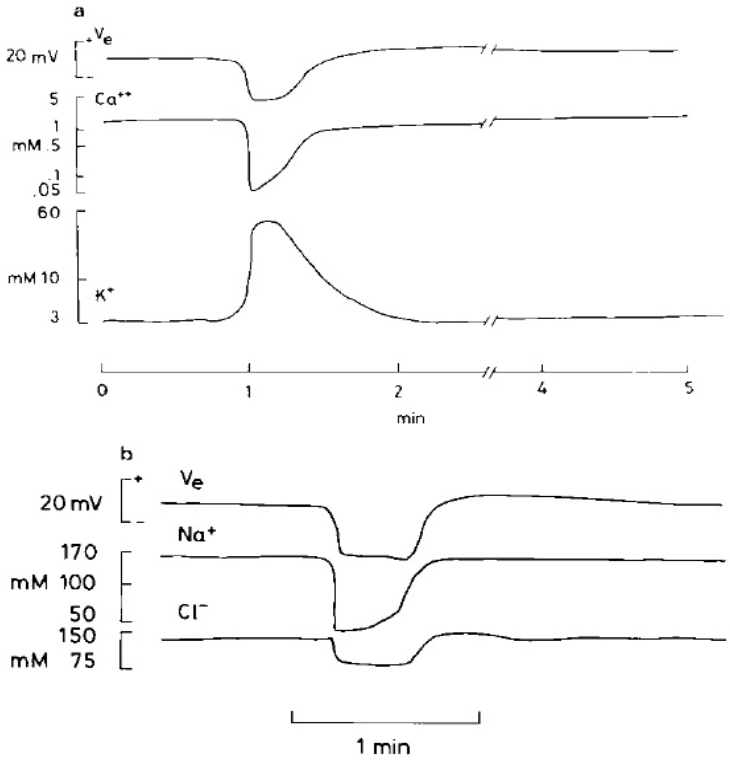
a
20 mV
V_e
5
1
mM .5
.1
.05
Ca^{++}
60
mM 10
3
K^+
0
1
2
4
5
min
b
20 mV
V_e
Na^+
170
mM 100
50
150
mM 75
Cl^-
1 min

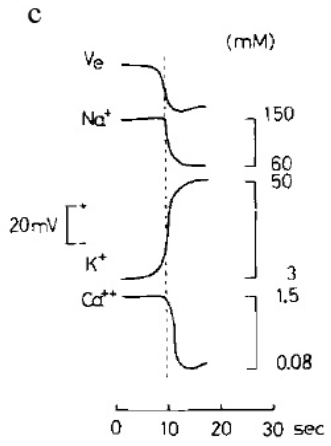
c
(mM)
V_e
Na^+
150
60
20mV
50
K^+
3
Ca^{++}
1,5
0.08
0
10
20
30 sec

exchanged one-for-one between intra- and extracellular solutions, because the reduction in $[Na^+]_o$ is greater than the increase in $[K^+]_o$ (Muller and Somjen, 2000). The mixed ion flux is possibly mediated by either opening of large conductance, non-selective ion channels or simultaneous activation of inward and outward currents through multiple channels.

1.3.2. Tissue pH changes

During SD, extracellular pH exhibits two components: an initial alkalinization that lasts for several seconds superimposed upon a more sustained acidification that recovers with a similar time course of ΔV_o (Kraig et al., 1983; Somjen, 1984; Tong and Chesler, 1999; Xiong and Stringer, 2000). The sustained extracellular acidosis component suggests a net efflux of protons, which might be associated with the acidic production from enhanced cellular metabolic activity. Lactate and CO_2 are the two best-known acidic products of cerebral metabolism which might contribute to this effect (Scheller et al., 1992a; Cruz et al., 1999). The interstitial acid shift is also temporally coincident with an intracellular alkaline shift of astrocytes (Chesler and Kraig, 1989), which is due to high $[K^+]_o$-induced astrocytic depolarization and Na^+/HCO_3^- cotransporter activities (Chesler, 2003). The initial transient extracellular alkalinization component is less easily explained. It might involve one or more of the following mechanisms: (1) the release of alkaline products from cells into interstitial fluid (Kraig and Cooper, 1987); (2) Ca^{2+}-dependent uptake of H^+ in response to activation of ionotropic glutamate receptors (Smith and Chesler, 1999); (3) HCO_3^- efflux across $GABA_A$ anion channels; and (4) opening of voltage-gated proton channels or the proton-permeable ion channels which mediate the large ion influx during SD (Decoursey, 2003).

Changes in the extracellular pH itself can also modify the generation and propagation of SD. A more acidic extracellular pH environment, which is accomplished by either decreasing saline

HCO_3^- or increasing the CO_2 content, increases the threshold for SD induction, slows down the propagation velocity, and shortens SD duration (Tong and Chesler, 2000). In contrast, an amplified extracellular alkalosis (eg. by the application of a carbonic anhydrase inhibitor) has a facilitatory effect on SD, and this effect can be reversed by NMDA receptor antagonists (Tong and Chesler, 1999). NMDA receptor activities are inhibited by protons with a 50% inhibitory concentration close to physiological pH (Traynelis and Cull-Candy, 1990). Under some pathological conditions like ischemia, the early transient alkalization may therefore contribute to cell damages induced by SD-like waves by relieving the proton block on NMDA receptors.

1.3.3. Extracellular space volume changes

Changes of extracellular volume fraction can be tested by measuring the extracellular concentration of certain membrane-impermeable substances, like tetramethylammonium (TMA^+), tetraethylammonium ions (TEA^+), hexafluoroarsenate (AsF_6^-), α-naphthalenesulfonate (α-NS^-) or choline, with ion-selective microelectrodes (Sykova and Nicholson, 2008). Studies have shown that the extracellular spaces shrink remarkably and then recover with a similar time course of ΔV_o during SD (Phillips and Nicholson, 1979; Jing et al., 1994). The volume of extracellular space can decrease by about 35-70%, and this value varies when measured with different probe ions (Hansen and Olsen, 1980; do Carmo and Martins-Ferreira, 1984; Hablitz and Heinemann, 1989; Lundbaek and Hansen, 1992). A possible explanation is that the decrease in cellular resistance during SD will increase the permeability to relatively smaller sized ion indicators, as supported by the studies of Phillips and Nicholson (1979), that the diameter of membrane channels that open during SD lies between 6 and 11 nm. More recent studies have shown that extracellular space occupies a volume fraction of about 20%-22% of adult rat

hippocampus (Mazel et al., 1998; Sykova et al., 1998), and this value decreases to about 5%-9% during SD (Mazel et al., 2002), which corresponds to about 17%-19% expansion of the average intracellular volume. In addition, the extracellular space volume fraction recovers to a value slightly higher than control and persists even one hour after SD, suggesting a long-lasting shrinkage of intracellular volumes.

The drastic extracellular space shrinkage of SD indubitably reflects cell swelling during SD. This was proven by early morphological studies in which brain tissue was quickly frozen and fixed immediately after SD was induced (Van Harreveld, 1958). Electron microscopy studies have revealed that the apical dendrites increase their diameter and this might account for the major fraction of swollen cellular elements (Van Harreveld and Khattab, 1967). However, very few studies have studied the cellular volume changes in living tissue. A recent study using *in vivo* two-photon microscopy indicates that SD induces transient neuronal swelling and dendritic beading, but does not affect astrocyte volumes (Takano et al., 2007). Given that astrocytic volumes are sensitive to elevated $[K^+]_o$, which is characteristic of SD, more studies will be required to explain this controversy.

1.3.4. Intrinsic optical signals

Intrinsic optical signal (IOS) is a functional neuroimaging technique that measures optical changes intrinsic to the tissue itself with second temporal resolution and micron spatial resolution (Frostig et al., 1990; Narayan et al., 1994; Cannestra et al., 1996). IOS is an appropriate approach to study SD because a large region of cortex can be imaged simultaneously and multiple time points can be collected over time as the wave spreads (O'Farrell et al., 2000; Ba et al., 2002). The IOS changes accompanying SD were first reported in the isolated frog retina by Gouras, who observed the visible “milky area” that expanded over the tissue together with the

electrical signals of SD (Gouras, 1958). This phenomenon was more thoroughly studied in chicken retina and was considered as a result of changing light scattering (Martins-Ferreira and de Castro, 1966). The IOS changes during SD have also been extensively studied in brain slices (Snow et al., 1983) or in anesthetized animal cortex (Yoon et al., 1996).

In the *in vivo* brain, there are three components of IOS that can be distinguished by different wavelength (Holthoff and Witte, 1996). The first component is from changes in blood volume that probably results from local capillary recruitment in an activated area (Lieke et al., 1989). It appears as an increase in hemoglobin absorption and dominates a peak wavelength between 500-700 nm. The second component originates from changes in the absorption or fluorescence of the transition states of NADH that indicates oxygen consumption changes. NADH has an emission peak at about 450 nm, while the oxidized form of the coenzyme does not fluoresce (Kasischke et al., 2004). The third component is relatively independent of wavelength and is based on scattered light (Holthoff and Witte, 1996). It dominates in the near infrared region above 800 nm since other components are absent in this region. It is possibly caused by the changes in the brain tissue after activation, like ion and water movement, expansion and contraction of extracellular spaces, capillary expansion, and neurotransmitter release (Lieke et al., 1989). In *in vitro* brain slices, the contribution of blood flow volume to the IOS changes is very minor. When imaged with near-infrared wavelength, only the third component of the IOSs can be observed. Light scattering affects light transmittance and reflectance in opposite ways: the more a medium scatters, the more light is reflected and the less is transmitted (Aitken et al., 1999).

Studies in brain slices have shown that rapid changes of IOS occur at the same time as the start of extracellular potential changes (Anderson and Andrew, 2002), suggesting that IOS imaging can be used reliably in visualizing the propagation pattern of SD waves. However, there are controversies in the observations of SD-related IOS from different research

groups. Some report that a decrease in light transmittance or increase in light reflectance, which is followed by a gradual recovery to baseline, is associated with the rapid negative potential shift of SD (Snow et al., 1983; Aitken et al., 1998; Tao, 2000; Vilagi et al., 2001; Buchheim et al., 2002). Other studies have shown that there is an initial brief (2-3 seconds) increase of light transmittance followed by a more gradual decrease. If the initial increase in transmittance is large, then the following decrease phase sometimes remains above the resting level (Basarsky et al., 1998; Anderson and Andrew, 2002; Fayuk et al., 2002). Despite the controversy, these studies all indicate that the start of IOS signals is temporally coincident with the onset of SD depolarization, suggesting that IOS imaging can adequately depict the status of the wave propagation. Many IOS studies have shown that the SD-associated IOS changes consist of multiple components, each of which may result from very distinct mechanisms (Fayuk et al., 2002). Different experimental conditions, like illumination wavelength, signal collection apparatus or recording chambers, may affect one or more component of the IOS, and then the overall changes in IOS could appear to be very different.

There are many factors that affect light scattering in brain slices, including particle size, particle number, membrane configuration and refractive index (Jarvis et al., 1999). These factors can be affected by various cellular processes associated with SD, among which one of the most important is cell swelling (Andrew and MacVicar, 1994). When water enters the cells, the refractive index of the cytosol becomes more similar to the extracellular fluid. This will reduce refraction at membrane interfaces and thus increase light transmittance. Cell swelling will also unfold plasma membrane to a more planar configuration, thereby increasing the probability of photon transmission (Jarvis et al., 1999). Swelling of intracellular organelles like mitochondria may also contribute to reducing light scattering by increasing particle size (Bahar et al., 2000). Dendritic beading, on the other hand, increases the number of particles as the single cylinder-

shaped dendrites change into multiple spherical ones, thus increasing the light scattering (Obeidat and Andrew, 1998). Finally, unlike brain slices, retina exhibits different IOS changes because they are initially transparent and have pronounced extracellular matrices that may increase light scattering when hydrated (Anderson and Andrew, 2002).

1.3.5. Cerebral blood flow and metabolic changes

Vascular changes during SD have been characterized with a variety of methodologies including observation of pial vessel diameter (Leão, 1944a), autoradiography (Lauritzen et al., 1982; Fabricius and Lauritzen, 1993), laser Doppler flowmetry (Fabricius and Lauritzen, 1996; Wolf et al., 1996; Dreier et al., 1998), and laser Doppler perfusion imaging (Lauritzen and Fabricius, 1995). SD is accompanied by multi-phase changes of the cerebral blood flow but the observations may be very different due to the experimental conditions and animal species. Generally, SD leads to a transient increase in blood flow and blood volume followed by a sustained reduction in blood flow in anesthetized animals, including rats (Lauritzen, 1984; Wahl et al., 1987), rabbits (Shibata et al., 1990, 1992), monkeys (Yokota et al., 2002) and cats (Wahl et al., 1987; Piper et al., 1991). The dilation of cerebral vessels and the increase in blood flow starts simultaneously with the ΔV_o of SD and lasts about 90 to 120 seconds (Fabricius et al., 1995). This increase has also been observed in non-anesthetized animals, although variable blood flow responses have been reported in awake rats (Duckrow, 1991; Shimazawa and Hara, 1996; Sonn and Mayevsky, 2006). The moderate but long-lasting suppression phase of cerebral blood flow, which is similar to the spreading oligemia observed in migraine patients (Olesen et al., 1981; Woods et al., 1994; Hadjikhani et al., 2001), can last over an hour after SD (Lauritzen et al., 1982; Piper et al., 1991; Lacombe et al., 1992; Mraovitch et al., 1992; Shibata et al., 1992;

Shimazawa and Hara, 1996). Additionally, the blood flow response in mice is unique compared with other species. Normally it does not show an obvious increase at SD onset, but rather exhibits a cerebral hypoperfusion or multiphase changes in a few minutes following SD (Ayata et al., 2004; Brennan et al., 2007; Takano et al., 2007). It has been reported that the constriction of intracortical arterioles is dependent on the astrocytic calcium waves in young mice (Chuquet et al., 2007). However, the reason for the complexity in mice is still unclear.

SD is accompanied by changes in energy metabolism, which is critical for restoration of membrane potential and ionic gradients following the profound depolarization (Gido et al., 1993). SD induces a remarkable increase in cerebral glucose utilization, and an increased net transfer of glucose from blood to brain (Shinohara et al., 1979; Gjedde et al., 1981; Lauritzen et al., 1990). Accordingly, both tissue glucose and glycogen levels decrease, and lactate level increases during SD (Krivanek, 1961; Lauritzen et al., 1990; Selman et al., 2004; Hashemi et al., 2009). SD induces an increase in tissue oxygen consumption and a decrease in basal tissue oxygen tension, which is adequately matched by an increase in local blood flow (Mayevsky and Weiss, 1991; Takano et al., 2007; Piilgaard and Lauritzen, 2009). A major increase in NADH oxidation has been observed temporally consistent with SD onset (Rosenthal and Somjen, 1973; Lothman et al., 1975; Rex et al., 1999; Takano et al., 2007). The time course of NADH level changes appears to correspond to the excitation and inhibition of neuronal metabolism (Rex et al., 1999). SD is accompanied by energy consumption, as indicated by rapidly elevated ATP and reduced ADP levels (Mies and Paschen, 1984; Kocher, 1990; Lauritzen et al., 1990; Selman et al., 2004). A decrease in phosphocreatine level has also been detected and the trend of the change is closely connected to the degree of depolarization accompanying SD (Krivanek, 1961; Lauritzen et al., 1990; Gault et al., 1994; Selman et al., 2004). These changes are consistent with increases in

oxygen metabolic rate, oxidation of NADH and glucose consumption, which might be required for pumping ions across plasma membranes during the recovery from SD.

1.4. Mechanisms of SD

SD is characterized by large depolarization and ion redistribution. Therefore, it is reasonable to postulate that the fundamental mechanisms underlying SD occurrence and progression rely on the activation of certain ion channels. Here, we will review the current understanding regarding the contribution of ion channels to the hypothetical mechanisms of SD.

1.4.1. Involvement of Na^+ channels

The rapid and large decrease of $[Na^+]_o$ in the extracellular space during SD suggests the occurrence of a profound inward Na^+ current (Kraig and Nicholson, 1978; Hansen and Zeuthen, 1981). Substituting extracellular Na^+ by choline or TMA^+ slows down the propagation of SD in a concentration-dependent manner in the isolated retina (Martins-Ferreira et al., 1974). This suggests that the Na^+ flow is required for SD. However, the VGSC blocker TTX does not exhibit a significant effect on the SD initiation and propagation (Sugaya et al., 1975; Tobiasz and Nicholson, 1982). This suggests that the Na^+ influx is mediated by other Na^+ permeable ion channels, such as ionotroptic glutamate receptors (see Chapter 1.4.4).

1.4.2. Involvement of Ca^{2+} channels

Studies have shown that extracellular Ca^{2+} drops remarkably with a similar time course of the decline of $[Na^+]_o$, suggesting an intense Ca^{2+} influx accompanying SD (Kraig and Nicholson, 1978; Hansen and Zeuthen, 1981; Herreras and Somjen, 1993b; Jing et al., 1993). Consistently, rapid increases of intracellular Ca^{2+} levels, by directly imaging with Ca^{2+} indicators, have also been reported during SD induced by either electrical stimulation (Kunkler and Kraig, 2004), focal high K^+ application or ouabain (Dietz et al., 2008). The non-selective Ca^{2+} channel blockers Co^{2+} and Ni^{2+} abolish the propagation of SD induced by focal high K^+ in hippocampal slices (Jing et al., 1993).

Among three types of high-threshold activated VGCCs, P/Q channel blockers are particularly effective in blocking the focal stimulation induced SD (Kunkler and Kraig, 2004). P/Q channels are critical for Ca^{2+}-dependent presynaptic neurotransmitter release throughout the brain. Impairment of depolarization-induced glutamate release by blocking P/Q channels may account for the impairment of SD propagation. The role of P/Q channels in SD has been supported by the findings that mutant P/Q channels were identified in FHM1 patients (see section 1.5.1.). Transgenic mice carrying the R192Q mutation gene of human P/Q channels exhibit increased Ca^{2+} currents, enhanced neurotransmitter release and lower threshold for SD (van den Maagdenberg et al., 2004; Tottene et al., 2009). These findings suggest that P/Q channels can facilitate SD by enhancing cell excitability and that they play an important role in focal stimulus-induced SD model.

However, blocking Ca^{2+} influx across plasma membrane has varied effects on different forms of SD. Removing extracellular Ca^{2+} completely blocks focal high K^+ application-induced SD in cortical slices (Footitt and Newberry, 1998; Peters et al., 2003), but has little effect on ouabain or

bath high KCl application-induced SD (Basarsky et al., 1998; Dietz et al., 2008). Here the question is why does blocking Ca^{2+} influx have varied effects in different SD models? One possibility is that Ca^{2+} channels may facilitate SD generation, but are not required to sustain SD propagation. Based on this assumption, other sources of the cytosolic Ca^{2+} increase, like Ca^{2+} released from endoplasmic reticulum or mitochondria, might be involved.

1.4.3. Involvement of K^+ channels

K^+ is believed to be an important factor since Grafstein first raised the K^+ hypothesis of SD (Grafstein, 1956): intense neuronal firing releases K^+ from neurons and thus accumulates in the interstitial space. Then the excessive K^+ can depolarize the same cell, or can diffuse and depolarize adjacent neurons and therefore release more K^+. This vicious cycle increases the susceptibility to SD and promotes the wave propagation. The K^+ hypothesis is supported by following two major evidences: (1) The voltage-gated K^+ channel blocker TEA reduces both extracellular K^+ level and the amplitude of extracellular potentials during SD in a dose-dependent manner in the chick retina (Scheller et al., 1998); (2) dramatic elevation of extracellular K^+ occurs simultaneously with the extracellular potential shift of SD. While these studies might best support the K^+ hypothesis, there are still questions regarding the principal role for K^+ in mediating SD propagation. First, even high doses of TEA cannot completely abolish SD in hippocampus (Jing et al., 1994), suggesting that the K^+ flow via TEA-sensitive voltage-gated K^+ channels is not the only player in promoting SD progression. Second, if SD is mediated by accumulated extracellular K^+, one might expect that the extracellular K^+ increase will occur before the depolarization of SD. However, extracellular K^+ changes and the extracellular DC voltage signals follow a similar temporal course. These studies suggest that the outflow of K^+

might be an important component in the positive feedback chain that generates SD, even if K^+ *per se* is not sufficient to initiate and sustain SD (Herreras, 2005).

1.4.4. Involvement of glutamate and glutamate receptors

Glutamate is the principal excitatory neurotransmitter in the central nervous system. Glutamate signaling plays a key physiological role by mediating the vast majority of excitatory synaptic transmission and is also responsible for excitotoxicity, the process that triggers neurodegeneration through glutamate receptor overactivation. Glutamate receptors are classified into ionotropic receptors and metabotropic receptors. The three types of ionotropic glutamate receptors are ligand-gated ion channels and are characterized by the names of their selective agonists, including NMDA, AMPA and kainate type of receptors. Metabotropic glutamate receptors are G-protein coupled receptors and are classified into eight subtypes that are subdivided into three groups based on sequence homology, signal pathways and agonist selectivity. All three classes of ionotropic receptors are permeable to Na^+, K^+ and/or Ca^{2+}, causing the consequent ion redistribution and neuronal depolarization. Nevertheless, neither AMPA nor KA receptor activation appear to be important for the initiation or propagation of SD, since AMPA/KA receptor antagonists have no effects on SD (Nellgard and Wieloch, 1992; Psarropoulou and Avoli, 1993; Kruger et al., 1999). Among all types of glutamate receptors, NMDA receptors make the most important contribution to SD.

Van Harreveld first proposed the glutamate hypothesis, which depicts glutamate as the key compound in mediating SD (Van Harreveld, 1959). According to this theory, glutamate is released by intensive neuronal activities and then activates more glutamate receptors on the same neuron or on adjacent neurons. These neighbouring neurons will also depolarize, fire, and

release more glutamate to form a positive feedback. In addition, the Na^+ influx via glutamate receptors may also explain the mechanism of Na^+ redistribution during SD since voltage gated Na^+ channels are not responsible. The glutamate hypothesis of SD is supported by the following evidences. First, glutamate is released during SD. A transient increase in the extracellular glutamate concentration has been detected by microdialysis or glutamate sensitive electrodes (Fabricius et al., 1993; Iijima et al., 1998). Second, SD can be elicited by application of glutamate receptor agonists onto the brain surface (Lauritzen et al., 1988; Lenti et al., 2009). Finally, SD is inhibited by various competitive (including APV, CPP and 2-amino-7-phosphonoheptanoate) and uncompetitive NMDA antagonists (including Mg^{2+}, ketamine, phencyclidine and MK-801 (Table 1.1).

There are, however, unresolved questions with this theory too. The insensitivity of SD to TTX and zero extracellular Ca^{2+} argues against the occurrence of glutamate release. With conventional views, neurotransmitter release is evoked by action potential-driven Ca^{2+} influx via presynaptic VGCCs. However, other mechanisms of glutamate release have also been reported. For instance, the reversed action of glutamate transporters can release glutamate from the cytosol under some pathological conditions like ischemia (Rossi et al., 2000). Glutamate efflux through astrocytic volume activated anion channels contributes to ouabain induced SD (Basarsky et al., 1999). Extracellular glutamate level can also be increased by action of cystein-glutamate exchangers or opening of gap junction hemichannels (Warr et al., 1999; Ye et al., 2003; Thompson et al., 2006). Astrocytes can also release glutamate via vesicular exocytosis that is dependent on calcium release from internal Ca^{2+} stores (Hua et al., 2004; Reyes and Parpura, 2008). These action potential- and VGCC-independent mechanisms may be involved in the glutamate release during SD.

Table 1.1. Effects of NMDA receptor antagonists on spreading depression

Anta-gonist	Properties	SD model	Observation	References
ketamine	Uncompetitive, open channel blocker	Focal injection of K^+ in anesthetized rat cortex	High dose (>25 mg/kg) completely blocks SD; lower doses suppress SD amplitude	(Hernandez-Caceres et al., 1987; Gorelova et al., 1987; Rashidy-Pour et al., 1995)
		DC stimulation in anesthetized rat cortex	Increases SD threshold; inhibits propagation; High dose (80 mg/kg) completely blocks SD	(Marrannes et al., 1988)
		Focal application of KCl in rate neocortical slices	100 μM reduces SD amplitude and duration	(Kruger et al., 1999)
MK-801	Uncompetitive, open channel blocker	Focal injection of K^+ in anesthetized rat cortex	2.5 mg/kg blocks SD initiation	(Hernandez-Caceres et al., 1987)
		DC stimulation in anesthetized rat cortex	Increases SD threshold; inhibits propagation; High dose (3.1 mg/kg) completely blocks SD	(Marrannes et al., 1988)
		Electrical stimulation in anesthetized rat cortex	10 mg/kg blocks both initation and propagation	(Lauritzen and Hansen, 1992)
		Ouabain-induced SD in hippocampal slices	Reduces the rate of propagation of SD	(Basarsky et al., 1999)
		Mechanical stimulation in anesthetized Cat cortex	Blocks SD	(Kaube and Goadsby, 1994)

Anta-gonist	Properties	SD model	Observation	References
Phency-clidine	Uncompetitive, open channel blocker	DC stimulation in anesthetized rat cortex	Increases SD threshold; inhibit propagation	(Marrannes et al., 1988)
CPP	Competitive antagonist	Microdialysis of K^+ in anesthetized rat hippocampus	Dialysis of 100-150 μM inhibits the second phase of ΔV_o without affecting the amplitude of first phase	(Herreras and Somjen, 1993b)
		4-AP induction in immature rate hippocampal slices	5 μM Largely inhibits the ΔV_o amplitude	(Psarropoulou and Avoli, 1992)
APV	Competitive antagonist	Focal injection of K^+ in anesthetized rat cortex	Blocks SD generation and propagation	(Hernandez-Caceres et al., 1987)
		Spontaneous SD by 0 Mg^{2+} solutions in rat hippocampal slices	Blocks generation of spontaneous SD	(Mody et al., 1987)
		Electrical stimulation in isolated turtle cerebellum	Blocks SD generation and increases the threshold	(Lauritzen et al., 1988)
		Spontaneous or focal electrical stimulation induced SD in human cortical slices	Blocks spontaneous SD and inhibits the second phase of ΔV_o when SD is induced by focal stimulation	(Avoli et al., 1991)
amino-7-phospho-noheptan oate (APH)	Competitive antagonist	DC stimulation in anesthetized rat cortex	Increases SD threshold; inhibits propagation; High dose (160 mg/kg) completely blocks SD	(Marrannes et al., 1988)
		Electrical stimulation in anesthetized rat cortex	4.5 mg/kg completely blocks SD even by superthreshold stimuli	(Lauritzen and Hansen, 1992)

Anta-gonist	Properties	SD model	Observation	References
Mg^{2+}	Non-competitive, voltage-dependent	Mechanical stimulation in chicken retina	Reduces SD propagating rate	(Martins-Ferreira et al., 1974)
CP-101,606	NR2B specific antagonist	Tetanus electrical stimulation in mouse cortex	Inhibits SD rate and amplitude	(Menniti et al., 2000)
Ifenprodil	NR2B specific antagonist	Tetanus electrical stimulation in mouse cortex	Abolishes SD occurrence	(Faria and Mody, 2004)

1.4.5. Astrocytic calcium signaling and gap junctions

Astrocytes exhibit waves of increased intracellular calcium that can propagate through gap junctions, and the calcium waves can also increase intracellular calcium in neighboring neurons (Nedergaard, 1994; Parpura et al., 1994; Hassinger et al., 1995). Astrocytic calcium waves and SD share a number of similar features. For instance, astrocytic calcium waves propagate at about 15-50 μm/second, which is similar to the rate of SD propagation (Cornell-Bell et al., 1990; Martins-Ferreira et al., 2000). Both phenomena can be effectively triggered by similar stimuli, such as high KCl, glutamate and electrical stimulation. Astrocyte calcium increments have been shown to precede neuronal depolarization during SD (Basarsky et al., 1998; Kunkler and Kraig, 1998). This has led to the hypothesis that astrocytic calcium waves might play an important role in SD (Nedergaard et al., 1995). The strongest evidence that support this idea is that both SD and astrocytic calcium waves depend on gap junction communication (Finkbeiner, 1992; Martins-Ferreira and Ribeiro, 1995; Nedergaard et al., 1995). The gap junction blockers, such as

heptanol, octanol and halothane, can block SD in chick retina (Nedergaard et al., 1995), rat hippocampus (Largo et al., 1997b; Kunkler and Kraig, 1998), and at least partially inhibit SD in mouse neocortex (Margineanu and Klitgaard, 2006). The gap-junction hypothesis of SD, however, is challenged by several issues. First, SD is not affected when astrocytic calcium waves are abolished by removing extracellular Ca^{2+} or by depletion of internal Ca^{2+} stores (Basarsky et al., 1998; Peters et al., 2003). Second, the selective glial metabolism blocker fluoroacetate does not inhibit SD (Largo et al., 1997a; Largo et al., 1997b). Finally, transgenic mice lacking astrocytic connexin43 gene exhibit an increase in the SD velocity (Theis et al., 2003). These evidences suggest that astrocytic calcium waves are not required for propagation of SD, raising the question about the role of gap junctions in SD.

Somjen has proposed an alternative hypothesis that SD propagates through inter-neuronal gap junctions. As mentioned in section 1.3.1, a brief burst of population spikes is detected in CA1 of hippocampus several seconds before the onset of the negative extracellular potential shift of SD. The population spikes are synchronized over considerable distances in the tissue (Herreras et al., 1994; Larrosa et al., 2006). It is hypothesized that the long-distance synchronization is mediated by the opening of normally closed electric junctions among neurons (Herreras and Somjen, 1993b; Herreras et al., 1994). This idea is supported by the findings that both the population spike and the propagation of SD are depressed by gap junction blockers (Largo et al., 1997a). However, the role of gap junctions in SD still needs to be confirmed by further evidences, like more specific pharmacological or genetic inhibition of neuronal gap junctions.

1.5. SD and Neurological Disorders

1.5.1. Migraine

Migraine is a common episodic brain disorder of neuronal and blood vessel dysfunction that affects more than ~15% of the population (Unger, 2006). Migraine attacks are typically characterized by repeated, episodic, frequently unilateral headaches that last several hours to days. In up to 30% of patients, the migraine attack is preceded or accompanied by transient and usually visual neurological symptoms called migraine aura (Goadsby, 2007). Migraine has a strong genetic component, which is higher in migraine with aura (MA) compared with migraine without aura, but the causative genes have not been identified yet (Wessman et al., 2002), except for familial hemiplegic migraine (FHM) that is a rare, autosomal dominant subtype of MA. SD is believed to underlie the aura symptoms of migraine, and activation and sensitization of the trigeminovascular system is critical for the pain generation itself (Goadsby et al., 2002; Pietrobon and Striessnig, 2003). Current acute and prophylactic treatments are not optimal as they are effective only in about half of the patients (Ramadan et al., 1997). We need more understanding of the migraine pathogenesis in order to prevent or treat this disorder.

1.5.1.1. SD and migraine aura

A typical migraine aura described by Lashley consists of a scotoma with a scintillating border drifting slowly across the visual field (Lashley, 1941). Usually, the disturbance starts at the centre of the visual field and spreads to the peripheral parts in about 10-15 minutes and returns to normal in another 10-15 minutes (Lauritzen, 2001). It is hypothesized that the scotoma results from a region of depressed neural activity and the scintillation results from a bordering region of

intense cortical excitation. The scotoma-scintillation moves across the visual cortex at speed of approximately 3 mm/min, which is similar to the propagation rate of SD. In addition, migraine aura and SD also share several other similarities. For example, both migraine aura and SD are likely to be initiated from brain regions with high neural density; they both propagate along the cortical surface; both tend to be restricted to one hemisphere; and both of them are repeatable (Lauritzen, 2001). These similarities lead to the hypothesis that SD is responsible for migraine aura.

1.5.1.2. Spreading oligemia in migraine patients

Cerebral blood flow undergoes a sequence of changes during migraine attacks in patients with MA (Skinhoj and Paulson, 1969; O'Brien, 1971; Mathew et al., 1976; Hachinski et al., 1977; Sakai and Meyer, 1978; Lauritzen et al., 1983b; Lauritzen et al., 1983a; Lauritzen and Olesen, 1984; Friberg et al., 1987; Andersen et al., 1988; Olesen et al., 1990; Cutrer et al., 1998; Cao et al., 1999). Normally, the migraine attack is accompanied by a reduction of cerebral blood flow (oligemia) that starts from the posterior part of the brain and spreads into the parietal and temporal lobes at a rate of 2-3 mm/min (Lauritzen, 2001). It has also been reported that a transient vasodilatation precedes the oligemia and the development of neurological sympotoms (Hadjikhani et al., 2001). The cerebral blood flow decreases by 30-40% and is still far above the ischemic level. Tests of the cerebral blood flow dynamics have revealed that blood pressure autoregulation in the oligemic region is normal, while the CO_2 reactivity and responses of cerebral blood flow to physiological activation is impaired (Lauritzen et al., 1983b; Lauritzen, 1984). These features are similar to the flow changes during SD (Table 1.2).

Table 1.2. A comparison between spreading oligemia of regional cerebral blood flow during migraine aura in man and Leão's cortical spreading depression in animals (from Tfelt-Hansen, Cephalalgia, 2009)

Factor	Migraine with aura	CSD in rats
Site of origin	Primary visual cortex	High neuron density
Way of spread	Continuous, cortical	Continuous, cortical
Excitation/depression	Yes	Yes
Rate of spread (mm/min)	3-5	2-6
Unilateral	Yes	Yes
Repeated waves	Yes	Yes
Initial hyperaemia	Yes	Yes
Oligemia lasting	Hours	1.5 h
Degree of hypoperfusion	Above ischemic threshold	Above ischemic threshold
Autoregulation	Preserved	preserved
CO_2 reactivity	Impaired	Impaired
Reaction to activation	Depressed	Depressed
Cerebral metabolism	Normal	Normal

1.5.1.3. Familial hemiplegic migraine

FHM diagnosis is based on the presence of one-sided motor weakness during the aura phase, and similar attacks in at least one first-degree or second-degree family member. Currently, there are three types of FHM that are genetically heterogenous with mutations in the CACNA1A (FHM1), the ATP1A2 (FHM2) and the SCNA1 (FHM3) genes (van den Maagdenberg et al., 2007).

The CACNA1A gene, which is located on chromosome 19p13, encodes the pore-forming alpha1A subunit of $Ca_V2.1$ (P/Q-type) voltage-gated calcium channels (Ophoff et al., 1996). This subunit consists of four repeated domains, each of which contains six transmembrane regions (S1-S6). 21 CACNA1A missense mutations associated with FHM1 have been identified since 1996 (Figure 1.4A) (de Vries et al., 2009), and these mutations are distributed in important functional regions throughout the channel, including the voltage sensor domains S4 and the pore loop domains between S5 and S6. Most investigated FHM1 mutations exhibit a gain-of-function effect at either single channel level or whole-cell level, like opening at more negative voltages and increased channel open probability (Hans et al., 1999; Tottene et al., 2002; Melliti et al., 2003; Mullner et al., 2004; van den Maagdenberg et al., 2004; Tottene et al., 2005). Consistent shifts to lower voltages of channel activation have also been reported by using whole-cell recordings in heterologous expression systems, transfected neurons and neurons of the knock-in mice (Hans et al., 1999; Tottene et al., 2002; Mullner et al., 2004; van den Maagdenberg et al., 2004). These gain-of-function effects lead to an enhanced Ca^{2+} current and transmitter release at presynaptic terminals.

The gene for FHM2, first identified in 2003, is mutant ATP1A2 gene that encodes the $\alpha 2$ subunit of the Na^+, K^+-ATPase (De Fusco et al., 2003). The Na^+, K^+-ATPase is a P-type ion pump that utilizes the energy of ATP to actively transport Na^+ out of and K^+ into the cell. It consists of two subunits, including a catalytic α subunit that contains the binding sites for ATP and the cations, and a regulatory β subunit. Now over thirty different missense mutations associated with FHM2 have been reported, all of which produce substitution of conserved amino acids in important functional regions including the intracellular loop 4-5 and extracellular loop 7-8. Functional studies have shown that most of the investigated mutations of FHM2 display either severe to

Figure. 1.4. Schematic representation of Sporadic Hemiplegic Migraine (SHM) and FHM mutations in FHM gene-encoded proteins. (a) Mutations in the α1A subunit of the voltage-gated $Ca_V2.1$ Ca^{2+} channel encoded by the FHM1 *CACNA1A* gene (Genbank Ac. nr. X99897). The protein is located in the plasma membrane and contains four repeated domains, each encompassing six transmembrane segments. (b) Mutations in the α2 subunit of the Na^+,K^+ ATPase encoded by the FHM2 *ATP1A2* gene (Genbank Ac. nr. NM_000702). The protein is located in the plasma membrane and contains ten transmembrane segments. (c) Mutations in the α1 subunit of the voltage-gated $Na_V1.1$ Na^+ channels encoded by the FHM3 *SCN1A* gene (Genbank Ac. nr. NM_006920). The protein is located in the plasma membrane and contains four repeated domains. Symbols: *Circle with solid line* FHM, *circle with dotted line* SHM, *circle with horizontal striped pattern* basilar-type migraine, *circle with vertical striped pattern* common migraine. *Asterisk* Mutation for which also SHM was reported, *black circles* mutation was tested for functional consequences, *white circle* mutation was not tested for functional consequences. Figure adapted from de Vries et al, Human Genetics, 2009, 126(1): 115-132.

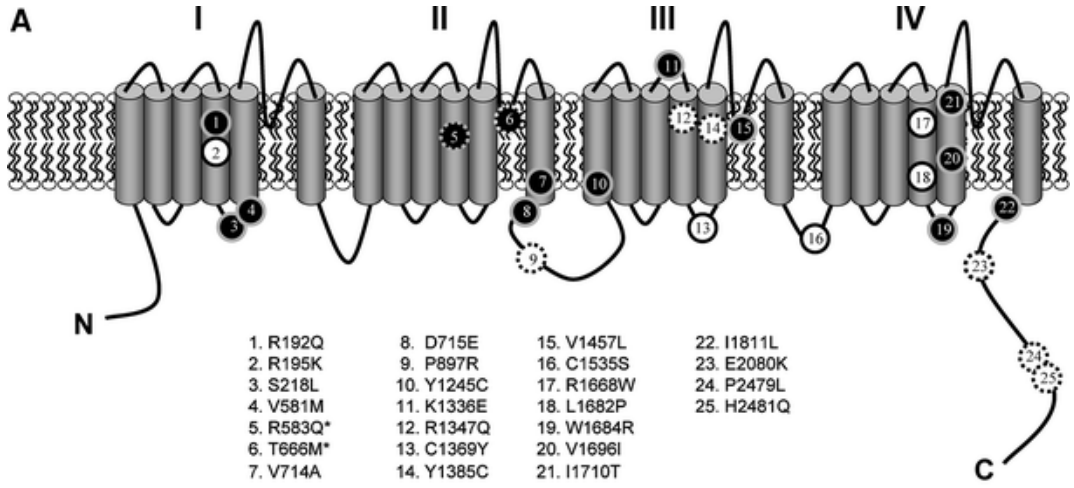

1. R192Q
2. R195K
3. S218L
4. V581M
5. R583Q*
6. T666M*
7. V714A
8. D715E
9. P897R
10. Y1245C
11. K1336E
12. R1347Q
13. C1369Y
14. Y1385C
15. V1457L
16. C1535S
17. R1668W
18. L1682P
19. W1684R
20. V1696I
21. I1710T
22. I1811L
23. E2080K
24. P2479L
25. H2481Q

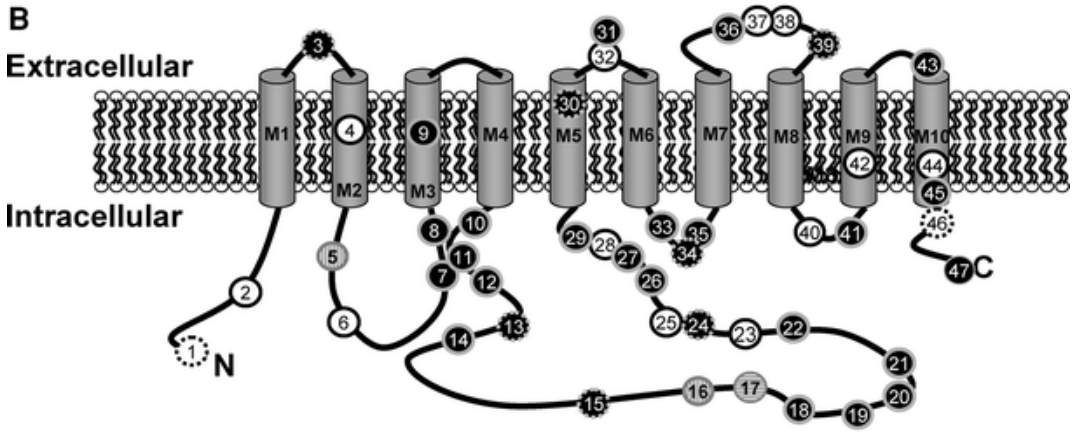

1. Y9N
2. R65W
3. E120A
4. V138A
5. E174K
6. R202Q
7. T263M
8. I286T
9. G301R
10. T345A
11. V362E
12. T376M
13. R383H
14. T415M
15. E492K
16. C515Y
17. R548H
18. R593W
19. A606T
20. G615R
21. V628M
22. R689Q
23. E700K
24. N717K
25. D718N
26. M731T
27. R763H
28. R763C
29. L764P
30. P786L
31. P796S
32. P796R
33. M829R
34. R834X
35. R834Q
36. W887R
37. G900R
38. E902K
39. R908Q
40. 935K-940Sdelinsl
41. R937P
42. S966fs
43. P979L
44. D999H
45. R1002Q
46. Y1009X
47. X1021R

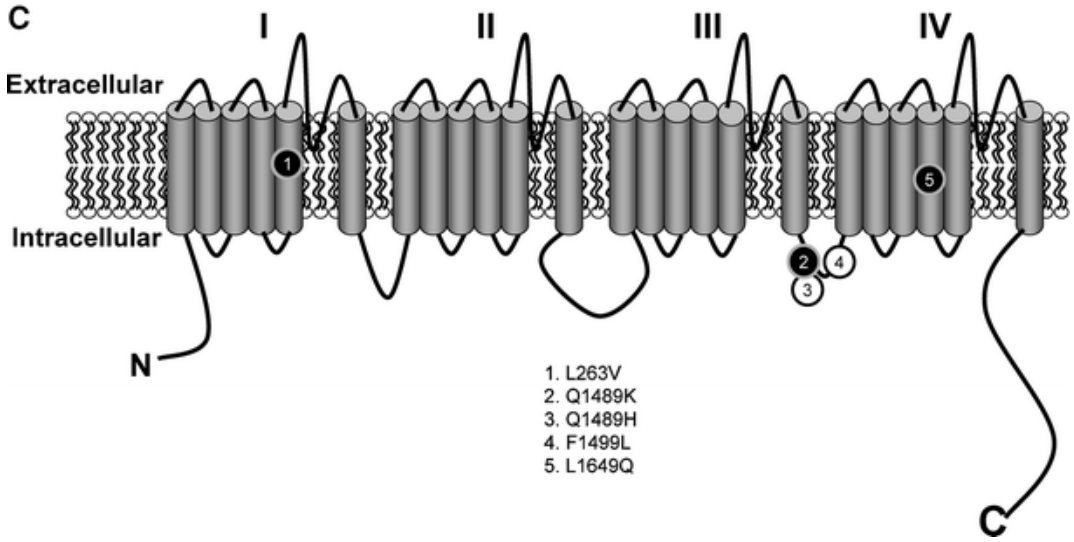

1. L263V
2. Q1489K
3. Q1489H
4. F1499L
5. L1649Q

complete loss-of-function of pump activity (De Fusco et al., 2003; Bassi et al., 2004; Capendeguy and Horisberger, 2004; Koenderink et al., 2005; Vanmolkot et al., 2006; Tavraz et al., 2008; Tavraz et al., 2009) or impaired potassium sensitivity that leads to slower clearance of extracellular K^+ and slower recovery from neuronal excitation (Segall et al., 2004; Segall et al., 2005).

The gene for FHM3 that encodes SCN1A, the α1 subunit of the voltage-gated sodium channel $Na_v1.1$, was first identified in 2005 (Dichgans et al., 2005). The pore-forming α1 subunit of the Na^+ channel is composed of six transmembrane segments repeated in four homologous domains. There are five identified FHM3 mutations so far and for three of them the functional studies have been shown. However the functional consequences of FHM3 mutations still remain controversial and require further confirmation (Vanmolkot et al., 2006; Vanmolkot et al., 2007; Kahlig et al., 2008; Tavraz et al., 2008).

1.5.1.4. Studies in FHM1 knock-in animal models

Two types of knock-in mice, which express R192Q or S218L mutations of FHM1, have been developed. In humans, patients with the R192Q mutation suffer from FHM only, whereas the S218L mutation is associated with both severe migraine and risk of developing severe cerebral edema and fatal coma (Kors et al., 2001). Mice carrying the R192Q mutation of the human FHM1 gene exhibit a gain-of-function of increased calcium current and lower activation voltage at both single channel and whole-cell level (van den Maagdenberg et al., 2004). These mice also showed lowered threshold for induction and increased velocity of propagation of SD. The high susceptibility to SD is likely induced by enhanced strength of cortical excitatory synaptic transmission due to increased action potential-evoked Ca^{2+} influx through the mutant

P/Q channels and the consequently increased glutamate release. In contrast with excitatory neurotransmission, inhibitory transmission is unchanged in these knock-in mice (Tottene et al., 2009). Consistent with the symptoms observed in humans, S218L mutant animals are associated with even higher susceptibility to SD and more severe neurological deficits compared with the R192Q mutations (Eikermann-Haerter et al., 2009b). Furthermore, female mutant mice are more susceptible to SD neurological deficits than their male equivalents. The sex difference can be eliminated by ovariectomy and be partially restored by estrogen replacement (Eikermann-Haerter et al., 2009b). Another study has shown that orchiectomy in male R192Q mice increases SD susceptibility by an androgen receptor-dependent mechanism (Eikermann-Haerter et al., 2009a). These findings suggest that sex hormones are responsible for the different susceptibility to SD between male and female. Interestingly, this is in line with the observations that genetic and hormonal factors are highly associated with migraine in humans (MacGregor, 2004), as indicated by a female preponderance for common types migraine (female:male ratio of 3:1), familial (5:2) and sporadic (4.25:1) hemiplegic migraine (Rasmussen et al., 1991; Thomsen et al., 2002; Thomsen et al., 2007). In summary, these studies may explain the pathological mechanisms for the FHM symptoms and strengthen the link between SD and migraine aura.

1.5.2. Ischemia

Leão has reported that a spreading depression-like event could be generated by carotid artery occlusion and hypothesized that such events could contribute to ischemic injury (Leão, 1947). In global ischemia or the core of focal lesions, large membrane depolarizations are caused by withdrawing oxygen itself, known as “hypoxic/ischemic depolarization” or “anoxic depolarization” (Hansen, 1985). In the penumbral regions surrounding the ischemic core,

recurrent SD-like events often originate from the edge of the infarcted areas, which is known as "peri-infarct depolarization" (Hossmann, 1996). Both of the phenomena have similar biophysical features as normal SD, however, it is noteworthy that they are generated by different mechanisms and they contribute differently to tissue damage following hypoxic conditions. These two phenomena will be discussed separately in this section.

1.5.2.1. Comparison of normoxic SD and anoxic depolarization

Hypoxia of cerebral tissue in either *in vivo* brains (Korf et al., 1988; Katayama et al., 1992; Lauritzen and Hansen, 1992; Xie et al., 1995) or *in vitro* slices (Balestrino and Somjen, 1986; Sick et al., 1987; Balestrino et al., 1989; Kral et al., 1993) results in a sequence of SD-like cellular events. It occurs between 60 and 180 seconds after onset of global ischemia *in situ*, and between 1 and 12 min after the onset in slices (Lipton, 1999). It is known that neurons first become hyperpolarized for a few minutes (Hansen, 1985; Luhmann and Heinemann, 1992). If oxygenation is not restored, the membrane potential undergoes a first gradual and then a rapid and profound decrease of about 10 to 30 mV. This precipitous depolarization is accompanied by a rise in extracellular K^+ (to about 60 mM), and by a decrease in extracellular Na^+ (to about 50 mM), Cl^-, and Ca^{2+} (to about 0.1 mM) (Lauritzen and Hansen, 1992; Kral et al., 1993; Xie et al., 1995). These biophysics features of the depolarization itself are very similar to what have been observed during SD (Table 1.3), except that the changes of membrane potential and ion gradients are normally irreversible if the shortage of oxygen supply persists beyond a critical period of time. Therefore, the hypoxia/ischemia induced depolarization is termed hypoxic/anoxic SD due to its similarities to normoxic SD, or terminal depolarization due to its inability of recovery (Somjen, 2001).

It has been long debated whether the normoxic SD and the large depolarization induced by cerebral hypoxia/ischemia are caused by the same mechanisms. Somjen has studied an *in vitro* hypoxia model in which brain slices in a gas-liquid interface chamber can be rapidly flooded with abundant oxygen compared with submerged slices. If oxygen is supplied shortly after the occurrence of the onset of ΔV_o, the cell membrane potential and ion gradients can recover in a time course very similar to normoxic SD (Czeh et al., 1993). In addition, short hypoxia-induced depolarization in the interfaced slices arose also focally, spreading with a similar pattern and velocity as normoxic SD (Aitken et al., 1998). Therefore, it is reasonable to postulate that the nature of depolarization itself during hypoxia is very similar to SD, while other metabolic changes might be different between the two. Hypoxia will cause more severe cell damages due to lack of energy supplies required for restoring normal membrane potential and ion homeostasis after the large depolarization.

There are, however, also other differences even if reversible hypoxic depolarization is induced under conditions described by Somjen. First, synaptic transmission is depressed a few minutes before the ΔV_o occurrence in hypoxia, while synaptic transmission disappears at ΔV_o onset during SD. A possible reason for this is that oxygen shortage impedes Ca^{2+} entry into, and therefore the release of transmitter from the presynaptic terminals (Young and Somjen, 1992; Czeh et al., 1993; Hershkowitz et al., 1993; Rosen and Morris, 1993). Second, selective permeability of cell membranes differs under the two conditions. For instance, TMA^+ enters cells and inorganic phosphate leaks out of the cytosol (Scheller et al., 1992b) during anoxic depolarization (Jing et al., 1994), but these changes are not seen during normoxic SD. Finally, there is a difference in the pharmacology between the two events. NMDA receptor antagonists are more effective in blocking SD than anoxic depolarization; TTX more greatly postpones

anoxic depolarization than SD; and the propagation of SD is more sensitive to the gap junction blockers.

Table 1.3. Comparison of normoxic SD and hypoxic SD-like depolarization

Cellular changes	Normoxic SD	Anoxic depolarization	References
Propagation rate	8.73 ± 0.92 mm/min measured electrically and 5.84 ± 0.63 mm/min measured optically	7.22 ± 1.60 mm/min measured electrically and 6.79 ± 0.42 mm/min measured optically	(Aitken et al., 1998)
Extracellular voltage shift (ΔV_o)	Similar amplitude and time course		(Aitken et al., 1998)
Membrane current	Membrane current amplitudes and reversal potentials are similar		(Czeh et al., 1993)
Interstitial Volume	about equally magnitude of shrinkage during SD and HSD		(Jing et al., 1994) (Hansen and Olsen, 1980)
Extracellular ion concentrations (including $[K^+]_o$, $[Na^+]_o$, $[Ca^{2+}]_o$, and $[Cl^-]_o$)	The magnitudes of extracellular ion concentration changes during the phase of the rapid ΔV_o are identical.		(Hansen and Zeuthen, 1981) (Vyskocil et al., 1972) (Nicholson et al., 1977)
Extracellular glutamate	The increase of released glutamate is much higher in ischemia than SD		(Van Harreveld and Kooiman, 1965; Fabricius et al., 1993) (Iijima et al., 1998)
IOS	Similar pattern		(Aitken et al., 1998; Bahar et al., 2000; Fayuk et al., 2002)

Cellular changes	Normoxic SD	Anoxic depolarization	References
pH_o	A first pronounced alkaline transient followed by a mild, sustained acid shift	Complete ischemia begins with a progressive acidification that eventually reaches a plateau of 6.6-6.8, and a transient alkaline is also observed at the onset of ΔV_o	(Kraig et al., 1983)
Sensitivity to TTX	No effect	TTX delays the onset of HSD and sometimes blocks the occurrence	(Aitken et al., 1991) (Xie et al., 1994; Muller and Somjen, 2000)
Sensitivity to NMDAR antagonists	Yes	No effect	(Hernandez-Caceres et al., 1987; Aitken et al., 1988; Lauritzen and Hansen, 1992)
Sensitivity to gap junction blockers	Yes	Gap junction blockers only delay the onset of HSD	(Aitken et al., 1998) (Largo et al., 1997b)

1.5.2.2. Peri-infarct depolarization

Peri-infarct depolarizations (PID) are spontaneous and recurrent waves of depolarization with all of the features of SD that occur in ischemic penumbra -- the region of ischemically threatened tissue adjacent to the infarct core zone following focal ischemia (Strong et al., 1983; Umegaki et al., 2005). PID arises differently from ischemic depolarizations. The most significant difference between the two is that the frequency of PID is reduced by antagonists of either NMDA or non-NMDA ionotropic glutamate receptors (Iijima et al., 1992; Chen et al., 1993; Mies et al., 1994;

Back et al., 1996), while anoxic depolarization is resistant to these blockers. PID is known to occur in stroke models of mouse, rat and cat (Gill et al., 1992; Strong et al., 2000), and also in human stroke (Dreier et al., 2006).

PID is generated in the border zone of the ischemic lesion and spread into the peri-infarct surrounding and accelerates growth of infarct size (Chen et al., 1993; Mies et al., 1993; Nedergaard and Hansen, 1993; Busch et al., 1996; Dijkhuizen et al., 1999). Factors that decrease the frequency of PID, such as glutamate receptor antagonists, iNOS blockers (Shimizu-Sasamata et al., 1998) and hypothermia, reduce the size of the infarct that develops in the penumbral region. Artificially increasing the frequency of PID by either KCl or electrical stimulation accelerates the growth of infarct region (Back et al., 1996; Busch et al., 1996). It is still unclear how PID contributes to the progression of ischemic cellular damage since SD alone in normal tissue appears to be non-harmful (Nedergaard and Hansen, 1988). The recurrent PID may augment glutamate release that evokes excitotoxicity and thus triggers neuronal damage (Kempski et al., 2000). Recent studies have shown that recurrent PIDs are associated with augmented vasoconstriction and diminished vasodilation, compared with normal SD that is accompanied by profound vasodilation. The enhanced vasoconstriction and hypoperfusion have been observed during hypoxia, after bilateral carotid occlusion and in focal ischemic penumbra (Sonn and Mayevsky, 2000; Shin et al., 2006; Strong et al., 2007). Hypoxia and hypotension might be an important factor in transforming the blood flow responses of SD from hyperemia into hypoperfusion under penumbra conditions (Sukhotinsky et al., 2008).

1.6. Rationale, Hypothesis and Objectives

The following interesting findings regarding the features of SD have led us to investigate the mechanisms of SD propagation. First, some studies have suggested a leading role for astrocytes in SD based on the observations that SD shares similarities with astrocytic calcium waves and that SD is dependent upon opening of gap-junctions (Martins-Ferreira et al., 2000). On the other hand, abolishing astrocytic calcium waves or incapacitation of astrocytic metabolism does not impair SD, but rather facilitate SD onset (Largo et al., 1997a; Basarsky et al., 1998). Questions still remain as to the role of astrocytes in mediating SD propagation. Second, propagation of SD wave is independent of action potentials, even though both the preceding population spikes and the depolarization itself rely on Na^+ conductance (Somjen, 2002). Third, activation of NMDA receptors is known to be a key step in SD progression, and glutamate is thought to be the key mediator of SD propagation (Lauritzen, 1994). However, the source of glutamate release still remains unknown. Finally, mitochondria exhibit enhanced activities during SD, and mitochondrial exchangers can be activated under pathological conditions causing transmitter release (Bahar et al., 2000; Garcia-Chacon et al., 2006). Nevertheless, it is still unclear how mitochondria contribute to SD.

These previous studies raise the questions of **what cell type and what cellular mechanisms mediate the propagation of SD**. We hypothesize that **neuronal signaling pathways involving glutamate and NMDA receptors are responsible for SD propagation**. Specifically, in chapter 2 we investigate the hypothesis that **neurons play a leading role in the pathophysiological responses during SD, while astrocytes merely respond passively to the elevated $[K^+]_o$ that accompanies SD**. In chapter 3, we test the hypothesis that **SD is mediated by a novel pathway**

of regenerative glutamate released that is different from classical synaptic transmission but instead is dependent upon NMDA receptors.

Objectives :

Aim 1. Examine specific pathophysiological responses of brain cells to SD in brain slices. SD is known to induce various phathophysiological events, such as cell swelling, tissue acidosis and energy metabolism changes, which may be responsible for the early or prolonged cellular damage following ischemic or traumatic stimuli. However, direct observations of these changes at single cell level are still lacking. We will test intracellular changes of cellular volume, intracellular pH and mitochondrial membrane potentials during SD by two-photon fluorescent imaging and electrophysiological methods.

Aim 2. Examine specific roles of neurons versus astrocytes in the SD-associated cellular responses. It has long been a discussion whether neurons or astrocytes play the leading role in mediating SD progression. Moreover, it is not clear how the two types of cells contribute to the SD-induced pathophysiology changes specifically. We will monitor changes of cellular swelling, pH and mitochondrial signaling in individual neurons and astrocytes in order to compare their contribution to SD.

Aim 3. Test whether glutamate is released during SD and whether the release is dependent upon action potential and VGCC-triggered vesicular exocytosis. It is believed that the

release and diffusion of glutamate mediate the propagation of SD. Interestingly, however, the propagation of SD is not affected by inhibition of either Na^+ or Ca^{2+} currents. We will test whether glutamate is released during SD under the condition of blocking both action potentials and Ca^{2+} influx from presynaptic Ca^{2+} channels and, if yes, whether glutamate is released via vesicular exocytosis.

Aim 4. Determine the mechanism of glutamate release during SD. Previous studies have shown that propagation of SD requires activation of NMDA receptors. Recent findings have suggested that NMDA receptors are expressed at presynaptic sites and can facilitate neurotransmitter release. The occurrence of SD in zero-calcium extracellular solutions suggests that Na^+ influx via NMDA receptors may play an important role in SD under this condition. Therefore, we will test the possibility that regenerative glutamate release during SD depends upon the activation of presynaptic NMDA receptors, and the action of mitochondrial Na^+/Ca^{2+} exchanger is an important step in this process.

Significance:

This work is expected to clarify the cellular mechanisms underlying the propagation of SD and the contribution of neurons versus astrocytes to SD. The proposed experiments will help us understand more about how SD is generated and how SD contributes to the related neuronal disorders. This study will also shed light towards future therapeutic targets for alleviating SD-associated complex disorders such as migraine, ischemia and brain trauma.

1.7. References

Aitken PG, Balestrino M, Somjen GG (1988) NMDA antagonists: lack of protective effect against hypoxic damage in CA1 region of hippocampal slices. Neurosci Lett 89:187-192.

Aitken PG, Jing J, Young J, Somjen GG (1991) Ion channel involvement in hypoxia-induced spreading depression in hippocampal slices. Brain Research 541:7-11.

Aitken PG, Tombaugh GC, Turner DA, Somjen GG (1998) Similar propagation of SD and hypoxic SD-like depolarization in rat hippocampus recorded optically and electrically. Journal of Neurophysiology 80:1514-1521.

Aitken PG, Fayuk D, Somjen GG, Turner DA (1999) Use of intrinsic optical signals to monitor physiological changes in brain tissue slices. Methods 18:91-103.

Amemori T, Gorelova NA, Bures J (1987) Spreading depression in the olfactory bulb of rats: reliable initiation and boundaries of propagation. Neuroscience 22:29-36.

Andersen AR, Friberg L, Olsen TS, Olesen J (1988) Delayed hyperemia following hypoperfusion in classic migraine. Single photon emission computed tomographic demonstration. Arch Neurol 45:154-159.

Anderson TR, Andrew RD (2002) Spreading depression: imaging and blockade in the rat neocortical brain slice. Journal of Neurophysiology 88:2713-2725.

Andrew RD, MacVicar BA (1994) Imaging cell volume changes and neuronal excitation in the hippocampal slice. Neuroscience 62:371-383.

Avoli M, Drapeau C, Louvel J, Pumain R, Olivier A, Villemure JG (1991) Epileptiform activity induced by low extracellular magnesium in the human cortex maintained in vitro. Ann Neurol 30:589-596.

Ayata C, Shin HK, Salomone S, Ozdemir-Gursoy Y, Boas DA, Dunn AK, Moskowitz MA (2004) Pronounced hypoperfusion during spreading depression in mouse cortex. J Cereb Blood Flow Metab 24:1172-1182.

Ba AM, Guiou M, Pouratian N, Muthialu A, Rex DE, Cannestra AF, Chen JW, Toga AW (2002) Multiwavelength optical intrinsic signal imaging of cortical spreading depression. Journal of Neurophysiology 88:2726-2735.

Back T, Ginsberg MD, Dietrich WD, Watson BD (1996) Induction of spreading depression in the ischemic hemisphere following experimental middle cerebral artery occlusion: effect on infarct morphology. J Cereb Blood Flow Metab 16:202-213.

Bahar S, Fayuk D, Somjen GG, Aitken PG, Turner DA (2000) Mitochondrial and intrinsic optical signals imaged during hypoxia and spreading depression in rat hippocampal slices. Journal of Neurophysiology 84:311-324.

Balestrino M, Somjen GG (1986) Chlorpromazine protects brain tissue in hypoxia by delaying spreading depression-mediated calcium influx. Brain Research 385:219-226.

Balestrino M, Aitken PG, Somjen GG (1989) Spreading depression-like hypoxic depolarization in CA1 and fascia dentata of hippocampal slices: relationship to selective vulnerability. Brain Research 497:102-107.

Balestrino M, Young J, Aitken P (1999) Block of (Na+,K+)ATPase with ouabain induces spreading depression-like depolarization in hippocampal slices. Brain Research 838:37-44.

Basarsky TA, Feighan D, MacVicar BA (1999) Glutamate release through volume-activated channels during spreading depression. J Neurosci 19:6439-6445.

Basarsky TA, Duffy SN, Andrew RD, MacVicar BA (1998) Imaging spreading depression and associated intracellular calcium waves in brain slices. J Neurosci 18:7189-7199.

Basser LS (1969) The relation of migraine and epilepsy. Brain 92:285-300.

Bassi MT, Bresolin N, Tonelli A, Nazos K, Crippa F, Baschirotto C, Zucca C, Bersano A, Dolcetta D, Boneschi FM, Barone V, Casari G (2004) A novel mutation in the ATP1A2 gene causes alternating hemiplegia of childhood. J Med Genet 41:621-628.

Bowyer SM, Aurora KS, Moran JE, Tepley N, Welch KM (2001) Magnetoencephalographic fields from patients with spontaneous and induced migraine aura. Ann Neurol 50:582-587.

Brennan KC, Beltran-Parrazal L, Lopez-Valdes HE, Theriot J, Toga AW, Charles AC (2007) Distinct vascular conduction with cortical spreading depression. Journal of Neurophysiology 97:4143-4151.

Buchheim K, Weissinger F, Siegmund H, Holtkamp M, Schuchmann S, Meierkord H (2002) Intrinsic optical imaging reveals regionally different manifestation of spreading depression in hippocampal and entorhinal structures in vitro. Exp Neurol 175:76-86.

Bures J, Buresova O, Janebova M (1968) The effect of spreading depression in the thalamus, corpus striatum and hippocampus on the activity of a chemically induced focus of paroxysmal activity in the rat cerebral cortex. Physiol Bohemoslov 17:533-540.

Busch E, Gyngell ML, Eis M, Hoehn-Berlage M, Hossmann KA (1996) Potassium-induced cortical spreading depressions during focal cerebral ischemia in rats: contribution to lesion growth assessed by diffusion-weighted NMR and biochemical imaging. J Cereb Blood Flow Metab 16:1090-1099.

Cannestra AF, Blood AJ, Black KL, Toga AW (1996) The evolution of optical signals in human and rodent cortex. Neuroimage 3:202-208.

Cao Y, Welch KM, Aurora S, Vikingstad EM (1999) Functional MRI-BOLD of visually triggered headache in patients with migraine. Arch Neurol 56:548-554.

Capendeguy O, Horisberger JD (2004) Functional effects of Na+,K+-ATPase gene mutations linked to familial hemiplegic migraine. Neuromolecular Med 6:105-116.

Case GR, Lavond DG, Thompson RF (2002) Cortical spreading depression and involvement of the motor cortex, auditory cortex, and cerebellum in eyeblink classical conditioning of the rabbit. Neurobiol Learn Mem 78:234-245.

Chen Q, Chopp M, Bodzin G, Chen H (1993) Temperature modulation of cerebral depolarization during focal cerebral ischemia in rats: correlation with ischemic injury. J Cereb Blood Flow Metab 13:389-394.

Chesler M (2003) Regulation and modulation of pH in the brain. Physiol Rev 83:1183-1221.

Chesler M, Kraig RP (1989) Intracellular pH transients of mammalian astrocytes. J Neurosci 9:2011-2019.

Chuquet J, Hollender L, Nimchinsky EA (2007) High-resolution in vivo imaging of the neurovascular unit during spreading depression. J Neurosci 27:4036-4044.

Collewijn H, Harreveld AV (1966) Membrane potential of cerebral cortical cells during spreading depression and asyxia. Exp Neurol 15:425-436.

Cornell-Bell AH, Finkbeiner SM, Cooper MS, Smith SJ (1990) Glutamate induces calcium waves in cultured astrocytes: long-range glial signaling. Science 247:470-473.

Cruz NF, Adachi K, Dienel GA (1999) Rapid efflux of lactate from cerebral cortex during K^+-induced spreading cortical depression. J Cereb Blood Flow Metab 19:380-392.

Cutrer FM, Sorensen AG, Weisskoff RM, Ostergaard L, Sanchez del Rio M, Lee EJ, Rosen BR, Moskowitz MA (1998) Perfusion-weighted imaging defects during spontaneous migrainous aura. Ann Neurol 43:25-31.

Czeh G, Aitken PG, Somjen GG (1992) Whole-cell membrane current and membrane resistance during hypoxic spreading depression. NeuroReport 3:197-200.

Czeh G, Aitken PG, Somjen GG (1993) Membrane currents in CA1 pyramidal cells during spreading depression (SD) and SD-like hypoxic depolarization. Brain Research 632:195-208.

De Fusco M, Marconi R, Silvestri L, Atorino L, Rampoldi L, Morgante L, Ballabio A, Aridon P, Casari G (2003) Haploinsufficiency of ATP1A2 encoding the Na+/K+ pump alpha2 subunit associated with familial hemiplegic migraine type 2. Nat Genet 33:192-196.

de Vries B, Frants RR, Ferrari MD, van den Maagdenberg AM (2009) Molecular genetics of migraine. Hum Genet 126:115-132.

Decoursey TE (2003) Voltage-gated proton channels and other proton transfer pathways. Physiol Rev 83:475-579.

Dichgans M, Freilinger T, Eckstein G, Babini E, Lorenz-Depiereux B, Biskup S, Ferrari MD, Herzog J, van den Maagdenberg AM, Pusch M, Strom TM (2005) Mutation in the neuronal voltage-gated sodium channel SCN1A in familial hemiplegic migraine. Lancet 366:371-377.

Dietz RM, Weiss JH, Shuttleworth CW (2008) Zn^{2+} influx is critical for some forms of spreading depression in brain slices. J Neurosci 28:8014-8024.

Dijkhuizen RM, Beekwilder JP, van der Worp HB, Berkelbach van der Sprenkel JW, Tulleken KA, Nicolay K (1999) Correlation between tissue depolarizations and damage in focal ischemic rat brain. Brain Research 840:194-205.

do Carmo RJ, Martins-Ferreira H (1984) Spreading depression of Leão probed with ion-selective microelectrodes in isolated chick retina. An Acad Bras Cienc 56:401-421.

Dreier JP, Kleeberg J, Alam M, Major S, Kohl-Bareis M, Petzold GC, Victorov I, Dirnagl U, Obrenovitch TP, Priller J (2007) Endothelin-1-induced spreading depression in rats is associated with a microarea of selective neuronal necrosis. Exp Biol Med (Maywood) 232:204-213.

Dreier JP, Korner K, Ebert N, Gorner A, Rubin I, Back T, Lindauer U, Wolf T, Villringer A, Einhaupl KM, Lauritzen M, Dirnagl U (1998) Nitric oxide scavenging by hemoglobin or nitric oxide synthase inhibition by N-nitro-L-arginine induces cortical spreading ischemia when K^+ is increased in the subarachnoid space. J Cereb Blood Flow Metab 18:978-990.

Dreier JP, Woitzik J, Fabricius M, Bhatia R, Major S, Drenckhahn C, Lehmann TN, Sarrafzadeh A, Willumsen L, Hartings JA, Sakowitz OW, Seemann JH, Thieme A, Lauritzen M, Strong AJ (2006) Delayed ischaemic neurological deficits after subarachnoid haemorrhage are associated with clusters of spreading depolarizations. Brain 129:3224-3237.

Dreier JP, Major S, Manning A, Woitzik J, Drenckhahn C, Steinbrink J, Tolias C, Oliveira-Ferreira AI, Fabricius M, Hartings JA, Vajkoczy P, Lauritzen M, Dirnagl U, Bohner G, Strong AJ (2009) Cortical spreading ischaemia is a novel process involved in ischaemic damage in patients with aneurysmal subarachnoid haemorrhage. Brain 132:1866-1881.

Duckrow RB (1991) Regional cerebral blood flow during spreading cortical depression in conscious rats. J Cereb Blood Flow Metab 11:150-154.

Eikermann-Haerter K, Baum MJ, Ferrari MD, van den Maagdenberg AM, Moskowitz MA, Ayata C (2009a) Androgenic suppression of spreading depression in familial hemiplegic migraine type 1 mutant mice. Ann Neurol 66:564-568.

Eikermann-Haerter K, Dilekoz E, Kudo C, Savitz SI, Waeber C, Baum MJ, Ferrari MD, van den Maagdenberg AM, Moskowitz MA, Ayata C (2009b) Genetic and hormonal factors modulate spreading depression and transient hemiparesis in mouse models of familial hemiplegic migraine type 1. J Clin Invest 119:99-109.

Fabricius M, Lauritzen M (1993) Transient hyperemia succeeds oligemia in the wake of cortical spreading depression. Brain Research 602:350-353.

Fabricius M, Lauritzen M (1996) Laser-Doppler evaluation of rat brain microcirculation: comparison with the [14C]-iodoantipyrine method suggests discordance during cerebral blood flow increases. J Cereb Blood Flow Metab 16:156-161.

Fabricius M, Jensen LH, Lauritzen M (1993) Microdialysis of interstitial amino acids during spreading depression and anoxic depolarization in rat neocortex. Brain Research 612:61-69.

Fabricius M, Akgoren N, Lauritzen M (1995) Arginine-nitric oxide pathway and cerebrovascular regulation in cortical spreading depression. Am J Physiol 269:H23-29.

Fabricius M, Fuhr S, Bhatia R, Boutelle M, Hashemi P, Strong AJ, Lauritzen M (2006) Cortical spreading depression and peri-infarct depolarization in acutely injured human cerebral cortex. Brain 129:778-790.

Faria LC, Mody I (2004) Protective effect of ifenprodil against spreading depression in the mouse entorhinal cortex. Journal of Neurophysiology 92:2610-2614.

Fayuk D, Aitken PG, Somjen GG, Turner DA (2002) Two different mechanisms underlie reversible, intrinsic optical signals in rat hippocampal slices. Journal of Neurophysiology 87:1924-1937.

Fifkova E, Bures J, Koshtoyants OK, Krivanek J, Weiss T (1961) Leão's spreading depression in the cerebellum of rat. Experientia 17:572-573.

Finkbeiner S (1992) Calcium waves in astrocytes-filling in the gaps. Neuron 8:1101-1108.

Footitt DR, Newberry NR (1998) Cortical spreading depression induces an LTP-like effect in rat neocortex in vitro. Brain Research 781:339-342.

Friberg L, Olsen TS, Roland PE, Lassen NA (1987) Focal ischaemia caused by instability of cerebrovascular tone during attacks of hemiplegic migraine. A regional cerebral blood flow study. Brain 110 (Pt 4):917-934.

Frostig RD, Lieke EE, Ts'o DY, Grinvald A (1990) Cortical functional architecture and local coupling between neuronal activity and the microcirculation revealed by in vivo high-resolution optical imaging of intrinsic signals. Proceedings of the National Academy of Sciences of the United States of America 87:6082-6086.

Garcia-Chacon LE, Nguyen KT, David G, Barrett EF (2006) Extrusion of Ca^{2+} from mouse motor terminal mitochondria via a Na^{+}-Ca^{2+} exchanger increases post-tetanic evoked release. J Physiol 574:663-675.

Gault LM, Lin CW, LaManna JC, Lust WD (1994) Changes in energy metabolites, cGMP and intracellular pH during cortical spreading depression. Brain Research 641:176-180.

Gido G, Katsura K, Kristian T, Siesjo BK (1993) Influence of plasma glucose concentration on rat brain extracellular calcium transients during spreading depression. J Cereb Blood Flow Metab 13:179-182.

Gill R, Andine P, Hillered L, Persson L, Hagberg H (1992) The effect of MK-801 on cortical spreading depression in the penumbral zone following focal ischaemia in the rat. J Cereb Blood Flow Metab 12:371-379.

Gjedde A, Hansen AJ, Quistorff B (1981) Blood-brain glucose transfer in spreading depression. Journal of Neurochemistry 37:807-812.

Goadsby PJ (2007) Recent advances in understanding migraine mechanisms, molecules and therapeutics. Trends Mol Med 13:39-44.

Goadsby PJ, Adner M, Edvinsson L (1996) Characterization of endothelin receptors in the cerebral vasculature and their lack of effect on spreading depression. J Cereb Blood Flow Metab 16:698-704.

Goadsby PJ, Lipton RB, Ferrari MD (2002) Migraine--current understanding and treatment. N Engl J Med 346:257-270.

Gorelova NA, Koroleva VI, Amemori T, Pavlik V, Bures J (1987) Ketamine blockade of cortical spreading depression in rats. Electroencephalography and Clinical Neurophysiology 66:440-447.

Gorji A, Zahn PK, Pogatzki EM, Speckmann EJ (2004) Spinal and cortical spreading depression enhance spinal cord activity. Neurobiol Dis 15:70-79.

Gouras P (1958) Spreading depression of activity in amphibian retina. Am J Physiol 195:28-32.

Grafstein B (1956) Mechanism of spreading cortical depression. Journal of Neurophysiology 19:154-171.

Guedes RC, Tsurudome K, Matsumoto N (2005) Spreading depression in vivo potentiates electrically-driven responses in frog optic tectum. Brain Research 1036:109-114.

Hablitz JJ, Heinemann U (1989) Alterations in the microenvironment during spreading depression associated with epileptiform activity in the immature neocortex. Brain Res Dev Brain Res 46:243-252.

Hachinski VC, Olesen J, Norris JW, Larsen B, Enevoldsen E, Lassen NA (1977) Cerebral hemodynamics in migraine. Can J Neurol Sci 4:245-249.

Hadjikhani N, Sanchez Del Rio M, Wu O, Schwartz D, Bakker D, Fischl B, Kwong KK, Cutrer FM, Rosen BR, Tootell RB, Sorensen AG, Moskowitz MA (2001) Mechanisms of migraine aura revealed by functional MRI in human visual cortex. Proceedings of the National Academy of Sciences of the United States of America 98:4687-4692.

Hans M, Luvisetto S, Williams ME, Spagnolo M, Urrutia A, Tottene A, Brust PF, Johnson EC, Harpold MM, Stauderman KA, Pietrobon D (1999) Functional consequences of mutations in the human alpha1A calcium channel subunit linked to familial hemiplegic migraine. J Neurosci 19:1610-1619.

Hansen AJ (1985) Effect of anoxia on ion distribution in the brain. Physiol Rev 65:101-148.

Hansen AJ, Olsen CE (1980) Brain extracellular space during spreading depression and ischemia. Acta physiologica Scandinavica 108:355-365.

Hansen AJ, Zeuthen T (1981) Extracellular ion concentrations during spreading depression and ischemia in the rat brain cortex. Acta physiologica Scandinavica 113:437-445.

Hansen AJ, Lauritzen M (1984) The role of spreading depression in acute brain disorders. An Acad Bras Cienc 56:457-479.

Hashemi P, Bhatia R, Nakamura H, Dreier JP, Graf R, Strong AJ, Boutelle MG (2009) Persisting depletion of brain glucose following cortical spreading depression, despite apparent hyperaemia: evidence for risk of an adverse effect of Leão's spreading depression. J Cereb Blood Flow Metab 29:166-175.

Hassinger TD, Atkinson PB, Strecker GJ, Whalen LR, Dudek FE, Kossel AH, Kater SB (1995) Evidence for glutamate-mediated activation of hippocampal neurons by glial calcium waves. Journal of Neurobiology 28:159-170.

Hernandez-Caceres J, Macias-Gonzalez R, Brozek G, Bures J (1987) Systemic ketamine blocks cortical spreading depression but does not delay the onset of terminal anoxic depolarization in rats. Brain Research 437:360-364.

Herreras O (2005) Electrical prodromals of spreading depression void Grafstein's potassium hypothesis. Journal of Neurophysiology 94:3656; author reply 3656-3657.

Herreras O, Somjen GG (1993a) Propagation of spreading depression among dendrites and somata of the same cell population. Brain Research 610:276-282.

Herreras O, Somjen GG (1993b) Analysis of potential shifts associated with recurrent spreading depression and prolonged unstable spreading depression induced by microdialysis of elevated K+ in hippocampus of anesthetized rats. Brain Research 610:283-294.

Herreras O, Largo C, Ibarz JM, Somjen GG, Martin del Rio R (1994) Role of neuronal synchronizing mechanisms in the propagation of spreading depression in the in vivo hippocampus. J Neurosci 14:7087-7098.

Hershkowitz N, Katchman AN, Veregge S (1993) Site of synaptic depression during hypoxia: a patch-clamp analysis. Journal of Neurophysiology 69:432-441.

Holthoff K, Witte OW (1996) Intrinsic optical signals in rat neocortical slices measured with near-infrared dark-field microscopy reveal changes in extracellular space. J Neurosci 16:2740-2749.

Hossmann KA (1996) Periinfarct depolarizations. Cerebrovasc Brain Metab Rev 8:195-208.

Hua X, Malarkey EB, Sunjara V, Rosenwald SE, Li WH, Parpura V (2004) Ca^{2+}-dependent glutamate release involves two classes of endoplasmic reticulum Ca^{2+} stores in astrocytes. J Neurosci Res 76:86-97.

Iijima T, Mies G, Hossmann KA (1992) Repeated negative DC deflections in rat cortex following middle cerebral artery occlusion are abolished by MK-801: effect on volume of ischemic injury. J Cereb Blood Flow Metab 12:727-733.

Iijima T, Shimase C, Iwao Y, Sankawa H (1998) Relationships between glutamate release, blood flow and spreading depression: real-time monitoring using an electroenzymatic dialysis electrode. Neurosci Res 32:201-207.

Jarvis CR, Lilge L, Vipond GJ, Andrew RD (1999) Interpretation of intrinsic optical signals and calcein fluorescence during acute excitotoxic insult in the hippocampal slice. Neuroimage 10:357-372.

Jing J, Aitken PG, Somjen GG (1993) Role of calcium channels in spreading depression in rat hippocampal slices. Brain Research 604:251-259.

Jing J, Aitken PG, Somjen GG (1994) Interstitial volume changes during spreading depression (SD) and SD-like hypoxic depolarization in hippocampal tissue slices. Journal of Neurophysiology 71:2548-2551.

Kahlig KM, Rhodes TH, Pusch M, Freilinger T, Pereira-Monteiro JM, Ferrari MD, van den Maagdenberg AM, Dichgans M, George AL, Jr. (2008) Divergent sodium channel defects in familial hemiplegic migraine. Proceedings of the National Academy of Sciences of the United States of America 105:9799-9804.

Katayama Y, Tamura T, Becker DP, Tsubokawa T (1992) Early cellular swelling during cerebral ischemia in vivo is mediated by excitatory amino acids released from nerve terminals. Brain Research 577:121-126.

Kaube H, Goadsby PJ (1994) Anti-migraine compounds fail to modulate the propagation of cortical spreading depression in the cat. Eur Neurol 34:30-35.

Kasischke KA, Vishwasrao HD, Fisher PJ, Zipfel WR, Webb WW (2004) Neural activity triggers neuronal oxidative metabolism followed by astrocytic glycolysis. Science 305:99-103.

Kempski O, Otsuka H, Seiwert T, Heimann A (2000) Spreading depression induces permanent cell swelling under penumbra conditions. Acta Neurochir Suppl 76:251-255.

Kleeberg J, Petzold GC, Major S, Dirnagl U, Dreier JP (2004) ET-1 induces cortical spreading depression via activation of the ETA receptor/phospholipase C pathway in vivo. Am J Physiol Heart Circ Physiol 286:H1339-1346.

Kocher M (1990) Metabolic and hemodynamic activation of postischemic rat brain by cortical spreading depression. J Cereb Blood Flow Metab 10:564-571.

Koenderink JB, Zifarelli G, Qiu LY, Schwarz W, De Pont JJ, Bamberg E, Friedrich T (2005) Na,K-ATPase mutations in familial hemiplegic migraine lead to functional inactivation. Biochim Biophys Acta 1669:61-68.

Korf J, Klein HC, Venema K, Postema F (1988) Increases in striatal and hippocampal impedance and extracellular levels of amino acids by cardiac arrest in freely moving rats. Journal of Neurochemistry 50:1087-1096.

Kors EE, Terwindt GM, Vermeulen FL, Fitzsimons RB, Jardine PE, Heywood P, Love S, van den Maagdenberg AM, Haan J, Frants RR, Ferrari MD (2001) Delayed cerebral edema and fatal coma after minor head trauma: role of the CACNA1A calcium channel subunit gene and relationship with familial hemiplegic migraine. Ann Neurol 49:753-760.

Kraig RP, Nicholson C (1978) Extracellular ionic variations during spreading depression. Neuroscience 3:1045-1059.

Kraig RP, Cooper AJ (1987) Bicarbonate and ammonia changes in brain during spreading depression. Can J Physiol Pharmacol 65:1099-1104.

Kraig RP, Ferreira-Filho CR, Nicholson C (1983) Alkaline and acid transients in cerebellar microenvironment. Journal of Neurophysiology 49:831-850.

Kral T, Luhmann HJ, Mittmann T, Heinemann U (1993) Role of NMDA receptors and voltage-activated calcium channels in an in vitro model of cerebral ischemia. Brain Research 612:278-288.

Krivanek J (1961) Some metabolic changes accompanying Leão's spreading cortical depression in the rat. Journal of Neurochemistry 6:183-189.

Kruger H, Heinemann U, Luhmann HJ (1999) Effects of ionotropic glutamate receptor blockade and 5-HT1A receptor activation on spreading depression in rat neocortical slices. NeuroReport 10:2651-2656.

Kunkler PE, Kraig RP (1998) Calcium waves precede electrophysiological changes of spreading depression in hippocampal organ cultures. J Neurosci 18:3416-3425.

Kunkler PE, Kraig RP (2004) P/Q Ca^{2+} channel blockade stops spreading depression and related pyramidal neuronal Ca^{2+} rise in hippocampal organ culture. Hippocampus 14:356-367.

Kunkler PE, Hulse RE, Schmitt MW, Nicholson C, Kraig RP (2005) Optical current source density analysis in hippocampal organotypic culture shows that spreading depression occurs with uniquely reversing currents. J Neurosci 25:3952-3961.

Lacombe P, Sercombe R, Correze JL, Springhetti V, Seylaz J (1992) Spreading depression induces prolonged reduction of cortical blood flow reactivity in the rat. Exp Neurol 117:278-286.

Largo C, Ibarz JM, Herreras O (1997a) Effects of the gliotoxin fluorocitrate on spreading depression and glial membrane potential in rat brain in situ. Journal of Neurophysiology 78:295-307.

Largo C, Tombaugh GC, Aitken PG, Herreras O, Somjen GG (1997b) Heptanol but not fluoroacetate prevents the propagation of spreading depression in rat hippocampal slices. Journal of Neurophysiology 77:9-16.

Larrosa B, Pastor J, Lopez-Aguado L, Herreras O (2006) A role for glutamate and glia in the fast network oscillations preceding spreading depression. Neuroscience 141:1057-1068.

Lashley KS (1941) Patterns of cerebral integration indicated by the scotoma of migraine. Archives of Neurology and Psychiatry 42:259-264.

Lauritzen M (1984) Long-lasting reduction of cortical blood flow of the brain after spreading depression with preserved autoregulation and impaired CO2 response. J Cereb Blood Flow Metab 4:546-554.

Lauritzen M (1994) Pathophysiology of the migraine aura. The spreading depression theory. Brain 117 (Pt 1):199-210.

Lauritzen M (2001) Cortical spreading depression in migraine. Cephalalgia 21:757-760.

Lauritzen M, Olesen J (1984) Regional cerebral blood flow during migraine attacks by Xenon-133 inhalation and emission tomography. Brain 107 (Pt 2):447-461.

Lauritzen M, Hansen AJ (1992) The effect of glutamate receptor blockade on anoxic depolarization and cortical spreading depression. J Cereb Blood Flow Metab 12:223-229.

Lauritzen M, Fabricius M (1995) Real time laser-Doppler perfusion imaging of cortical spreading depression in rat neocortex. NeuroReport 6:1271-1273.

Lauritzen M, Skyhoj Olsen T, Lassen NA, Paulson OB (1983a) Changes in regional cerebral blood flow during the course of classic migraine attacks. Ann Neurol 13:633-641.

Lauritzen M, Olsen TS, Lassen NA, Paulson OB (1983b) Regulation of regional cerebral blood flow during and between migraine attacks. Ann Neurol 14:569-572.

Lauritzen M, Rice ME, Okada Y, Nicholson C (1988) Quisqualate, kainate and NMDA can initiate spreading depression in the turtle cerebellum. Brain Research 475:317-327.

Lauritzen M, Hansen AJ, Kronborg D, Wieloch T (1990) Cortical spreading depression is associated with arachidonic acid accumulation and preservation of energy charge. J Cereb Blood Flow Metab 10:115-122.

Lauritzen M, Jorgensen MB, Diemer NH, Gjedde A, Hansen AJ (1982) Persistent oligemia of rat cerebral cortex in the wake of spreading depression. Ann Neurol 12:469-474.

Leão AAP (1944a) Pial circulation and spreading depression of activity in the cerebral cortex. Journal of Neurophysiology 7:391-396.

Leão AAP (1944b) Spreading depression of activity in the cerebral cortex. Journal of Neurophysiology 7:357-390.

Leão AAP (1945) Propagation of spreading cortical depression. Journal of Neurophysiology 8:33-45.

Leão AAP (1947) Further observations on the spreading depression of activity in the cerebral cortex. Journal of Neurophysiology 10:409-414.

Leão AAP (1987) On the inferred relationship of migraine and spreading depression. London: John Libbey & Co.

Lenti L, Domoki F, Gaspar T, Snipes JA, Bari F, Busija DW (2009) N-Methyl-D-Aspartate Induces Cortical Hyperemia through Cortical Spreading Depression-Dependent and -Independent Mechanisms in Rats. Microcirculation:1-11.

Lieke EE, Frostig RD, Arieli A, Ts'o DY, Hildesheim R, Grinvald A (1989) Optical imaging of cortical activity: real-time imaging using extrinsic dye-signals and high resolution imaging based on slow intrinsic-signals. Annu Rev Physiol 51:543-559.

Lipton P (1999) Ischemic cell death in brain neurons. Physiol Rev 79:1431-1568.

Lothman E, Lamanna J, Cordingley G, Rosenthal M, Somjen G (1975) Responses of electrical potential, potassium levels, and oxidative metabolic activity of the cerebral neocortex of cats. Brain Research 88:15-36.

Luhmann HJ, Heinemann U (1992) Hypoxia-induced functional alterations in adult rat neocortex. Journal of Neurophysiology 67:798-811.

Lundbaek JA, Hansen AJ (1992) Brain interstitial volume fraction and tortuosity in anoxia. Evaluation of the ion-selective micro-electrode method. Acta Physiologica Scandinavica 146:473-484.

MacGregor EA (2004) Oestrogen and attacks of migraine with and without aura. Lancet Neurol 3:354-361.

Margineanu DG, Klitgaard H (2006) The connexin 36 blockers quinine, quinidine and mefloquine inhibit cortical spreading depression in a rat neocortical slice model in vitro. Brain Res Bull 71:23-28.

Marrannes R, Willems R, De Prins E, Wauquier A (1988) Evidence for a role of the N-methyl-D-aspartate (NMDA) receptor in cortical spreading depression in the rat. Brain Research 457:226-240.

Martins-Ferreira H, de Castro GO (1966) Light-scattering changes accompanying spreading depression in isolated retina. Journal of Neurophysiology 29:715-726.

Martins-Ferreira H, Ribeiro LJ (1995) Biphasic effects of gap junctional uncoupling agents on the propagation of retinal spreading depression. Brazilian Journal of Medical and Biological Research.

Martins-Ferreira H, Nedergaard M, Nicholson C (2000) Perspectives on spreading depression. Brain Res Brain Res Rev 32:215-234.

Martins-Ferreira H, De Oliveira Castro G, Struchiner CJ, Rodrigues PS (1974) Circling spreading depression in isolated chick retina. Journal of Neurophysiology 37:773-784.

Mathew NT, Hrastnik F, Meyer JS (1976) Regional cerebral blood flow in the diagnosis of vascular headache. Headache 15:252-260.

Mayevsky A, Weiss HR (1991) Cerebral blood flow and oxygen consumption in cortical spreading depression. J Cereb Blood Flow Metab 11:829-836.

Mazel T, Simonova Z, Sykova E (1998) Diffusion heterogeneity and anisotropy in rat hippocampus. NeuroReport 9:1299-1304.

Mazel T, Richter F, Vargova L, Sykova E (2002) Changes in extracellular space volume and geometry induced by cortical spreading depression in immature and adult rats. Physiol Res 51 Suppl 1:S85-93.

Melliti K, Grabner M, Seabrook GR (2003) The familial hemiplegic migraine mutation R192Q reduces G-protein-mediated inhibition of P/Q-type (Ca(V)2.1) calcium channels expressed in human embryonic kidney cells. J Physiol 546:337-347.

Menniti FS, Pagnozzi MJ, Butler P, Chenard BL, Jaw-Tsai SS, Frost White W (2000) CP-101,606, an NR2B subunit selective NMDA receptor antagonist, inhibits NMDA and injury induced c-fos expression and cortical spreading depression in rodents. Neuropharmacology 39:1147-1155.

Mies G, Paschen W (1984) Regional changes of blood flow, glucose, and ATP content determined on brain sections during a single passage of spreading depression in rat brain cortex. Exp Neurol 84:249-258.

Mies G, Iijima T, Hossmann KA (1993) Correlation between peri-infarct DC shifts and ischaemic neuronal damage in rat. NeuroReport 4:709-711.

Mies G, Kohno K, Hossmann KA (1994) Prevention of periinfarct direct current shifts with glutamate antagonist NBQX following occlusion of the middle cerebral artery in the rat. J Cereb Blood Flow Metab 14:802-807.

Milner PM (1958) Note on a possible correspondence between the scotomas of migraine and spreading depression of Leão. Electroencephalography and Clinical Neurophysiology 10:705.

Mody I, Lambert JD, Heinemann U (1987) Low extracellular magnesium induces epileptiform activity and spreading depression in rat hippocampal slices. Journal of Neurophysiology 57:869-888.

Monakhov KK, Fifkova E, Bures J (1962) Steady potential field of hippocampal spreading depression. J Cell Comp Physiol 59:155-161.

Mraovitch S, Calando Y, Goadsby PJ, Seylaz J (1992) Subcortical cerebral blood flow and metabolic changes elicited by cortical spreading depression in rat. Cephalalgia 12:137-141; discussion 127.

Muller M, Somjen GG (2000) Na^+ and K^+ concentrations, extra- and intracellular voltages, and the effect of TTX in hypoxic rat hippocampal slices. Journal of Neurophysiology 83:735-745.

Mullner C, Broos LA, van den Maagdenberg AM, Striessnig J (2004) Familial hemiplegic migraine type 1 mutations K1336E, W1684R, and V1696I alter Cav2.1 Ca2+ channel gating: evidence for beta-subunit isoform-specific effects. J Biol Chem 279:51844-51850.

Narayan SM, Santori EM, Blood AJ, Burton JS, Toga AW (1994) Imaging optical reflectance in rodent barrel and forelimb sensory cortex. Neuroimage 1:181-190.

Nedergaard M (1994) Direct signaling from astrocytes to neurons in cultures of mammalian brain cells. Science 263:1768-1771.

Nedergaard M, Hansen AJ (1988) Spreading depression is not associated with neuronal injury in the normal brain. Brain Research 449:395-398.

Nedergaard M, Hansen AJ (1993) Characterization of cortical depolarizations evoked in focal cerebral ischemia. J Cereb Blood Flow Metab 13:568-574.

Nedergaard M, Cooper AJ, Goldman SA (1995) Gap junctions are required for the propagation of spreading depression. Journal of Neurobiology 28:433-444.

Nellgard B, Wieloch T (1992) NMDA-receptor blockers but not NBQX, an AMPA-receptor antagonist, inhibit spreading depression in the rat brain. Acta Physiologica Scandinavica 146:497-503.

Nicholson C (1984) Comparative Neurophysiology of spreading depression in the cerebellum. An Acad Bras Cienc 56:481-494.

Nicholson C, Kraig RP (1975) Chloride and potassium changes measured during spreading depression in catfish cerebellum. Brain Research 96:384-389.

Nicholson C, Bruggencate GT, Steinberg R, Stockle H (1977) Calcium modulation in brain extracellular microenvironment demonstrated with ion-selective micropipette. Proceedings of the National Academy of Sciences of the United States of America 74:1287-1290.

Nilsson P, Hillered L, Olsson Y, Sheardown MJ, Hansen AJ (1993) Regional changes in interstitial K^+ and Ca^{2+} levels following cortical compression contusion trauma in rats. J Cereb Blood Flow Metab 13:183-192.

O'Brien MD (1971) Cerebral blood changes in migraine. Headache 10:139-143.

O'Farrell AM, Rex DE, Muthialu A, Pouratian N, Wong GK, Cannestra AF, Chen JW, Toga AW (2000) Characterization of optical intrinsic signals and blood volume during cortical spreading depression. NeuroReport 11:2121-2125.

Obeidat AS, Andrew RD (1998) Spreading depression determines acute cellular damage in the hippocampal slice during oxygen/glucose deprivation. Eur J Neurosci 10:3451-3461.

Obrenovitch TP, Zilkha E, Urenjak J (1996) Evidence against high extracellular glutamate promoting the elicitation of spreading depression by potassium. J Cereb Blood Flow Metab 16:923-931.

Olesen J, Larsen B, Lauritzen M (1981) Focal hyperemia followed by spreading oligemia and impaired activation of rCBF in classic migraine. Ann Neurol 9:344-352.

Olesen J, Friberg L, Olsen TS, Iversen HK, Lassen NA, Andersen AR, Karle A (1990) Timing and topography of cerebral blood flow, aura, and headache during migraine attacks. Ann Neurol 28:791-798.

Ophoff RA, Terwindt GM, Vergouwe MN, van Eijk R, Oefner PJ, Hoffman SM, Lamerdin JE, Mohrenweiser HW, Bulman DE, Ferrari M, Haan J, Lindhout D, van Ommen GJ, Hofker MH, Ferrari MD, Frants RR (1996) Familial hemiplegic migraine and episodic ataxia type-2 are caused by mutations in the Ca^{2+} channel gene CACNL1A4. Cell 87:543-552.

Parpura V, Basarsky TA, Liu F, Jeftinija K, Jeftinija S, Haydon PG (1994) Glutamate-mediated astrocyte-neuron signalling. Nature 369:744-747.

Peters O, Schipke CG, Hashimoto Y, Kettenmann H (2003) Different mechanisms promote astrocyte Ca^{2+} waves and spreading depression in the mouse neocortex. J Neurosci 23:9888-9896.

Phillips JM, Nicholson C (1979) Anion permeability in spreading depression investigated with ion-sensitive microelectrodes. Brain Research 173:567-571.

Pietrobon D, Striessnig J (2003) Neurobiology of migraine. Nat Rev Neurosci 4:386-398.

Piilgaard H, Lauritzen M (2009) Persistent increase in oxygen consumption and impaired neurovascular coupling after spreading depression in rat neocortex. J Cereb Blood Flow Metab 29:1517-1527.

Piper RD, Lambert GA, Duckworth JW (1991) Cortical blood flow changes during spreading depression in cats. Am J Physiol 261:H96-102.

Psarropoulou C, Avoli M (1992) CPP, an NMDA-receptor antagonist, blocks 4-aminopyridine-induced spreading depression episodes but not epileptiform activity in immature rat hippocampal slices. Neurosci Lett 135:139-143.

Psarropoulou C, Avoli M (1993) 4-Aminopyridine-induced spreading depression episodes in immature hippocampus: developmental and pharmacological characteristics. Neuroscience 55:57-68.

Ramadan NM, Schultz LL, Gilkey SJ (1997) Migraine prophylactic drugs: proof of efficacy, utilization and cost. Cephalalgia 17:73-80.

Rashidy-Pour A, Motaghed-Larijani Z, Bures J (1995) Tolerance to ketamine-induced blockade of cortical spreading depression transfers to MK-801 but not to AP5 in rats. Brain Research 693:64-69.

Rasmussen BK, Jensen R, Schroll M, Olesen J (1991) Epidemiology of headache in a general population--a prevalence study. J Clin Epidemiol 44:1147-1157.

Reuter U, Weber JR, Gold L, Arnold G, Wolf T, Dreier J, Lindauer U, Dirnagl U (1998) Perivascular nerves contribute to cortical spreading depression-associated hyperemia in rats. Am J Physiol 274:H1979-1987.

Rex A, Pfeifer L, Fink F, Fink H (1999) Cortical NADH during pharmacological manipulations of the respiratory chain and spreading depression in vivo. J Neurosci Res 57:359-370.

Reyes RC, Parpura V (2008) Mitochondria modulate Ca^{2+}-dependent glutamate release from rat cortical astrocytes. J Neurosci 28:9682-9691.

Richter F, Bauer R, Lehmenkuhler A, Schaible HG (2008) Spreading depression in the brainstem of the adult rat: electrophysiological parameters and influences on regional brainstem blood flow. J Cereb Blood Flow Metab 28:984-994.

Rosen AS, Morris ME (1993) Anoxic depression of excitatory and inhibitory postsynaptic potentials in rat neocortical slices. Journal of Neurophysiology 69:109-117.

Rosenthal M, Somjen G (1973) Spreading depression, sustained potential shifts, and metabolic activity of cerebral cortex of cats. Journal of Neurophysiology 36:739-749.

Rossi DJ, Oshima T, Attwell D (2000) Glutamate release in severe brain ischaemia is mainly by reversed uptake. Nature 403:316-321.

Sakai F, Meyer JS (1978) Regional cerebral hemodynamics during migraine and cluster headaches measured by the 133Xe inhalation method. Headache 18:122-132.

Scheller D, Kolb J, Tegtmeier F (1992a) Lactate and pH change in close correlation in the extracellular space of the rat brain during cortical spreading depression. Neurosci Lett 135:83-86.

Scheller D, Tegtmeier F, Schlue WR (1998) Dose-dependent effects of tetraethylammonium on circling spreading depressions in chicken retina. J Neurosci Res 51:85-89.

Scheller D, Kolb J, Tegtmeier F, Lehmenkuhler A (1992b) Extracellular changes of inorganic phosphate are different during spreading depression and global cerebral ischemia of rats. Neurosci Lett 141:269-272.

Segall L, Mezzetti A, Scanzano R, Gargus JJ, Purisima E, Blostein R (2005) Alterations in the alpha2 isoform of Na,K-ATPase associated with familial hemiplegic migraine type 2. Proceedings of the National Academy of Sciences of the United States of America 102:11106-11111.

Segall L, Scanzano R, Kaunisto MA, Wessman M, Palotie A, Gargus JJ, Blostein R (2004) Kinetic alterations due to a missense mutation in the Na,K-ATPase alpha2 subunit cause familial hemiplegic migraine type 2. J Biol Chem 279:43692-43696.

Selman WR, Lust WD, Pundik S, Zhou Y, Ratcheson RA (2004) Compromised metabolic recovery following spontaneous spreading depression in the penumbra. Brain Research 999:167-174.

Shibata M, Leffler CW, Busija DW (1990) Cerebral hemodynamics during cortical spreading depression in rabbits. Brain Research 530:267-274.

Shibata M, Leffler CW, Busija DW (1992) Pial arteriolar constriction following cortical spreading depression is mediated by prostanoids. Brain Research 572:190-197.

Shimazawa M, Hara H (1996) An experimental model of migraine with aura: cortical hypoperfusion following spreading depression in the awake and freely moving rat. Clin Exp Pharmacol Physiol 23:890-892.

Shimizu-Sasamata M, Bosque-Hamilton P, Huang PL, Moskowitz MA, Lo EH (1998) Attenuated neurotransmitter release and spreading depression-like depolarizations after focal ischemia in mutant mice with disrupted type I nitric oxide synthase gene. J Neurosci 18:9564-9571.

Shin HK, Dunn AK, Jones PB, Boas DA, Moskowitz MA, Ayata C (2006) Vasoconstrictive neurovascular coupling during focal ischemic depolarizations. J Cereb Blood Flow Metab 26:1018-1030.

Shinohara M, Dollinger B, Brown G, Rapoport S, Sokoloff L (1979) Cerebral glucose utilization: local changes during and after recovery from spreading cortical depression. Science 203:188-190.

Sick TJ, Solow EL, Roberts EL, Jr. (1987) Extracellular potassium ion activity and electrophysiology in the hippocampal slice: paradoxical recovery of synaptic transmission during anoxia. Brain Research 418:227-234.

Skinhoj E, Paulson OB (1969) Regional blood flow in internal carotid distribution during migraine attack. Br Med J 3:569-570.

Smith SE, Chesler M (1999) Effect of divalent cations on AMPA-evoked extracellular alkaline shifts in rat hippocampal slices. Journal of Neurophysiology 82:1902-1908.

Snow RW, Taylor CP, Dudek FE (1983) Electrophysiological and optical changes in slices of rat hippocampus during spreading depression. Journal of Neurophysiology 50:561-572.

Somjen GG (1984) Acidification of interstitial fluid in hippocampal formation caused by seizures and by spreading depression. Brain Research 311:186-188.

Somjen GG (2001) Mechanisms of spreading depression and hypoxic spreading depression-like depolarization. Physiol Rev 81:1065-1096.

Somjen GG (2002) Ion regulation in the brain: implications for pathophysiology. Neuroscientist 8:254-267.

Sonn J, Mayevsky A (2000) Effects of brain oxygenation on metabolic, hemodynamic, ionic and electrical responses to spreading depression in the rat. Brain Research 882:212-216.

Sonn J, Mayevsky A (2006) Effects of anesthesia on the responses to cortical spreading depression in the rat brain in vivo. Neurol Res 28:206-219.

Strong AJ, Venables GS, Gibson G (1983) The cortical ischaemic penumbra associated with occlusion of the middle cerebral artery in the cat: 1. Topography of changes in blood flow, potassium ion activity, and EEG. J Cereb Blood Flow Metab 3:86-96.

Strong AJ, Fabricius M, Boutelle MG, Hibbins SJ, Hopwood SE, Jones R, Parkin MC, Lauritzen M (2002) Spreading and synchronous depressions of cortical activity in acutely injured human brain. Stroke 33:2738-2743.

Strong AJ, Smith SE, Whittington DJ, Meldrum BS, Parsons AA, Krupinski J, Hunter AJ, Patel S, Robertson C (2000) Factors influencing the frequency of fluorescence transients as markers of peri-infarct depolarizations in focal cerebral ischemia. Stroke 31:214-222.

Strong AJ, Anderson PJ, Watts HR, Virley DJ, Lloyd A, Irving EA, Nagafuji T, Ninomiya M, Nakamura H, Dunn AK, Graf R (2007) Peri-infarct depolarizations lead to loss of perfusion in ischaemic gyrencephalic cerebral cortex. Brain 130:995-1008.

Sugaya E, Takato M, Noda Y (1975) Neuronal and glial activity during spreading depression in cerebral cortex of cat. Journal of Neurophysiology 38:822-841.

Sukhotinsky I, Dilekoz E, Moskowitz MA, Ayata C (2008) Hypoxia and hypotension transform the blood flow response to cortical spreading depression from hyperemia into hypoperfusion in the rat. J Cereb Blood Flow Metab 28:1369-1376.

Sykova E, Nicholson C (2008) Diffusion in brain extracellular space. Physiol Rev 88:1277-1340.

Sykova E, Mazel T, Simonova Z (1998) Diffusion constraints and neuron-glia interaction during aging. Exp Gerontol 33:837-851.

Takano T, Tian GF, Peng W, Lou N, Lovatt D, Hansen AJ, Kasischke KA, Nedergaard M (2007) Cortical spreading depression causes and coincides with tissue hypoxia. Nat Neurosci 10:754-762.

Tao L (2000) Light scattering in brain slices measured with a photon counting fiber optic system. J Neurosci Methods 101:19-29.

Tavraz NN, Friedrich T, Durr KL, Koenderink JB, Bamberg E, Freilinger T, Dichgans M (2008) Diverse functional consequences of mutations in the Na^+/K^+-ATPase alpha2-subunit causing familial hemiplegic migraine type 2. J Biol Chem 283:31097-31106.

Tavraz NN, Durr KL, Koenderink JB, Freilinger T, Bamberg E, Dichgans M, Friedrich T (2009) Impaired plasma membrane targeting or protein stability by certain ATP1A2 mutations identified in sporadic or familial hemiplegic migraine. Channels (Austin) 3:82-87.

Tfelt-Hansen PC (2009) History of migraine with aura and cortical spreading depression from 1941 and onwards. Cephalalgia doi:10.1111/j.1468-2982.2009.02015.x.

Theis M, Jauch R, Zhuo L, Speidel D, Wallraff A, Doring B, Frisch C, Sohl G, Teubner B, Euwens C, Huston J, Steinhauser C, Messing A, Heinemann U, Willecke K (2003) Accelerated hippocampal spreading depression and enhanced locomotory activity in mice with astrocyte-directed inactivation of connexin43. J Neurosci 23:766-776.

Thompson RJ, Zhou N, MacVicar BA (2006) Ischemia opens neuronal gap junction hemichannels. Science 312:924-927.

Thomsen LL, Eriksen MK, Roemer SF, Andersen I, Olesen J, Russell MB (2002) A population-based study of familial hemiplegic migraine suggests revised diagnostic criteria. Brain 125:1379-1391.

Thomsen LL, Kirchmann M, Bjornsson A, Stefansson H, Jensen RM, Fasquel AC, Petursson H, Stefansson M, Frigge ML, Kong A, Gulcher J, Stefansson K, Olesen J (2007) The genetic spectrum of a population-based sample of familial hemiplegic migraine. Brain 130:346-356.

Tobiasz C, Nicholson C (1982) Tetrodotoxin resistant propagation and extracellular sodium changes during spreading depression in rat cerebellum. Brain Research 241:329-333.

Tong CK, Chesler M (1999) Endogenous pH shifts facilitate spreading depression by effect on NMDA receptors. Journal of Neurophysiology 81:1988-1991.

Tong CK, Chesler M (2000) Modulation of spreading depression by changes in extracellular pH. Journal of Neurophysiology 84:2449-2457.

Tottene A, Pivotto F, Fellin T, Cesetti T, van den Maagdenberg AM, Pietrobon D (2005) Specific kinetic alterations of human CaV2.1 calcium channels produced by mutation S218L causing familial hemiplegic migraine and delayed cerebral edema and coma after minor head trauma. J Biol Chem 280:17678-17686.

Tottene A, Fellin T, Pagnutti S, Luvisetto S, Striessnig J, Fletcher C, Pietrobon D (2002) Familial hemiplegic migraine mutations increase Ca^{2+} influx through single human CaV2.1 channels and decrease maximal CaV2.1 current density in neurons. Proceedings of the National Academy of Sciences of the United States of America 99:13284-13289.

Tottene A, Conti R, Fabbro A, Vecchia D, Shapovalova M, Santello M, van den Maagdenberg AM, Ferrari MD, Pietrobon D (2009) Enhanced excitatory transmission at cortical synapses as the basis for facilitated spreading depression in Ca(v)2.1 knockin migraine mice. Neuron 61:762-773.

Trachtenberg MC, Hull CD, Buchwald NA (1970) Electrophysiological concomitants of spreading depression in caudate and thalamic nuclei of the cat. Brain Research 20:219-231.

Traynelis SF, Cull-Candy SG (1990) Proton inhibition of N-methyl-D-aspartate receptors in cerebellar neurons. Nature 345:347-350.

Umegaki M, Sanada Y, Waerzeggers Y, Rosner G, Yoshimine T, Heiss WD, Graf R (2005) Peri-infarct depolarizations reveal penumbra-like conditions in striatum. J Neurosci 25:1387-1394.

Unger J (2006) Migraine headaches: a historical prospective, a glimpse into the future, and migraine epidemiology. Dis Mon 52:367-384.

van den Maagdenberg AM, Haan J, Terwindt GM, Ferrari MD (2007) Migraine: gene mutations and functional consequences. Curr Opin Neurol 20:299-305.

van den Maagdenberg AM, Pietrobon D, Pizzorusso T, Kaja S, Broos LA, Cesetti T, van de Ven RC, Tottene A, van der Kaa J, Plomp JJ, Frants RR, Ferrari MD (2004) A Cacna1a knockin migraine mouse model with increased susceptibility to cortical spreading depression. Neuron 41:701-710.

Van Harreveld A (1958) Changes in the diameter of apical dendrites during spreading depression. Am J Physiol 192:457-463.

Van Harreveld A (1959) Compounds in brain extracts causing spreading depression of cerebral cortical activity and contraction of crustacean muscle. Journal of Neurochemistry 3:300-315.

Van Harreveld A, Kooiman M (1965) Amino Acid Release from the Cerebral Cortex during Spreading Depression and Asphyxiation. Journal of Neurochemistry 12:431-439.

Van Harreveld A, Khattab FI (1967) Changes in cortical extracellular space during spreading depression investigated with the electron microscope. Journal of Neurophysiology 30:911-929.

Vanmolkot KR, Stroink H, Koenderink JB, Kors EE, van den Heuvel JJ, van den Boogerd EH, Stam AH, Haan J, De Vries BB, Terwindt GM, Frants RR, Ferrari MD, van den Maagdenberg AM (2006) Severe episodic neurological deficits and permanent mental retardation in a child with a novel FHM2 ATP1A2 mutation. Ann Neurol 59:310-314.

Vanmolkot KR, Babini E, de Vries B, Stam AH, Freilinger T, Terwindt GM, Norris L, Haan J, Frants RR, Ramadan NM, Ferrari MD, Pusch M, van den Maagdenberg AM, Dichgans M (2007) The novel p.L1649Q mutation in the SCN1A epilepsy gene is associated with familial hemiplegic migraine: genetic and functional studies. Mutation in brief #957. Online. Hum Mutat 28:522.

Vilagi I, Klapka N, Luhmann HJ (2001) Optical recording of spreading depression in rat neocortical slices. Brain Research 898:288-296.

Vyskocil F, Kritz N, Bures J (1972) Potassium-selective microelectrodes used for measuring the extracellular brain potassium during spreading depression and anoxic depolarization in rats. Brain Research 39:255-259.

Wadman WJ, Juta AJ, Kamphuis W, Somjen GG (1992) Current source density of sustained potential shifts associated with electrographic seizures and with spreading depression in rat hippocampus. Brain Research 570:85-91.

Wahl M, Lauritzen M, Schilling L (1987) Change of cerebrovascular reactivity after cortical spreading depression in cats and rats. Brain Research 411:72-80.

Warr O, Takahashi M, Attwell D (1999) Modulation of extracellular glutamate concentration in rat brain slices by cystine-glutamate exchange. J Physiol 514 (Pt 3):783-793.

Weiss T, Fifkova E (1963) The Effect of Neocortical and Caudatal Spreading Depression on "Circling Movements" Induced from the Caudate Nucleus. Physiol Bohemoslov 12:332-338.

Wessman M et al. (2002) A susceptibility locus for migraine with aura, on chromosome 4q24. Am J Hum Genet 70:652-662.

Wolf T, Lindauer U, Obrig H, Dreier J, Back T, Villringer A, Dirnagl U (1996) Systemic nitric oxide synthase inhibition does not affect brain oxygenation during cortical spreading depression in rats: a noninvasive near-infrared spectroscopy and laser-Doppler flowmetry study. J Cereb Blood Flow Metab 16:1100-1107.

Woods RP, Iacoboni M, Mazziotta JC (1994) Brief report: bilateral spreading cerebral hypoperfusion during spontaneous migraine headache. N Engl J Med 331:1689-1692.

Xie Y, Zacharias E, Hoff P, Tegtmeier F (1995) Ion channel involvement in anoxic depolarization induced by cardiac arrest in rat brain. J Cereb Blood Flow Metab 15:587-594.

Xie Y, Dengler K, Zacharias E, Wilffert B, Tegtmeier F (1994) Effects of the sodium channel blocker tetrodotoxin (TTX) on cellular ion homeostasis in rat brain subjected to complete ischemia. Brain Research 652:216-224.

Xiong ZQ, Stringer JL (2000) Extracellular pH responses in CA1 and the dentate gyrus during electrical stimulation, seizure discharges, and spreading depression. Journal of Neurophysiology 83:3519-3524.

Ye ZC, Wyeth MS, Baltan-Tekkok S, Ransom BR (2003) Functional hemichannels in astrocytes: a novel mechanism of glutamate release. J Neurosci 23:3588-3596.

Yokota C, Kuge Y, Hasegawa Y, Tagaya M, Abumiya T, Ejima N, Tamaki N, Yamaguchi T, Minematsu K (2002) Unique profile of spreading depression in a primate model. J Cereb Blood Flow Metab 22:835-842.

Yoon RS, Tsang PW, Lenz FA, Kwan HC (1996) Characterization of cortical spreading depression by imaging of intrinsic optical signals. NeuroReport 7:2671-2674.

Young JN, Somjen GG (1992) Suppression of presynaptic calcium currents by hypoxia in hippocampal tissue slices. Brain Research 573:70-76.

2. TRANSIENT SWELLING, ACIDIFICATION AND MITOCHONDIRAL DEPOLARIZATION OCCURS IN NEURONS BUT NOT ASTROCYTES DURING SPREADING DEPRESSION[1]

2.1. Introduction

SD in cerebral cortex occurs in several neurological disorders including migraine (Pietrobon and Striessnig 2003; Sanchez-del-Rio and Reuter 2004), brain trauma (Fabricius et al. 2006) and stroke (Strong and Dardis 2005). SD is a slowly propagating wave of neuronal and glial depolarization that spreads out at 30-50 μm/s. The depolarization occurs at the wave front of SD, which causes a large field potential shift and profound ion redistributions (Leão 1944; Somjen 2001).

It has been hotly debated whether neurons or astrocytes are the primary contributor to SD generation and propagation (for review, see Somjen 2001). Some reports indicate that neuronal depolarization is best timed with the SD wave front (Muller and Somjen 2000), whereas others support the contrary view, that astrocyte depolarization shows better temporal coincidence (Sugaya et al. 1975). Imaging calcium in both cell types during SD has helped this deliberation but has not resolved it. Previous work found that the propagation rate of SD was similar to astrocyte calcium waves (Nedergaard et al. 1995), suggesting that this astrocyte signal might drive SD. However, neuronal calcium waves evoked during SD were found to precede the change in astrocytic calcium, and diminishing astrocyte calcium waves did not block SD (Basarsky et al. 1998; Chuquet et al. 2007). These latter studies suggest the astrocyte may be a

[1] A version of this chapter has been published. Zhou N, Gordon GRJ, Feighan D, & MacVicar BA. (2010). Transient swelling, acidification and mitochondrial depolarization occurs in neurons but not astrocytes during spreading depression. Cerebral Cortex. Advance Access published Febuary 22, 2010, doi: 10.1093/cercor/bhq018

mere passive responder to the SD wave and lend credence to the idea that neurons are the principal culprit. However, calcium signals alone cannot adequately place this model on solid footing, especially because calcium entry into cells seems to have little role in the mechanisms underlying SD (Basarsky et al., 1998). When combined with the contradictory electrophysiological evidence of the time course of SD in each cell type, it is clear that other cellular parameters must be examined to see if this discrepancy between neurons and astrocytes still holds.

Changes in cell volume, pH homeostasis, and oxidative metabolism occur rapidly, and cumulating evidence suggests that these cellular changes are important to the pathophysiology of SD by initiating damage processes. First, the interstitial space shrinks dramatically following SD (Jing et al. 1994), suggesting the occurrence of cytotoxic cerebral edema caused by cell swelling, which is a possible cause for brain injury in trauma and ischemic stroke (Kimelberg 1995). Second, cortical extracellular pH (pH_o) shows a rapid alkaline transient at SD onset, followed by prolonged acidosis (Menna et al. 2000). Disturbance of pH homeostasis has been postulated to contribute to cell death and genesis of infarction following cerebral ischemia (Lipton 1999; Nedergaard et al. 1991). Third, SD induces mitochondrial membrane depolarization (Bahar et al. 2000), which plays an important role in apoptotic pathways (Orrenius et al. 2003). However, it is still unknown what the relative contributions are of neurons and astrocytes to these pathophysiological changes during SD.

In the present study, we use simultaneous electrophysiological and two-photon imaging approaches to examine cell swelling, pH changes and mitochondrial membrane potentials in individual neurons and astrocytes during the onset and progression of SD. Changes in these pathophysiological responses 1) provide a tool for examining the temporal profile of cellular activation of both neurons and astrocytes, 2) help establish which cell type is the main

contributor to SD propagation as well as SD pathophysiology, and 3) offer needed insight into the cellular mechanisms underlying SD-related neural disorders. We demonstrate that SD evokes a sequence of cellular responses unique to neurons in cortical slices that are not reflected in astrocytes. SD induces a remarkably rapid and reversible cell volume increase, a transient intracellular pH (pH_i) decrease and mitochondrial membrane potential changes exclusively in neurons. In contrast, astrocytes did not exhibit any of these responses during SD, suggesting that they play a passive role by only responding to neuronal activity.

2.2. Materials and Methods

2.2.1. Neocortical slice preparation and induction of SD

Slices from parietal cortex were prepared from 20- to 30-day-old thy1–yellow fluorescent protein-positive (YFP^+) mice (Feng et al. 2000; C57BL/J and CBA F1 hybrids) and from 14- to 21-day-old Sprague Dawley rats, according to standard procedures. Our experiments were approved by the Canadian Council for Animal Care and the University of British Columbia Animal Care Committee. All experiments were conducted in strict accordance with National Institutes of Health Guide for the Care and Use of Laboratory Animals. Briefly, the animals were anesthetized deeply with halothane and decapitated. The brain was removed quickly, and 400-µm coronal cortical slices (from Bregma 0 to Bregma -3 mm of rat brain) were cut with a vibratome (VT100; Leica, Willowdale, Ontario, Canada) in chilled (0–4 °C) slicing solution containing the following (in mM): 230 sucrose, 26 $NaHCO_3$, 10 D-glucose, 2.5 KCl, 1.25 NaH_2PO_4, 0.5 $CaCl_2$, and 10 $MgSO_4$, pH 7.3. Then the slices were transferred to a storage chamber with fresh artificial cerebrospinal fluid (ACSF) containing the following (in mM): 126 NaCl, 2.5 KCl, 2.0 $MgCl_2$, 2.0 $CaCl_2$, 1.25 NaH_2PO_4, 26 $NaHCO_3$, and 10 D-glucose, pH 7.3,

and were incubated at room temperature for >1 h before recording. All solutions were saturated with 95% O_2/5% CO_2. Brain slices from YFP^+ mice were used in experiments measuring neuronal volume. In all the other experiments, brain slices from rats were utilized.

Individual slices were transferred to a recording chamber with slice supports (Warner Instruments, Hamden, CT) that permit solution flow both above and below the slice and perfused rapidly with oxygenated ACSF (3 ml/min) at 30-32 °C. SD was induced by perfusing ACSF containing 40 mM KCl (high K^+) for 80-90 s. The high K^+ solution was made by an equimolar replacement of 40 mM KCl for NaCl. The high K^+ solution reached 50% of maximal concentration in ~24 s and reached 80% in ~55 s in the bath. The high K^+ solution contains the following (in mM): 88.5 NaCl, 40 KCl, 2.0 $MgCl_2$, 2.0 $CaCl_2$, 1.25 NaH_2PO_4, 26 $NaHCO_3$, and 10 D-glucose, pH 7.3. SD could be reliably induced in 2 min from the perfusion of high K^+ ACSF. There was a low probability of inducing SD if the perfusion speed was less than 0.6 ml/min, even when applied for 2-3 min. At this speed, the $[K^+]$ in the bath reached 50% of maximum in ~50 s and 80% in ~120 s. The slower perfusion rate probably inactivates certain ion channels due to the slower rate of depolarization as external K^+ slowly increases. Tetrodotoxin (TTX; 1 μM) was bath applied to block sodium currents in all the experiments. This allowed us to more selectively examine the cellular changes induced by SD itself and not from alterations in action potential firing that are triggered secondary to SD.

2.2.2. Two-photon imaging and analysis

We performed imaging with a two-photon laser scanning microscope (Zeiss LSM510-Axioskop-2 fitted with a 40X-W/0.80 numerical aperture objective lens) directly coupled to a Mira

Ti:sapphire laser (~100-fs pulses, 76 MHz, pumped by a 5 W Verdi laser; Coherent). We imaged both neurons and astrocytes at depths >50 μm from the slice surface. Fluorescent neurons were selected from Layer IV and V of the upper somatosensory cortex (S1HL and S1FL). In this region, pyramidal neurons were identified by their shape and the presence of a single, large apical dendrite extending vertically toward the pial surface and clearly distinct from the small circular interneurons. Astrocytes were loaded with sulforhodamine 101 (SR101, Molecular Probes, Eugene, OR) by bath application (25 μM for 20 min) followed by washing for at least 20 min. To load astrocytes with 2',7'-bis-(2-carboxyethyl)-5-(and-6)-carboxyfluorescein, acetoxymethyl ester (BCECF/AM, Molecular Probes), slices were incubated with 20 μM of BCECF/AM (in 0.3% DMSO) for 1 hr. To load astrocytes with Rhodamine 123 (Rh123, Molecular Probes), slices were incubated with 10 μM Rh123 for 5 min. Neurons were labeled with YFP or by injection of BCECF (free acid, Molecular Probes), Rh123 or Fluor® 594 hydrazide (Molecular Probes) from the recording electrode. YFP was excited at 890 nm and was detected with external detectors with a 535-nm (30 nm bandpass) filter. The BCECF and Rh123 fluorophores were excited at 840 nm and were detected with detectors with a 535-nm (30 nm bandpass) filter (figure 2.1A). The SR101 fluorophore was excited at 840 or 890 nm and was detected with external detectors with a 630-nm (60 nm bandpass) filter. The Alexa 594 fluorophore was excited at 840 nm and was detected with detectors with a 630-nm (60 nm bandpass) filter. Changes of intrinsic optical signals (IOSs) were imaged by acquiring the two-photon IR laser light (840-890 nm) in the transmitted optical path with an external photomultiplier (PMT) simultaneously with acquisition of epifluorescence signals via a separate set of PMTs.

Figure 2.1. Imaging BCECF by two-photon microscopy. (A) Two-photon excitation spectrum of BCECF. (B) Representative traces showing changes in BCECF (ΔF/F), Alexa 594 (ΔF/F) and normalized BCECF with Alexa 594 (ΔF/R) when images were obtained with excitation wavelength at 840 nm.

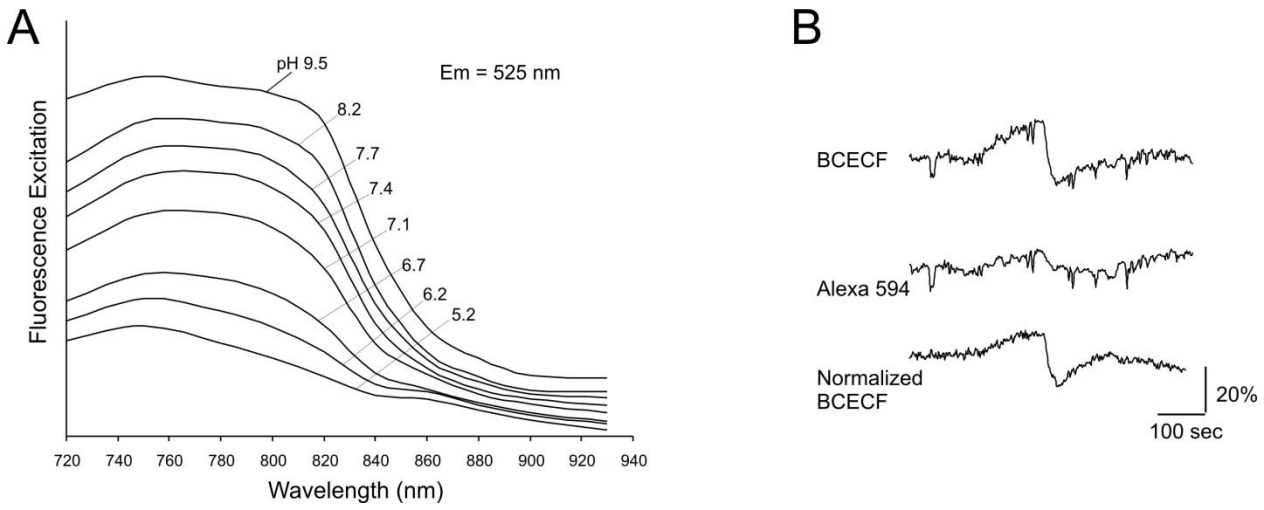
A
pH 9.5
Em = 525 nm
8.2
7.7
7.4
7.1
6.7
6.2
5.2
Fluorescence Excitation
720
740
760
780
800
820
840
860
880
900
920
940
Wavelength (nm)
B
BCECF
Alexa 594
Normalized
BCECF
20%
100 sec

Fluorescence signals were defined as $\Delta F/F = [(F_1 - B_1) - (F_0 - B_0)]/(F_0 - B_0)$, where F_1 and F_0 represent fluorescence within the cell cytoplasm at any given time point and at the beginning of the experiment respectively, and B_1 and B_0 are the background fluorescence at the same time point and at the beginning of the experiment, respectively. Background values were taken from an adjacent area of the imaged cell. To control for changes in BCECF or Rh123 fluorescence induced by changes in cell volume, we loaded the cells with another inert dye with different emission spectra (Alexa 594 or SR101) to ratio and normalize BCECF or Rh123 fluorescence intensity. The fluorescent intensity of the point of interest was selected from cell soma not including the nucleus region. Normalized fluorescence signals were defined as $\Delta F/R = (\Delta F/F) / (\Delta F_{inert}/F_{inert})$ where $\Delta F/F$ is fluorescence from BCECF or Rh123 fluorophore, and $\Delta F_{inert}/F_{inert}$ is fluorescence from the inert dye Alexa 594 or SR101. A representative fluorescence change of normalized BCECF intensity is shown in figure 2.1B.

Normalized IOSs were defined as $\Delta T = (T_1 - T_0)/T_0$, where T_1 and T_0 are transmitted light intensity of a small region in the field of view at a certain time point and at the beginning, respectively. The rate of change for IOS was determined by the first derivative of ΔT ($d\Delta T/dt$, where ΔT is the change in IOS and t is time). We developed criteria using the maximal rate of rise of the IOS change to quantitatively differentiate between the fast component of the IOS, which we show to be associated with SD, and the slow components of the IOS response that are caused by the elevated $[K^+]_o$ (Figure 2.2B). In 10 randomly selected experiments, the maximal rate of rise of the slow component was <2.0% ΔT/s (mean 0.95±0.10% ΔT/s, n=10). Therefore, if the maximum rate of rise exceeded 2.0% ΔT/s, it was regarded as the fast component and thus indicated the occurrence of SD (arrows in Figure 2.2B). The time when the rate obviously exceeded the baseline was taken as SD onset. The validity of the threshold criterion was

confirmed as the peak rate of rise after SD onset (7.47±0.18% ΔT/s, n=9) was significantly larger than the peak rate of rise when SD was not induced (0.86±0.09% ΔT/s, n=10, $p<0.001$ Figure 2.2C).

For imaging cell volume changes, three-dimensional time-lapse images were taken during the perfusion of high K^+ ACSF. At each time point, a two-dimensional projection image was made of the three-dimensional image that was composed of a Z-stack of 5 or 6 frames obtained at 2-μm increments. All the imaging experiments were recorded with Zeiss LSM 3.2, and images were exported into a series of time-lapse images. The image sequences were recentered, and the volume changes were calculated as the changes of cross-section area with the "analysis particles" function of ImageJ 1.32. When a specific threshold value was set to the whole image sequence, the analysis particles function automatically outlined the cell shape and calculate the cross-section area at all the time points.

2.2.3. Electrophysiology

Whole-cell voltage-clamp recordings from cortical neurons were obtained at 30-32 °C. Patch electrodes (5-7 MΩ) were pulled from 1.5 mm outer diameter thin-walled glass capillaries (150F-4; World Precision Instruments, Sarasota, FL) in three stages on a Flaming-Brown micropipette puller (model P-97; Sutter Instruments, Novato, CA) and were filled with intracellular solution containing the following: 135 mM K-Gluconate, 10 mM HEPES, 1.1 mM EGTA, 0.1 mM $CaCl_2$, 4 mM Mg-ATP, 0.5 mM Na-GTP, pH 7.2; 20 μM of Ru360 (Merck, Darmstadt, Germany) or 10 μM of cyclosporin A (CsA; Sigma, St Louis, MO) was included in the intracellular solution for the corresponding experiment. For imaging experiments, 100 μM of

BCECF (free acid), 10 μM of Rh123, or 25 μM of Alexa 594 was also included in the intracellular solution. Normally, the intracellular fluorescence became stable within 10 min of establishing whole-cell recordings. Membrane potentials were voltage clamped at –70 mV in neurons and at –80 mV in astrocytes. Membrane potential measurements were obtained with respect to the bath ground not the extracellular voltage in the brain slice so that there may be a small voltage measurement error during the 3-5 mV external DC shifts of SD. DC-coupled field potentials were recorded with glass micropipettes filled with ACSF (resistance, 1–3MΩ). Membrane currents and field potentials were monitored with MultiClamp 700B amplifier (Molecular Devices, Union City, CA), acquired via a Digidata 1320 series analog-to-digital interface onto a Pentium computer with Clampex 9.0 software (Molecular Devices). Data were sampled at 10 kHz, and most were low-pass filtered (four-pole Bessel) at 1 kHz.

2.2.4. Statistical analysis

In all cases Student's *t* tests were used for statistical comparisons, with $p < 0.01$ considered significant. Values are reported as the mean ± SEM.

2.3. Results

2.3.1. Imaging cortical SD with IOS

Changes in tissue light scattering or transmittance (Andrew and MacVicar 1994; MacVicar and Hochman 1991), have been used to monitor SD propagation in brain tissue (Anderson and Andrew 2002; Basarsky *et al.* 1998). We observed that a wave of SD in cortical slices was

reliably induced by perfusing ACSF containing 40 mM of KCl with a high speed (3 ml/min) (Anderson and Andrew 2002) and caused dramatic alterations to the IOS (Figure 2.2A). High perfusion rates alone, without elevated K^+, did not induce SD. The IOS changes that occurred when high K^+ was perfused and successfully induced SD consisted of two components: an initial transient peak in light transmittance that appeared on top of a much slower IOS increase (Figure 2.2B). Even though these two IOS components were easily discernable, plotting the rate of the IOS change made their difference even more dramatic. The rate of change in the initial component displayed a rapid increase and a sharp peak, followed by a rapid decrease and overshoot past baseline (peak rate of rise: 7.47±0.18% ΔT/s, n=9; Figure 2.2B). This method of analysis also revealed that this IOS component propagated through the tissue with the SD wave at 26.0±4.0 μm/s (n=9) (Figure 2.2D, E & F). This speed is approximately 50% of the SD propagation rate reported without TTX and is most likely due to a TTX-mediated reduction in the total SD-inward current (Muller and Somjen 1998, 2000). In contrast, the rate of change in the second slower IOS component was much slower (rate of rise: 0.35±0.06% ΔT/s, n=10, $p<0.001$, Figure 2.2B) showing no distinct peak and no apparent propagation through the tissue. This indicated that the slow secondary IOS change was not directly associated with SD and was instead due to a general slice swelling as a result of the elevated $[K^+]_o$ *per se* (Anderson and Andrew 2002). To confirm this idea, we perfused cortical slices with high K^+ at a lower perfusion speed (<0.6 ml/min), so that SD was not evoked. As expected, instead of the biphasic response, the IOS showed a gradual, nonpropagating increase (rate of rise: 0.27±0.04% ΔT/s, n=10, Figure 2.2C), similar to the slow, secondary IOS component observed during SD ($p=0.24$). The timing differences between the initial SD-relevant and the secondary SD-irrelevant IOS allowed us to quantitatively differentiate between them (see Methods) and use the initial rapid IOS component as an indicator of the occurrence of SD for subsequent optical experiments.

Figure 2.2. Imaging of spreading depression in cortex. (A) Pseudocolor staining of IOS changes (ΔT) during SD induced by ACSF containing 40 mM KCl. Scale: 100 μm. (B) The upper trace shows a representative IOS change during SD. The red part indicates the rapid IOS component that represented SD and the blue part indicates the slow IOS component. The lower trace shows the rate of rise for the IOS (calculated by $d\Delta T/dt$). (C) The representative IOS changes and rate of IOS change without evoking SD. (D) The time course of changes in the IOS, measured from a, b, and c three areas shown in panel A as a change in transmittance (ΔT). (E) The rate of IOS changes corresponding to the traces in D (ΔT/sec). (F) Expanded time courses of rate of changes in IOS from the region between dotted lines in E showing the propagation of the rapid IOS transient between the regions labelled in (A).

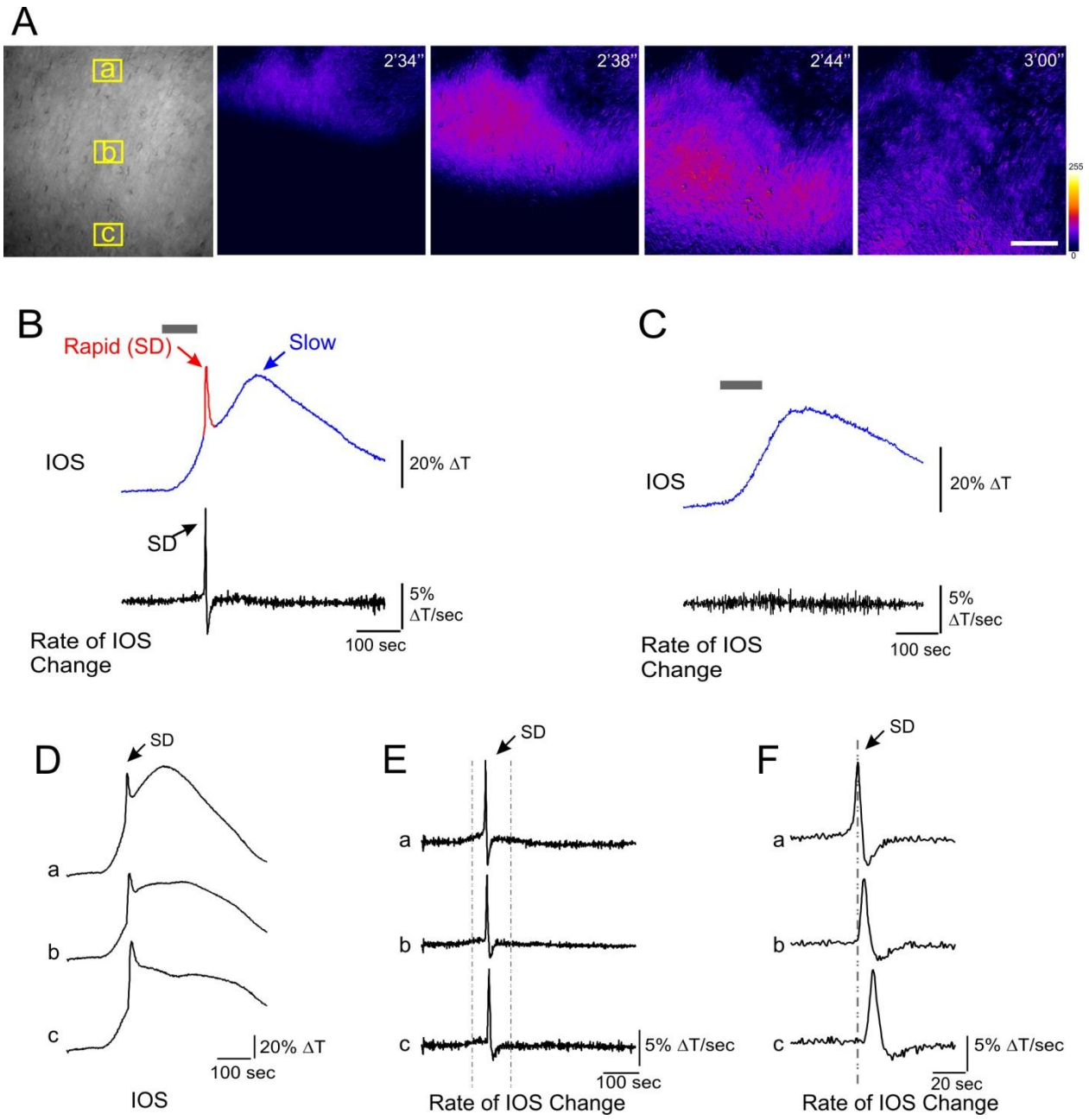
A
a
b
c
2'34"
2'38"
2'44"
3'00"
255
0
B
Rapid (SD)
Slow
IOS
20% ΔT
SD
5%
ΔT/sec
100 sec
Rate of IOS
Change
C
IOS
20% ΔT
5%
ΔT/sec
100 sec
Rate of IOS
Change
D
SD
a
b
c
20% ΔT
100 sec
IOS
E
SD
a
b
c
5% ΔT/sec
100 sec
Rate of IOS Change
F
SD
a
b
c
5% ΔT/sec
20 sec
Rate of IOS Change

2.3.2. The IOS at single-cell resolution was temporally correlated with electrophysiological signals during SD

We then examined how the IOS components correlated with the electrophysiological signals generated by SD (Czeh et al. 1993) to determine how the IOS could be used as a marker of the time course of SD. In order to ascertain which electrophysiological phase of SD was correlated with the rapid IOS component we simultaneously imaged IOS signals and recorded either extracellular field potentials or whole-cell membrane currents (Figure 2.3). In response to an SD wave, a field potential shift, measured with an extracellular electrode placed adjacent to a neuron soma (<10 μm), occurred temporally coincident with propagation of the rapid IOS component (centre of Figure 2.3A; Figure 2.3B). Whole-cell voltage-clamp recordings from individual neurons showed that typically a slowly developing inward current was first induced reflecting the membrane depolarization due to high K^+ perfusion (amplitude 14.5±3.4 pA/pF, n=8) before an SD wave was triggered. However, at the initiation of SD, a rapid onset, large amplitude inward current (28.3±5.5 pA/pF, n=8) was observed that peaked at the same time as the rapid IOS increase (Figure 2.3C). This current, which we termed I_{SD}, caused the depolarization observed in SD and has been shown previously to be coincident with the extracellular potential shift (Czeh *et al.* 1993). I_{SD} was not observed in the absence of SD (as indicated by the IOS). Only the initial inward current from the high K^+ perfusion itself continued to slowly develop (amplitude 17.8±3.4 pA/pF, n=6, Figure 2.3D). Whole-cell recording from astrocytes showed a much smaller I_{SD} with an amplitude of 9.2±3.9 pA/pF (n=4). The occurrence of I_{SD} in astrocytes was also coincident with the IOS change (Figure 2.4). These data demonstrated that the rapid IOS change reliably denotes the onset of SD as measured by either the extracellular potential shift or the depolarizing inward current from individual cells.

Figure 2.3. The rapid rate of change of IOS was coincident with the depolarizing currents and field potentials of SD. (A) High magnification imaging of a single neuron during SD. IOS changes are shown as ΔT. Scale: 10 μm. (B) Time course of the IOS change and extracellular field potential during SD. (C) Time course of the IOS change and whole-cell current during SD in a representative neuron. (D) Time course of the IOS change and whole-cell current showing that without the induction of SD there was no rapid, transient IOS component.

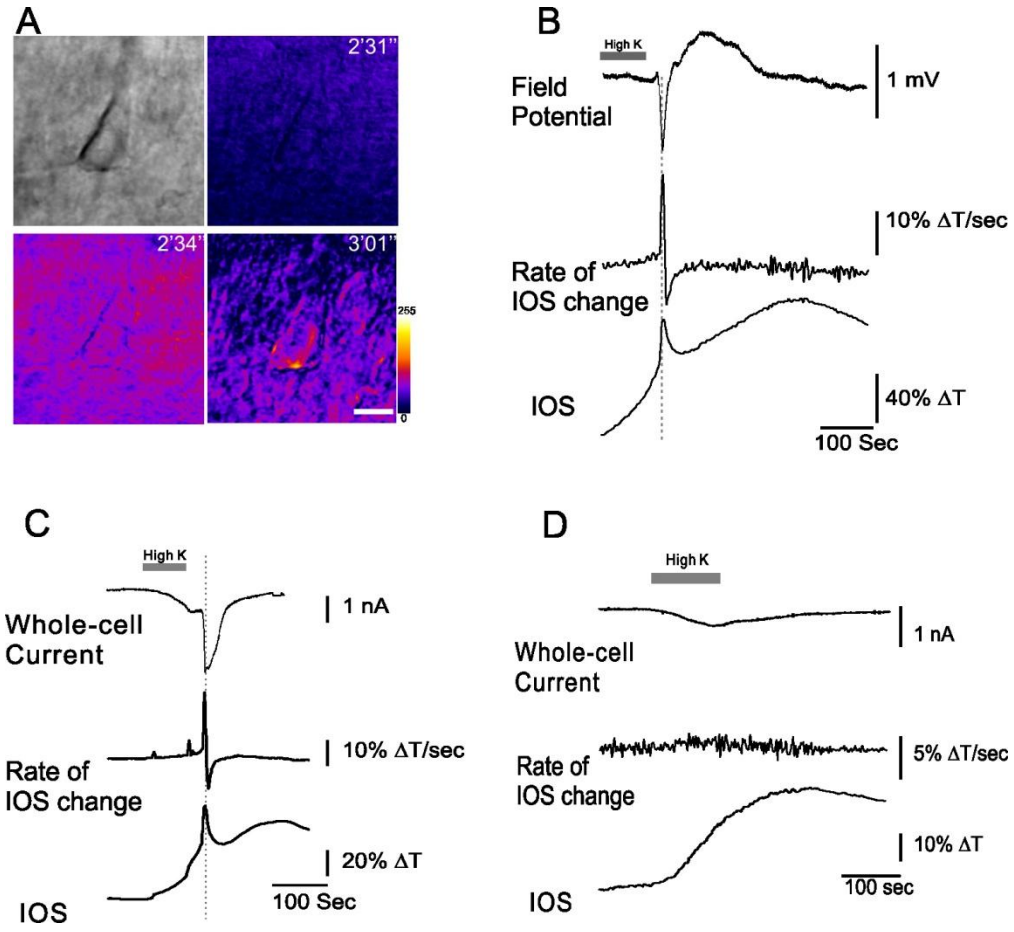
A
2'31"
2'34"
3'01"
255
0
B
High K
Field
Potential
1 mV
10% ΔT/sec
Rate of
IOS change
IOS
40% ΔT
100 Sec
C
High K
Whole-cell
Current
1 nA
10% ΔT/sec
Rate of
IOS change
20% ΔT
IOS
100 Sec
D
High K
1 nA
Whole-cell
Current
5% ΔT/sec
Rate of
IOS change
10% ΔT
IOS
100 sec

Figure 2.4. Time course of whole-cell current (top trace), IOS (bottom) and changes in the IOS (middle) during SD in a representative astrocyte.

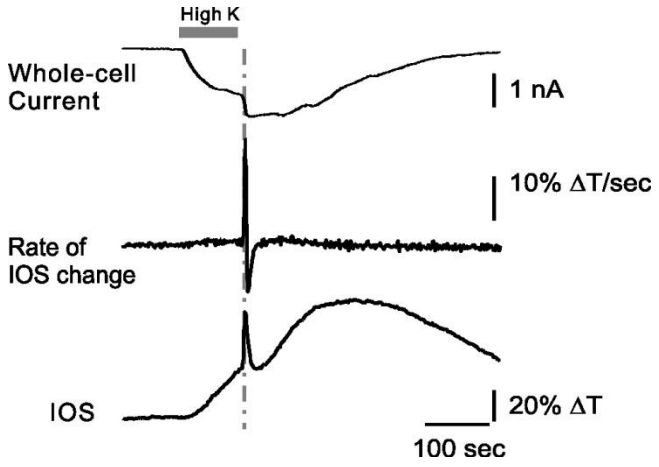
High K
Whole-cell
Current
1 nA
10% ΔT/sec
Rate of
IOS change
IOS
20% ΔT
100 sec

2.3.3. Neuronal and astrocytic volume changes evoked by SD

We next imaged neuronal and astrocytic morphological changes to determine which type of cell contributes to the interstitial space shrinkage during SD. Measurements of cell volume were acquired simultaneously with either the IOS or electrophysiological indicators to verify the occurrence of SD and to determine how volume changes were temporally related to SD onset. We first examined whether neurons underwent swelling by imaging single YFP-positive cortical neurons in mouse slices and measuring their maximal cross-sectional area from a Z-stack of images as described in the Materials and Methods. When high K^+ was perfused at a lower speed so that SD was not induced, there was no obvious neuronal volume change (0.8±0.5%, n=10, Figure 2.5B top), consistent with a previous report showing that neuron volume is resistant to osmolarity changes (Andrew et al. 2007). Interestingly, at SD onset, a rapid increase in neuronal volume was initiated, reaching a maximum (11.0±0.9%, $p<0.001$) in 72±3 seconds (n=10), followed by gradual recovery to baseline in 5-7 minutes (Figure 2.5A, B bottom). To determine whether astrocytes exhibit similar volume changes, we imaged astrocytes stained with SR101 (Nimmerjahn et al. 2004). In contrast to neurons that were resistant to slow increases in $[K^+]_o$, astrocytes gradually swelled (35.6±3.4%, n=10) (Kimelberg 2000) when high $[K^+]_o$ was perfused and gradually recovered their volume during washout (Figure 2.5C top). The change in astrocyte volume coincided with the slow phase of the IOS change, indicating a standard swelling response from the elevated $[K^+]_o$. When SD was induced, astrocytes did not show any further swelling (40.2±1.7%, n=10, $p=0.62$ compared to slow perfusion, Figure 2.5C bottom and E). These results indicate that astrocytes only display passive swelling in response to high K^+, whereas neurons exhibit a concerted and SD-specific volume increase that is distinct from standard osmotic swelling. These data also suggest that the pathophysiological reduction of interstitial volume observed at SD onset (Jing *et al.* 1994) is of neuronal, rather than astrocytic origin.

Figure 2.5. Transient volume increases in neurons but not astrocytes during SD. (A) The image sequence of a neuron before, during, and after SD in mouse slice. The right panel shows the overlap (yellow region) of images before (green component) and during SD (red component). This shows graphically the larger cross-sectional area in red of the swollen neuron in SD. (B) Representative traces showing the time course of the high K^+-induced IOS rate (black) and neuronal volume changes (red) without (top) and with (bottom) SD. The transient increase in neurons occurred at the onset of SD but was not observed when SD did not occur. (C) Representative traces showing the time course of the high K^+-induced IOS (black) and astrocytic volume changes (red) without (top) and with (bottom) SD in rat slice. There were no additional changes in astrocytes during SD as compared to the changes solely induced by the perfusion of high K^+. (D) Summary graphs (means ±s.e.m) showing neuronal volume changes (D) were only observed when SD was induced by high K^+ whereas astrocytic volume changes (E) occurred with just high K^+ and there were no additional changes associated with SD.

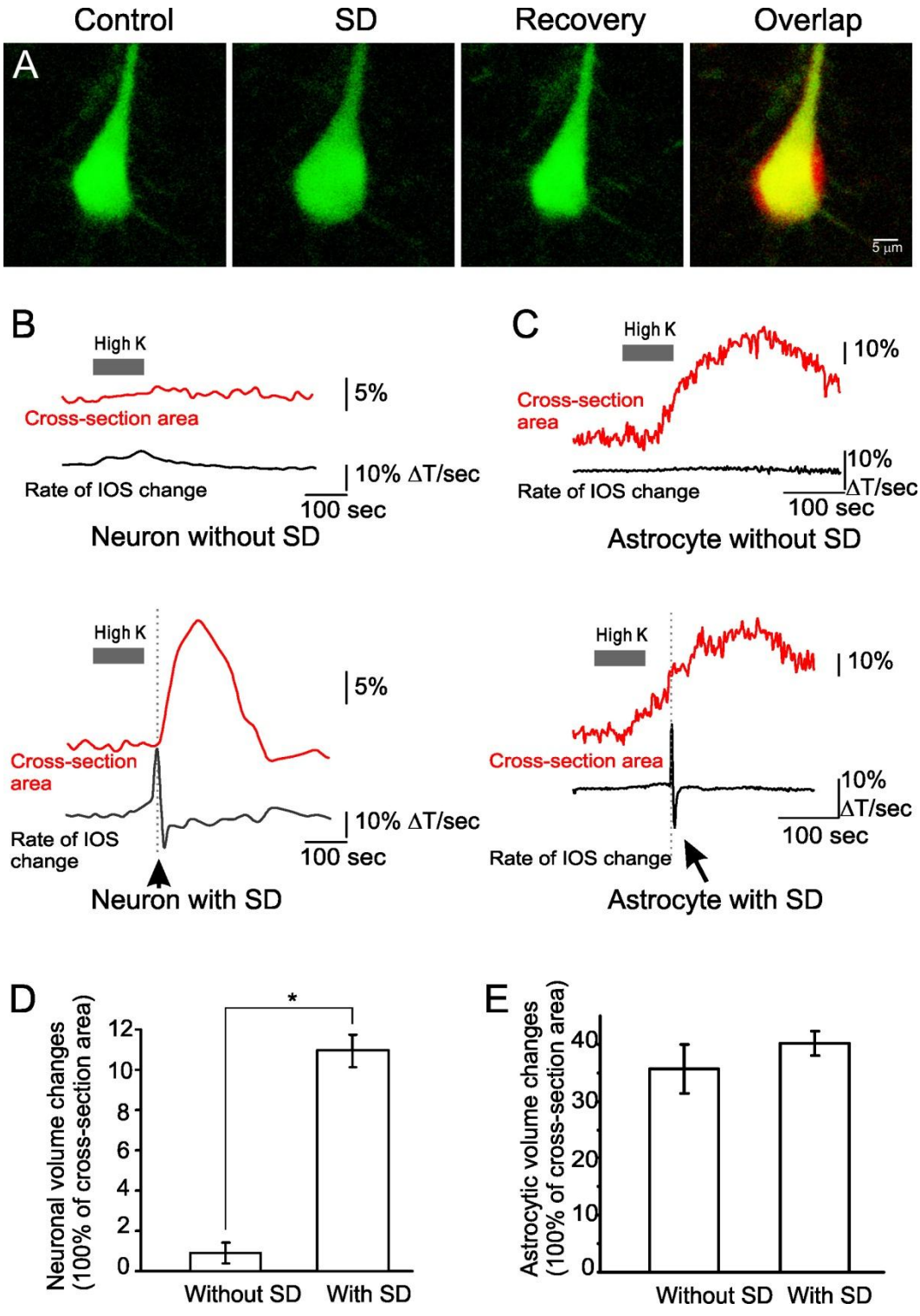
Control
SD
Recovery
Overlap
A
5 μm
B
High K
5%
Cross-section area
10% ΔT/sec
Rate of IOS change
100 sec
Neuron without SD
C
High K
10%
Cross-section area
10%
ΔT/sec
Rate of IOS change
100 sec
Astrocyte without SD
High K
5%
Cross-section area
10% ΔT/sec
Rate of IOS change
100 sec
Neuron with SD
High K
10%
Cross-section area
10%
ΔT/sec
Rate of IOS change
100 sec
Astrocyte with SD
D
Neuronal volume changes (100% of cross-section area)
12
10
8
6
4
2
0
*
Without SD
With SD
E
Astrocytic volume changes (100% of cross-section area)
40
30
20
10
0
Without SD
With SD

2.3.4. Neuronal versus astrocytic intracellular pH changes during SD

To gain insight into the dysregulation of pH homeostasis during SD (Menna *et al.* 2000), we used the pH indicator BCECF to examine the pH_i dynamics in neurons and astrocytes. Neurons were loaded with cell-impermeable BCECF through the patch pipette. A cell labeled with BCECF showed quite uniform staining in the cytosol and the nucleus. To control for changes in BCECF fluorescence induced by changes in cell volume, another inert dye, Alexa 594, was also injected intracellularly and was used to ratio and thus normalize BCECF fluorescence intensity (Figure 2.6A). When SD was not evoked, high K^+ induced an increase in BCECF fluorescence in neurons (7.8±1.5% ΔF/R, n=7, Figure 2.6B), suggesting a slight alkaline shift. In contrast, when SD was induced, the BCECF fluorescence showed a transient decrease that was temporally coincident with the rapid IOS change and I_{SD} (-21.7±1.9% ΔF/R, n=7, Figure 2.6C), indicating a pH_i decrease at the onset of SD. To examine pH_i changes in astrocytes, these cells were loaded with the cell permeable BCECF/AM and SR101. The latter provided a control for volume-induced changes by normalizing BCECF fluorescence to that of SR101 (Figure 2.6D). Either BCECF injected through the patch pipette or bulk loading of BCECF/AM resulted in an even staining in the cell soma without showing specific incorporation in the nucleus. Without the induction of SD, high K^+ *per se* caused a gradual increase in astrocytic BCECF fluorescence (19.7±3.6% ΔF/R, n=5, Figure 2.6E), indicating an intracellular alkalization that was similar but relatively greater than that observed in neurons. However, in direct contrast to neurons, astrocytes did not show a transient decrease of BCECF fluorescence at the onset of SD but instead showed an increase similar to that observed in response to high K^+ itself (27.1±3.8% ΔF/R, n=8, Figure 2.6F). To test the possibility that the astrocytic pH response to SD was concealed by the pH_i increase to high K^+ alone, we locally injected a small volume of KCl (3 M) in a distant and discrete region of the cortex to evoke an SD wave that would then propagate into

Figure 2.6. Imaging intracellular pH changes show neurons display a transient acidification during SD. (A) Fluorescence images from a neuron loaded with BCECF (top panels) and Alexa 594 (bottom panels) before (left panels) and during (right panels) SD. (B, C) Representative traces showing BCECF fluorescence normalized to Alexa fluorescence (top trace), IOS (middle) and whole-cell current in a neuron without SD (B) as compared to a neuron with SD (D). (D) Astrocytes stained with SR101 (red, top panels), BCECF (green, middle panels), and overlap (bottom panels) before (left panels) and during (right panels) SD in astrocytes. Measurements were taken from the regions of overlap. (E, F) Representative traces showing BCECF fluorescence normalized to SR101 fluorescence (top trace), IOS (middle) and whole-cell current in astrocytes without SD (E) compared to astrocytes with SD.

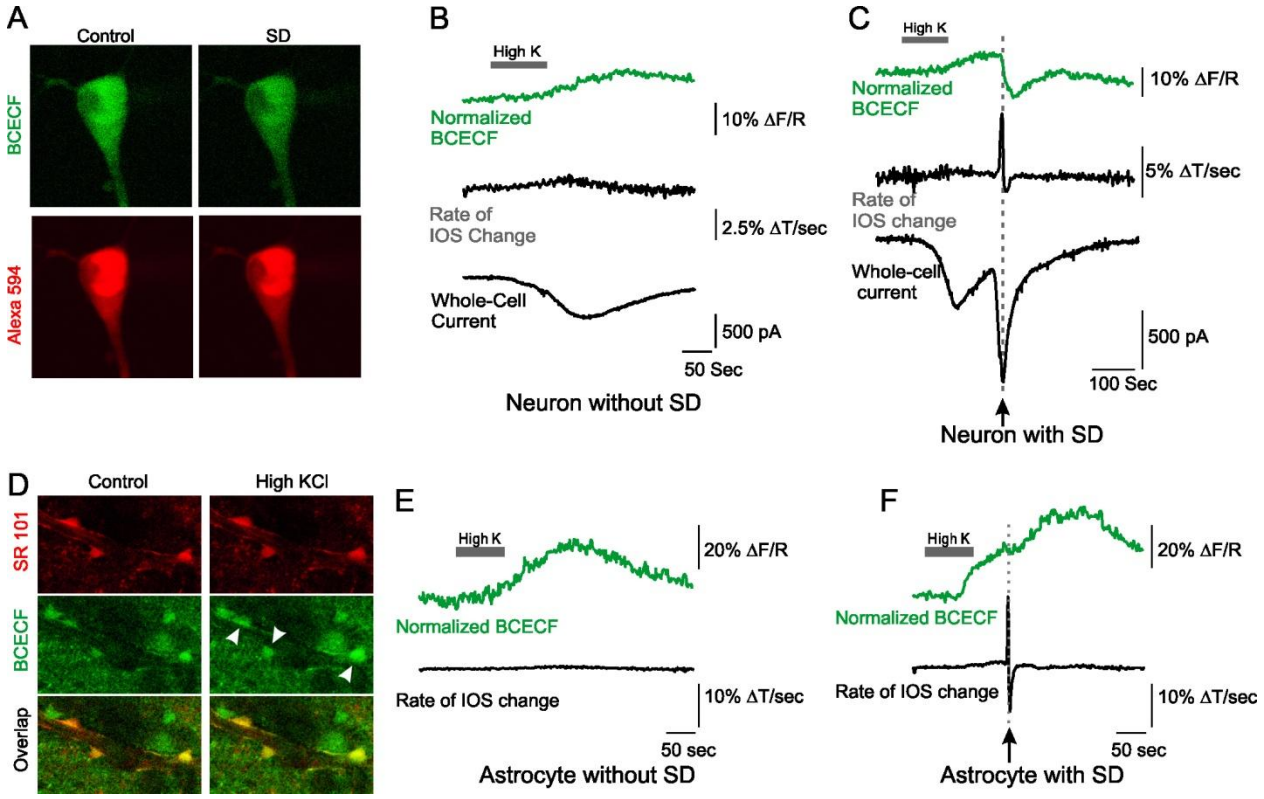
A
Control
SD
BCECF
Alexa 594
B
High K
Normalized BCECF
10% ΔF/R
Rate of IOS Change
2.5% ΔT/sec
Whole-Cell Current
500 pA
50 Sec
Neuron without SD
C
High K
Normalized BCECF
10% ΔF/R
Rate of IOS change
5% ΔT/sec
Whole-cell current
500 pA
100 Sec
Neuron with SD
D
Control
High KCl
SR 101
BCECF
Overlap
E
High K
20% ΔF/R
Normalized BCECF
Rate of IOS change
10% ΔT/sec
50 sec
Astrocyte without SD
F
High K
20% ΔF/R
Normalized BCECF
Rate of IOS change
10% ΔT/sec
50 sec
Astrocyte with SD

the imaged region (Figure 2.7). Under these conditions, astrocytes displayed an immediate increase in BCECF fluorescence, indicating a rapid alkalization of pH_i at SD onset. This effect is likely due to the rapid increase in the $[K^+]_o$ caused by SD (Brinley et al. 1960) which is known to raise pH_i in astrocytes (Chesler and Kraig 1989). These data demonstrate that neurons, but not astrocytes, display a distinct acidification during SD. This transient acidosis experienced by neurons may be associated with the interstitial pH changes at SD onset reported by others (Menna *et al.* 2000).

2.3.5. Mitochondrial membrane potential changes during SD

As SD induces mitochondrial membrane depolarization (Bahar *et al.* 2000), which is thought to play an important role in apoptosis (Orrenius *et al.* 2003), we used the mitochondrial membrane potential ($\Delta\psi_m$) indicator Rh123 to examine $\Delta\psi_m$ dynamics in brain slices (Kovacs et al. 2005) during SD. To observe the $\Delta\psi_m$ in neurons, Rh123 was included in the whole-cell patch pipette. Because Rh123 is membrane permeable, Rh123 also stained cells in the surrounding neuropil, resulting in some puncta background staining. To differentiate the boundary of the recorded neuron and the Rh123 signal from adjacent cells, Alexa 594 was also included in the intracellular solution (Figure 2.8A). Before SD onset, high K^+ induced a relatively small and gradual increase in Rh123 fluorescence (Figure 2.8C). Immediately following the onset of SD, the cytosol Rh123 fluorescence increased (21.2±2.0% $\Delta F/R$, n=6) with a rapid time course, reaching a maximum approximately 2 s later than the rapid IOS change and I_{SD} (Figure 2.8D,F). This indicated that a profound but transient mitochondrial membrane depolarization occurs in neurons just after SD onset (Figure 2.8D, F). Because calcium homeostasis is a crucial factor in mitochondrial

Figure 2.7. IOS and pH_i changes during SD induced by local injection of high KCl. (A) IOS during SD that was induced by local injection of 3 M of KCl (left colume) or bath perfusion of 40 mM of KCl (right column). (B) Time course of IOS measured from (A). Left: local injection of KCl; Right: bath perfusion of KCl. (C) Representative traces showing IOS (top trace), changes in IOS (middle) and BCECF fluorescence normalized to SR101 fluorescence in single astrocytes (bottom) induced by local injection of KCl. (D) Averaged time course of BCECF fluorescence during SD.

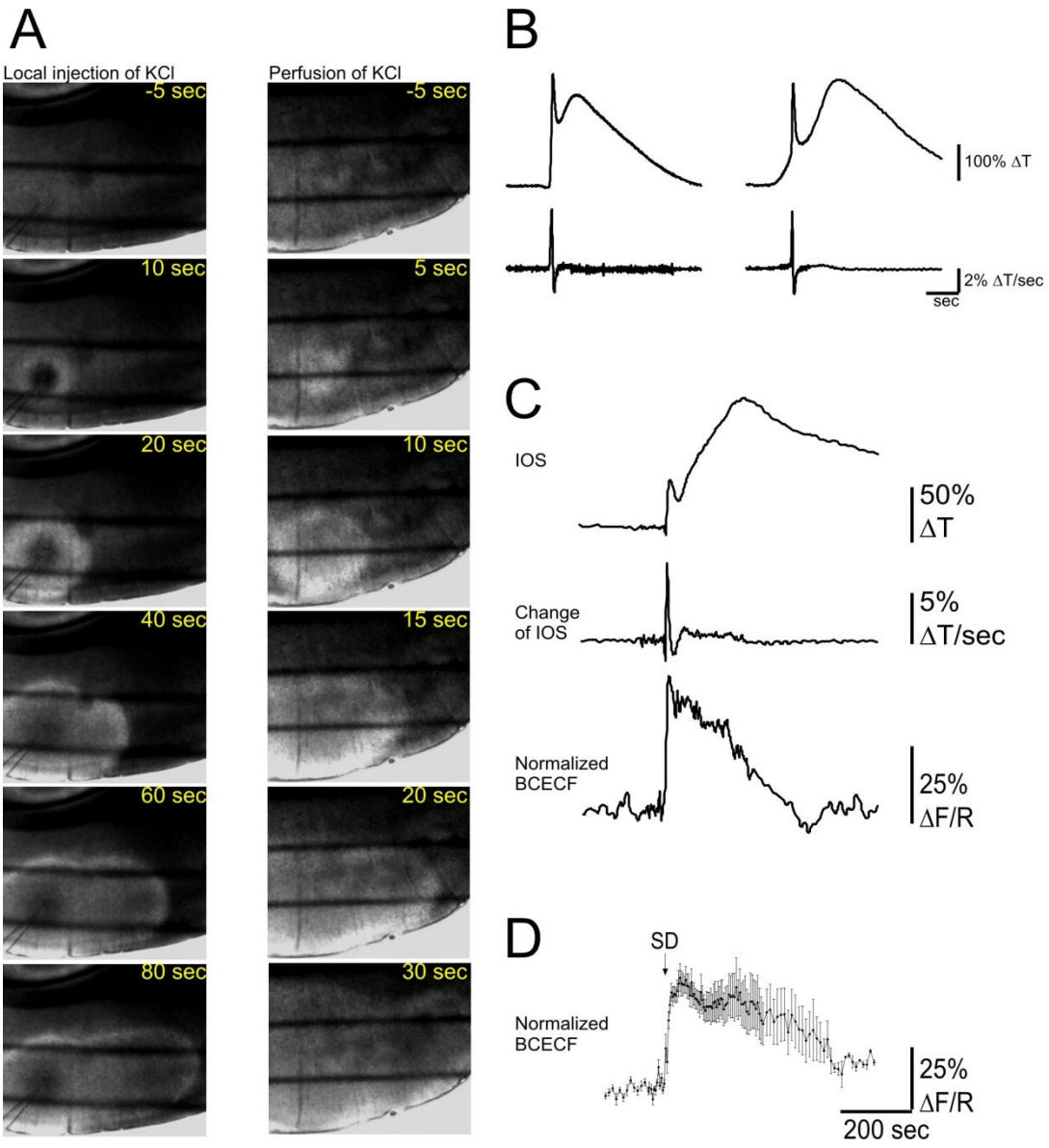
A
Local injection of KCl
Perfusion of KCl
-5 sec
-5 sec
10 sec
5 sec
20 sec
10 sec
40 sec
15 sec
60 sec
20 sec
80 sec
30 sec
B
100% ΔT
2% ΔT/sec
sec
C
IOS
50%
ΔT
Change
of IOS
5%
ΔT/sec
Normalized
BCECF
25%
ΔF/R
D
SD
Normalized
BCECF
25%
ΔF/R
200 sec

Figure 2.8. Neuronal mitochondrial changes during SD. (A) Representative neuron stained with Rh123 (green) and Alexa 594 (red). The yellow region shows the neuronal area where the Rh123 measurements were taken and the red is the neuronal nucleus. (B-E) Pseudocolour image of Rh123 fluorescence intensity before (B, C), during (D) and after (E) the onset of SD (time points are shown in traces in F). (F) Changes of IOS, Rh123 intensity and whole-cell current during SD. (G) Summary of means ± s.e.m showing Rh123 changes in neurons during SD with control, ACSF containing 0 mM of Ca^{2+}, 20 μM of Ru360, or 10 μM of CsA in the intracellular solution. Ru360, which inhibits the mitochondrial calcium uniporter significantly depressed Rh123 changes and 0 mM external Ca^{2+} totally blocked them. In contrast the MPTP inhibitor CsA had no effect. (H) Representative traces of the changes of IOS, Rh123 fluorescence intensity and whole-cell current during SD in 0-Ca^{2+} ACSF showing that the SD depolarizing current was still observed in 0-Ca^{2+} ACSF.

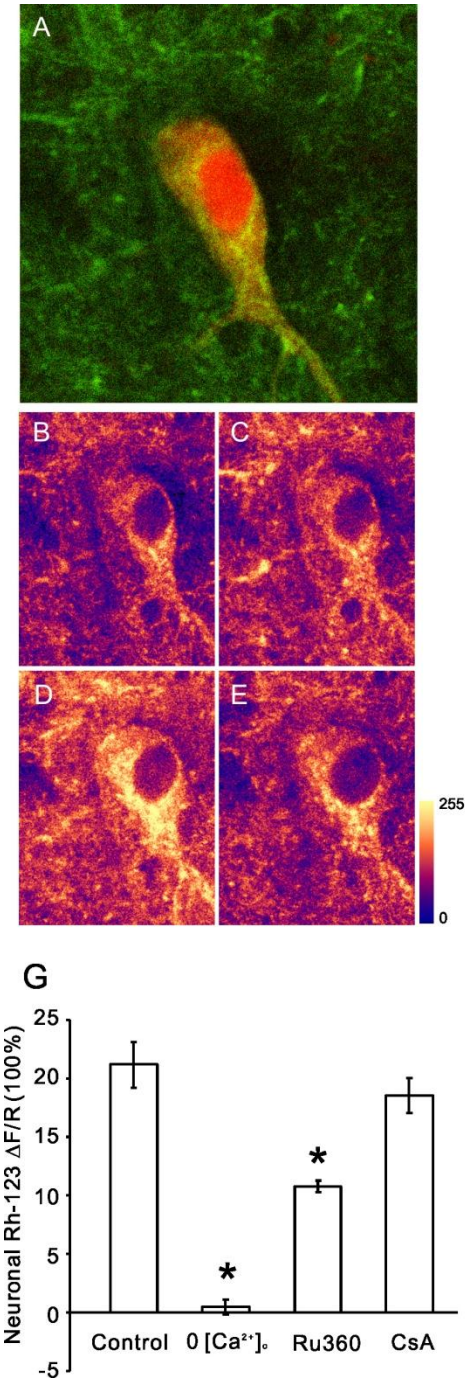
A
B
C
D
E
255
0
G
Neuronal Rh-123 ΔF/R (100%)
25
20
15
10
5
0
-5
Control
0 [Ca²⁺]ₒ
Ru360
CsA
*
*
F
KCl
B
C
D
E
10% ΔF/R
Rh-123
10% ΔT/sec
Rate of
IOS Change
Whole-cell
Current
500 pA
100 Sec
H
0 [Ca²⁺]ₒ
KCl
Rh-123
10% ΔF/R
Rate of
IOS Change
10% ΔT/sec
Whole-cell
Current
500 pA
100 sec

function (Duchen 2004), we tested the role for calcium entry during SD by perfusing slices with Ca^{2+}-free extracellular solutions to determine whether the mitochondrial depolarization was dependent upon increased cytosolic [Ca^{2+}]. Consistent with previous studies (Basarsky *et al.* 1998), SD induction and propagation (15±3 μm/sec, n=5) was not blocked by removal of extracellular calcium. However, the maximal rate of rise in the IOS was slower in Ca^{2+}-free solutions (2.3±0.4% ΔT/s, n=5, $p<0.001$) compared to control (7.5±0.5% ΔT/s, n=9). In the absence of extracellular calcium the SD-induced mitochondrial depolarization was completely abolished compared to control (0.5±0.6%, $p<0.001$, n=5, Figure 2.8G, H). The $\Delta\psi_m$ depolarization may result from either opening of the mitochondrial permeability transition pore (MPTP), which is induced by uptake of excessive calcium into mitochondria (Nicholls 2008; Skulachev 2006), or uptake of cytosolic calcium through the mitochondrial uniporter (Kirichok et al. 2004). We tested the potential role of the MPTP by including the inhibitor CsA in the intracellular solution (Kovacs *et al.* 2005) but found no significant change in the $\Delta\psi_m$ depolarization induced by SD compared to control (18.5±1.5% ΔF/R, $p=0.29$, Figure 2.8G). However, in the presence of Ru360, a specific inhibitor for the calcium uniporter, the $\Delta\psi_m$ depolarization was markedly reduced during SD (10.7±0.5% ΔF/R, n=5, $p<0.01$). Collectively, these data suggest that SD-induced mitochondrial depolarization depends upon calcium influx into the cytosol of the neuron and subsequent uptake into mitochondria through the calcium uniporter. This effect, however, is not required for the induction or propagation of SD but instead reflects a consequence of the SD event.

We next examined Rh123 changes in astrocytes and compared the responses with that observed in neurons. Astrocytes were loaded with Rh123 using bath application that led to bright labeling of these cells, which was confirmed by co-labeling with SR101 (Figure 2.9). When high K^+ was perfused but did not evoke SD, astrocytes showed a gradual increase in Rh123 fluorescence

Figure 2.9. Astrocytic mitochondrial changes were not associated with SD. (A) Brightfield image of region shown in panels B-D. Astrocytes were stained with SR101 (B) and with Rh123 (C) and the merged image is shown in (D). (E, F) Representative traces showing the Rh123 signal changes in 4 individual astrocytes and the corresponding IOS changes induced by high K^+ solution without the induction of SD (E) and the changes during SD (F). There were no additional changes beyond those induced by the perfusion of high K^+. (G) Summary of means ± s.e.m showing Rh123 fluorescence in astrocytes when SD was initiated versus when there was no SD. There was no significant difference.

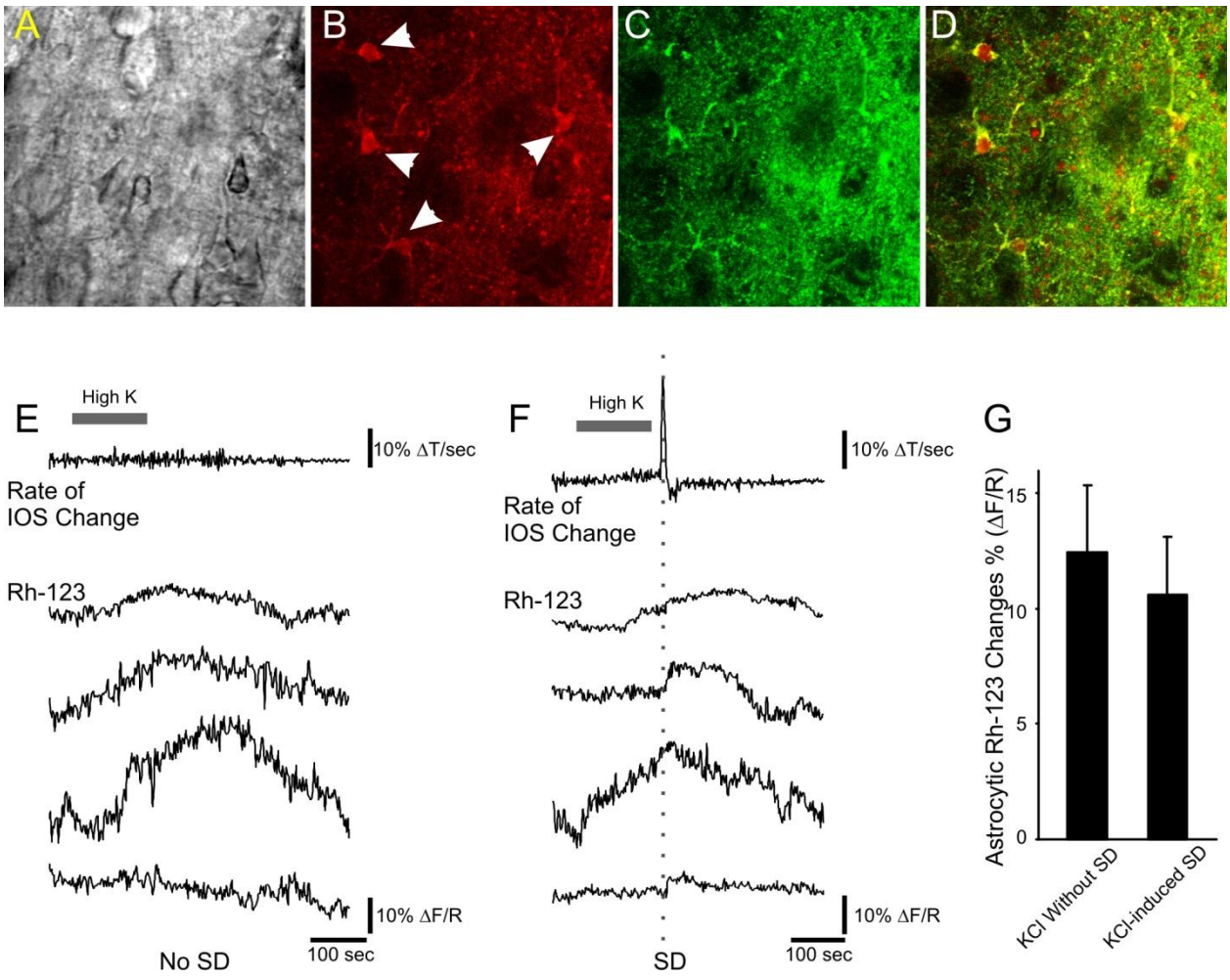
A
B
C
D
E
High K
10% ΔT/sec
Rate of
IOS Change
Rh-123
10% ΔF/R
No SD
100 sec
F
High K
10% ΔT/sec
Rate of
IOS Change
Rh-123
10% ΔF/R
SD
100 sec
G
Astrocytic Rh-123 Changes % (ΔF/R)
15
10
5
0
KCl Without SD
KCl-induced SD

(10.6±2.5% ΔF/R, n=12), similar to that of neurons. However, the degree of the fluorescence change was variable among astrocytes within the same field of view (Figure 2.9E). When SD occurred, most astrocytes did not show an additional increase in Rh123 intensity (Figure 2.9F) and the average maximal increase of Rh123 fluorescence was not significantly different from high K^+ alone (12.4±2.9% ΔF/R, n=17, p=0.65, Figure 2.9G). Therefore, these results indicate that neurons are the major locus for the mitochondrial membrane potential changes induced by SD propagation.

2.4. Discussion

We have used a combination of two-photon laser scanning microscopy (TPLSM) and electrophysiological techniques to show changes in cell volume, pH_i, and mitochondrial membrane potential in neurons versus astrocytes during SD in cerebral cortex *in vitro*. A transient increase in light transmittance was observed to be coincident with electrophysiological signals of SD, indicating that imaging IOS changes using the infrared ultrafast laser can be used as a reliable indicator of the SD onset. Imaging individual YFP-labelled neurons showed that SD evoked a rapid but transient volume increase in neurons, but not in astrocytes. At the onset of SD, neurons also showed a transient decrease of pH_i and a transient mitochondrial membrane depolarization. The $\Delta\psi_m$ was dependent upon cytosolic calcium changes and was caused by calcium uptake into mitochondria through calcium uniporters. Astrocytes did not exhibit the same changes in pH_i and $\Delta\psi_m$ during the onset of SD.

2.4.1. IOS and KCl induction of SD

SD-related IOS changes are complex, involving multiple underlying mechanisms such as cell swelling, dendritic beading, neuronal secretion, and/or mitochondrial volume changes (Aitken et al. 1999; Salzberg et al. 1985). We observed that the SD-related IOS showed a transient change that consisted of an initial increase followed by a rapid decrease in transmitted light, a pattern consistent with several previous reports (Anderson and Andrew 2002; Fayuk et al. 2002). Contrary to these results, some studies have shown an increase in light scattering, which decreases light transmittance during the initial phase of SD (Aitken et al. 1998; Snow et al. 1983; Buchheim et al. 2002; Vilagi et al. 2001). These differences may be due to the arrangement of the optical detectors or the wavelengths used in the experiment. We examined this transmitted image at infrared wavelengths, in which IOSs are principally generated by light scattering (Ba et al. 2002), resulting in an increase in light transmittance as cells swell. Despite the complexity of the IOS though, our data clearly shows that by taking the first derivative of this signal, the rapid rise and peak is a robust and faithful indicator of the SD wave front and an indispensable tool for temporally aligning SD with other pathophysiological events within the cortical slice.

Our results provide evidence for the existence of differential signals generated by neurons as compared with astrocytes during SD and high K^+. The rapid IOS component that was correlated with SD onset occurred simultaneously with several events only observed in neurons. The most dramatic change observed was a remarkably large yet quickly reversible swelling, which showed maximal volume increase 60 sec after the peak IOS. This latency suggests that this effect may be caused by the large conductance associated with the rapid depolarization of SD, as massive and prolonged ion influx would dramatically enable sustained water movement into the cell. The shorter time course of the IOS transient compared with the duration of neuronal swelling suggests that the transient increase in light transmittance was not solely due to neuronal volume

changes in the soma and dendritic shafts but perhaps additionally reflects yet to be described cellular processes. Finally, the slow nonpropagating IOS increase induced by KCl was coincident with the astrocytic volume increase. This was similar in all slices whether or not SD was evoked. Therefore, the slower component of IOS was likely due to the change in light scattering caused by astrocytic swelling.

2.4.2. Contribution of neurons versus astrocytes to the interstitial volume changes

Based on measurements of the concentration of extracellular cell-impermeable indicators like TMA^+ and TEA^+ it has been concluded that the interstitial space shrinks rapidly at SD onset (Hansen and Olsen 1980; Jing *et al.* 1994). However, in these studies, it was unclear which cell type was responsible. A recent study has shown that neuronal swelling was likely to be the main cause for the tissue swelling during SD *in vivo* (Takano et al. 2007). Our observations demonstrate that astrocytes swell only as a result of the elevated $[K^+]_o$ and not because of SD, while neurons were essentially opposite, showing resistance to elevated $[K^+]_o$ and only swelled in response to SD. In astrocytes, the high K^+ would lead to potassium uptake followed by water entry through aquaporins to compensate for the subsequent osmolarity shift (Kimelberg 2000). This is consistent with data showing that astrocytes express high levels of aquaporin 4 (Nielsen et al. 1997). In contrast, neurons lack aquaporin channels (Badaut et al. 2004; Rash et al. 1998), explaining their inability to osmotically respond to K^+ elevation. These ideas have been supported in a recent imaging study, in which neurons fail to change cellular volume during acute osmotic stress whereas astrocytes rapidly swell (Andrew *et al.* 2007). Our results suggest that SD-induced neuronal swelling is probably due to the ionic fluxes during the large

conductance increase during SD. However, it is currently unclear which ion channels are opening to allow the movement of water.

2.4.3. Intracellular pH changes

Another novel observation in our study is that pH_i rapidly acidifies in neurons during SD. Previous studies of pH measurements mainly focused on pH_o. For instance, Kraig et al. have used a double-barrelled liquid membrane pH ion-selective micropipette to obtain rapid and repeatable pH_o measurements during SD (Kraig et al. 1983). They reported that SD was accompanied by an initial small alkaline shift in pH_o and was followed by a long-lasting acid phase (Kraig *et al.* 1983; Tong and Chesler 1999). Although this study showed that the pH_o changes resulted from the membrane transport of H^+ and HCO_3^-, these extracellular measurements could not differentiate between the contributions of pH transients in neurons versus astrocytes. The development of fluorescent pH indicators provided the ability to obtain continuous real-time monitoring of pH_i in individual cells. BCECF is the most widely used pH indicator because it is well retained in cells (i.e. low leakage rate), its pK_a (6.98) is close to natural pH_i, and it can be used for quantitive pH measurements with ratiometric imaging (Paradiso et al. 1984) or for imaging qualitative pH changes using TPLSM. We used BCECF imaging with TPLSM to provide spatiotemporal determination of pH_i changes in neurons versus astrocytes. During SD we observed remarkably different pH_i transients in neurons versus astrocytes. The rapid pH_i decrease in neurons suggests a transient proton influx or HCO_3^- efflux, which accompanies the large ionic flux at the onset of SD. In contrast to the neurons, astrocytes increased pH_i gradually when $[K^+]_o$ was elevated, but they did not exhibit any unique changes to SD. The gradual pH_i change in high K^+ was consistent with previous studies which showed that

raising $[K^+]_o$ or electrical stimulation caused intracellular alkalization in astrocytes (Chesler and Kraig 1987, 1989). This alkalization is due to the astrocytic Na^+-HCO_3^- cotransporter, which transported 2 or 3 HCO_3^- for each Na^+. Astrocytic membrane depolarization induced by elevated $[K^+]_o$ shifts the electrochemical gradient towards increased influx of HCO_3^- thereby raising pH_i (Chesler 2003). This suggests that neuronal activities likely account for the pH_o transients at the onset of SD.

2.4.4. $\Delta\psi_m$ changes during SD

There are several mechanisms underlying mitochondrial depolarization, including mitochondrial Ca^{2+} cycling that is dependent on the calcium uniporter and Na^+/Ca^{2+} exchanger, Ca^{2+}-dependent mitochondrial membrane transition, or a disruption of the ADP/ATP and the NAD^+/NADH ratio (Duchen 2004). Under normal physiological conditions, the electrochemical potential gradient across the mitochondrial membrane drives the uptake of calcium from cytosol into mitochondria. The calcium is taken up through the uniporter on the inner membrane and it therefore depolarizes $\Delta\psi_m$ (Gunter et al. 1994). It has been reported that mitochondrial calcium uptake follows the cytosolic calcium elevation with a time lag (Rakhit et al. 2001). This is in line with our observations that the mitochondrial signal occurs later than the IOS and electric signals. The measured increase in cytosolic Rh123 fluorescence during SD suggests depolarized mitochondrial membrane potential (Baracca et al. 2003), which would reduce oxygen consumption by mitochondria thereby possibly transiently increasing pO_2 (Kadenbach 2003).

In conclusion our results suggest that astrocytes are not active contributors to the generation of SD. Astrocytes appear to merely follow the intense depolarization of neurons and respond to the increased $[K^+]_o$ which is known to occur during SD. The neuronal depolarization we observed

during SD is unusual in that it still propagated in TTX and calcium-free external solutions, a combination that blocked both Na^+ and Ca^{2+} dependent spikes and synaptic transmission. Our imaging experiments suggest that it is most likely a nonselective cation conductance that allowed the substantial changes to pH. In addition, the depolarization during SD triggered calcium influx into neurons that led to mitochondrial depolarization. Our observations suggest that neurons are the key locus for the pathogenesis induced by ischemia or other disorders that involved SD. It will be important to extend our observations to *in vivo* models of SD (Takano *et al.* 2007) as an intact blood supply may differentially affect SD mitochondrial responses. However, our results are consistent with the conclusion from Somjen's overview of the literature that "in SD, neurons lead and glial cells follow" (Somjen 2001). These data help clarify the role of neurons and astrocytes in SD and provide an important framework towards a mechanistic comprehension of the neuropathology.

2.5. References

Aitken PG, Fayuk D, Somjen GG, Turner DA. 1999. Use of intrinsic optical signals to monitor physiological changes in brain tissue slices. Methods. 18: 91-103.

Aitken PG, Tombaugh GC, Turner DA, Somjen GG. 1998. Similar propagation of SD and hypoxic SD-like depolarization in rat hippocampus recorded optically and electrically. J Neurophysiol. 80: 1514-1521.

Anderson TR, Andrew RD. 2002. Spreading depression: imaging and blockade in the rat neocortical brain slice. J Neurophysiol. 88: 2713-2725.

Andrew RD, Labron MW, Boehnke SE, Carnduff L, Kirov SA. 2007. Physiological evidence that pyramidal neurons lack functional water channels. Cereb Cortex. 17: 787-802.

Andrew RD, MacVicar BA. 1994. Imaging cell volume changes and neuronal excitation in the hippocampal slice. Neuroscience. 62: 371-383.

Ba AM, Guiou M, Pouratian N, Muthialu A, Rex DE, Cannestra AF, Chen JW, Toga AW. 2002. Multiwavelength optical intrinsic signal imaging of cortical spreading depression. J Neurophysiol. 88: 2726-2735.

Badaut J, Petit JM, Brunet JF, Magistretti PJ, Charriaut-Marlangue C, Regli L. 2004. Distribution of Aquaporin 9 in the adult rat brain: preferential expression in catecholaminergic neurons and in glial cells. Neuroscience. 128: 27-38.

Bahar S, Fayuk D, Somjen GG, Aitken PG, Turner DA. 2000. Mitochondrial and intrinsic optical signals imaged during hypoxia and spreading depression in rat hippocampal slices. J Neurophysiol. 84: 311-324.

Baracca A, Sgarbi G, Solaini G, Lenaz G. 2003. Rhodamine 123 as a probe of mitochondrial membrane potential: evaluation of proton flux through F(0) during ATP synthesis. Biochim Biophys Acta. 1606: 137-146.

Basarsky TA, Duffy SN, Andrew RD, MacVicar BA. 1998. Imaging spreading depression and associated intracellular calcium waves in brain slices. J Neurosci. 18: 7189-7199.

Brinley FJ, Jr., Kandel ER, Marshall WH. 1960. Potassium outflux from rabbit cortex during spreading depression. J Neurophysiol. 23: 246-256.

Buchheim K, Weissinger F, Siegmund H, Holtkamp M, Schuchmann S, Meierkord H. 2002. Intrinsic optical imaging reveals regionally different manifestation of spreading depression in hippocampal and entorhinal structures in vitro. Exp Neurol. 175: 76-86.

Chesler M. 2003. Regulation and modulation of pH in the brain. Physiol Rev. 83: 1183-1221.

Chesler M, Kraig RP. 1987. Intracellular pH of astrocytes increases rapidly with cortical stimulation. Am J Physiol. 253: R666-670.

Chesler M, Kraig RP. 1989. Intracellular pH transients of mammalian astrocytes. J Neurosci. 9: 2011-2019.

Chuquet J, Hollender L, Nimchinsky EA. 2007. High-resolution in vivo imaging of the neurovascular unit during spreading depression. J Neurosci. 27: 4036-4044.

Czeh G, Aitken PG, Somjen GG. 1993. Membrane currents in CA1 pyramidal cells during spreading depression (SD) and SD-like hypoxic depolarization. Brain Res. 632: 195-208.

Duchen MR. 2004. Mitochondria in health and disease: perspectives on a new mitochondrial biology. Mol Aspects Med. 25: 365-451.

Fabricius M, Fuhr S, Bhatia R, Boutelle M, Hashemi P, Strong AJ, Lauritzen M. 2006. Cortical spreading depression and peri-infarct depolarization in acutely injured human cerebral cortex. Brain. 129: 778-790.

Fayuk D, Aitken PG, Somjen GG, Turner DA. 2002. Two different mechanisms underlie reversible, intrinsic optical signals in rat hippocampal slices. J Neurophysiol. 87: 1924-1937.

Feng G, Mellor RH, Bernstein M, Keller-Peck C, Nguyen QT, Wallace M, Nerbonne JM, Lichtman JW, Sanes JR. 2000. Imaging neuronal subsets in transgenic mice expressing multiple spectral variants of GFP. Neuron. 28: 41-51.

Gunter TE, Gunter KK, Sheu SS, Gavin CE. 1994. Mitochondrial calcium transport: physiological and pathological relevance. Am J Physiol. 267: C313-339.

Hansen AJ, Olsen CE. 1980. Brain extracellular space during spreading depression and ischemia. Acta Physiol Scand. 108: 355-365.

Jing J, Aitken PG, Somjen GG. 1994. Interstitial volume changes during spreading depression (SD) and SD-like hypoxic depolarization in hippocampal tissue slices. J Neurophysiol. 71: 2548-2551.

Kadenbach B. 2003. Intrinsic and extrinsic uncoupling of oxidative phosphorylation. Biochim Biophys Acta. 1604: 77-94.

Kimelberg HK. 1995. Current concepts of brain edema. Review of laboratory investigations. J Neurosurg. 83: 1051-1059.

Kimelberg HK. 2000. Cell volume in the CNS: regulation and implications for nervous system function and pathology. The neuroscientist. 6: 14-25.

Kirichok Y, Krapivinsky G, Clapham DE. 2004. The mitochondrial calcium uniporter is a highly selective ion channel. Nature. 427: 360-364.

Kovacs R, Kardos J, Heinemann U, Kann O. 2005. Mitochondrial calcium ion and membrane potential transients follow the pattern of epileptiform discharges in hippocampal slice cultures. J Neurosci. 25: 4260-4269.

Kraig RP, Ferreira-Filho CR, Nicholson C. 1983. Alkaline and acid transients in cerebellar microenvironment. J Neurophysiol. 49: 831-850.

Leão AAP. 1944. Spreading depression of activity in the cerebral cortex. J Neurophysiol. 7: 357-390.

Lipton P. 1999. Ischemic cell death in brain neurons. Physiol Rev. 79: 1431-1568.

MacVicar BA, Hochman D. 1991. Imaging of synaptically evoked intrinsic optical signals in hippocampal slices. J Neurosci. 11: 1458-1469.

Menna G, Tong CK, Chesler M. 2000. Extracellular pH changes and accompanying cation shifts during ouabain-induced spreading depression. J Neurophysiol. 83: 1338-1345.

Muller M, Somjen GG. 1998. Inhibition of major cationic inward currents prevents spreading depression-like hypoxic depolarization in rat hippocampal tissue slices. Brain Res. 812: 1-13.

Muller M, Somjen GG. 2000. Na^+ and K^+ concentrations, extra- and intracellular voltages, and the effect of TTX in hypoxic rat hippocampal slices. J Neurophysiol. 83: 735-745.

Nedergaard M, Cooper AJ, Goldman SA. 1995. Gap junctions are required for the propagation of spreading depression. J Neurobiol. 28: 433-444.

Nedergaard M, Goldman SA, Desai S, Pulsinelli WA. 1991. Acid-induced death in neurons and glia. J Neurosci. 11: 2489-2497.

Nicholls DG. 2008. Oxidative stress and energy crises in neuronal dysfunction. Ann N Y Acad Sci. 1147: 53-60.

Nielsen S, Nagelhus EA, Amiry-Moghaddam M, Bourque C, Agre P, Ottersen OP. 1997. Specialized membrane domains for water transport in glial cells: high-resolution immunogold cytochemistry of aquaporin-4 in rat brain. J Neurosci. 17: 171-180.

Nimmerjahn A, Kirchhoff F, Kerr JN, Helmchen F. 2004. Sulforhodamine 101 as a specific marker of astroglia in the neocortex in vivo. Nat Methods. 1: 31-37.

Orrenius S, Zhivotovsky B, Nicotera P. 2003. Regulation of cell death: the calcium-apoptosis link. Nat Rev Mol Cell Biol. 4: 552-565.

Paradiso AM, Tsien RY, Machen TE. 1984. Na^+-H^+ exchange in gastric glands as measured with a cytoplasmic-trapped, fluorescent pH indicator. Proc Natl Acad Sci U S A. 81: 7436-7440.

Pietrobon D, Striessnig J. 2003. Neurobiology of migraine. Nat Rev Neurosci. 4: 386-398.

Rakhit RD, Mojet MH, Marber MS, Duchen MR. 2001. Mitochondria as targets for nitric oxide-induced protection during simulated ischemia and reoxygenation in isolated neonatal cardiomyocytes. Circulation. 103: 2617-2623.

Rash JE, Yasumura T, Hudson CS, Agre P, Nielsen S. 1998. Direct immunogold labeling of aquaporin-4 in square arrays of astrocyte and ependymocyte plasma membranes in rat brain and spinal cord. Proc Natl Acad Sci U S A. 95: 11981-11986.

Salzberg BM, Obaid AL, Gainer H. 1985. Large and rapid changes in light scattering accompany secretion by nerve terminals in the mammalian neurohypophysis. J Gen Physiol. 86: 395-411.

Sanchez-del-Rio M, Reuter U. 2004. Migraine aura: new information on underlying mechanisms. Curr Opin Neurol. 17: 289-293.

Skulachev VP. 2006. Bioenergetic aspects of apoptosis, necrosis and mitoptosis. Apoptosis. 11: 473-485.

Snow RW, Taylor CP, Dudek FE. 1983. Electrophysiological and optical changes in slices of rat hippocampus during spreading depression. J Neurophysiol. 50: 561-572.

Somjen GG. 2001. Mechanisms of spreading depression and hypoxic spreading depression-like depolarization. Physiol Rev. 81: 1065-1096.

Strong AJ, Dardis R. 2005. Depolarisation phenomena in traumatic and ischaemic brain injury. Adv Tech Stand Neurosurg. 30: 3-49.

Sugaya E, Takato M, Noda Y. 1975. Neuronal and glial activity during spreading depression in cerebral cortex of cat. J Neurophysiol. 38: 822-841.

Takano T, Tian GF, Peng W, Lou N, Lovatt D, Hansen AJ, Kasischke KA, Nedergaard M. 2007. Cortical spreading depression causes and coincides with tissue hypoxia. Nat Neurosci. 10: 754-762.

Tong CK, Chesler M. 1999. Endogenous pH shifts facilitate spreading depression by effect on NMDA receptors. J Neurophysiol. 81: 1988-1991.

Vilagi I, Klapka N, Luhmann HJ. 2001. Optical recording of spreading depression in rat neocortical slices. Brain Res. 898: 288-296.

3. A NOVEL FORM OF REGENERATIVE GLUTAMATE RELEASE BY NMDA RECEPTORS CAUSES SPREADING DEPRESSION[2]

3.1. Introduction

Spreading depression (SD) is a slowly propagating wave of neuronal depolarization (Leão, 1944) that underlies migraine aura (Bowyer et al., 2001; Hadjikhani et al., 2001; Pietrobon and Striessnig, 2003) and also contributes to damage progress following ischemia (Dreier et al., 2006) and brain trauma (Strong et al., 2002; Fabricius et al., 2006). At the SD wavefront there is a profound depolarization indicated by extracellular potential shift of 5 to 10 mV and neuronal depolarization to approximately 0 mV for several minutes. SD spreads in a radial pattern from the initiation point and propagates in all directions through the cerebral cortex at a rate of 3-5 mm/min (Somjen, 2001). Van Harreveld first hypothesized that glutamate mediates SD, by diffusing from the releasing site and depolarizing adjacent cells and fibers, which in turn release more glutamate (Van Harreveld, 1959). This hypothesis was supported by evidence that glutamate was released during SD (Fabricius et al., 1993), and that glutamate initiated SD when applied to the brain (Van Harreveld, 1959). However, traditional synaptic transmission is not responsible for SD, because SD still propagates after the blockade of action potentials and VGCCs (Somjen, 2001). This raises the questions of first, whether significant glutamate release still occurs during SD after action potentials and VGCCs are blocked and second, what are the novel mechanisms underlying release of glutamate during SD.

The NMDA type glutamate receptor (NMDAR) plays a critical role in cortical and cerebellar SD, since SD can be suppressed by NMDAR antagonists (Lauritzen and Hansen, 1992; Lauritzen,

[2] A version of this chapter will be submitted for publication. Zhou N, Rungta RL, Feighan D, & MacVicar BA. A novel form of regenerative glutamate release by NMDA receptors causes spreading depression.

1994) and evoked by NMDAR agonists (Lauritzen et al., 1988). However, again the observations of SD propagation after action potentials and synaptic transmission were blocked, make it difficult to envisage a mechanism by which postsynaptic activation of NMDARs could lead to further release of glutamate at distant presynaptic sites. Even if the NMDAR-induced dendritic depolarization were sufficient to electrotonically depolarize presynaptic terminals without action potential generation (Alle and Geiger, 2006; Shu et al., 2006), transmitter release would still require VGCCs as the calcium source should be located close to presynaptic vesicles (Meinrenken et al., 2002). Given that SD propagation requires neither action potentials nor VGCC, it is reasonable to postulate that NMDARs contribute to SD by other mechanisms. Another mechanism is suggested by the recent compelling evidence that NMDARs are expressed at presynaptic terminals and enhance neurotransmission (Corlew et al., 2008). Electron microscopy has been used to directly visualize the presynaptic location of NMDARs in neocortex (Aoki et al., 1994; Corlew et al., 2007), hippocampus (Siegel et al., 1994; Jourdain et al., 2007), amygdale (Farb et al., 1995) and spinal cord (Liu et al., 1994). Physiological recordings have shown that presynaptic NMDARs can facilitate both spontaneous and evoked neurotransmitter release (Sjostrom et al., 2003; Bender et al., 2006; Corlew et al., 2007; Li and Han, 2007; Brasier and Feldman, 2008). Therefore we hypothesize that presynaptic NMDARs induce glutamate release during SD and that NMDAR induced-glutamate release could excite more NMDARs to trigger a regenerative glutamate release. If this mechanism is responsible for SD propagation, then one would predict the following. First, vesicular glutamate release during SD will still occur after blocking action potentials and VGCCs. Second, glutamate release during SD should be blocked by NMDAR antagonists. Third, direct activation of NMDARs should be able to trigger glutamate release independent of action potentials and VGCCs. Finally,

if the NMDARs are activated in a small area, the released glutamate should activate adjacent neurons to release more glutamate, resulting in a SD-like propagating wave.

Here, we used enzyme based glutamate electrodes in combination with electrophysiological recordings and intrinsic optical signals (IOS) to show that SD propagation is mediated by an unusual form of vesicular glutamate release that requires neither VGCCs nor neuronal spiking. This process depends on opening of presynaptic NMDARs and the consequent activation of NCX_{mito}. In addition, NMDAR activation alone is sufficient to induce glutamate release and generate an SD wave. As the released glutamate can diffuse to neighbouring terminals, this results in a vicious cycle of glutamate-induced glutamate release, underling the propagation of SD.

3.2. Methods

3.2.1. Slice preparation

Hippocampal and neocortical slices were prepared from 19-23 day old Sprague-Dawley rats. Treatment of animals was approved by the University of British Columbia Animal Care and Use Committee. Rats were anaesthetized with halothane (Sigma), decapitated and the brains removed into ice-cold slicing solution containing (in mM): 230 sucrose, 26 $NaHCO_3$, 10 D-glucose, 2.5 KCl, 1.25 NaH_2PO_4, 0.5 $CaCl_2$, and 10 $MgSO_4$. 400 μm thick transverse hemi-sections from hippocampus or cortical hemi-sections from neocortex (from Bregma 0 to Bregma -3 mm of rat brain) were sliced (Leica vibratome) in the slicing solution. Then the slices were transferred to a storage chamber with fresh ACSF containing the following (in mM): 128 NaCl, 2.5 KCl, 0.6 $MgCl_2$, 2.0 $CaCl_2$, 1.25 NaH_2PO_4, 26 $NaHCO_3$, and 10 D-glucose, and were

incubated at room temperature for >1 h before recording. All solutions were saturated with 95% O_2/5% CO_2.

3.2.2. Induction of SD

Individual slices were transferred to a recording chamber with slice supports that permit solution flow both above and below the slice and perfused rapidly with oxygenated ACSF (3 ml/min) at 30-32 °C. SD was induced by perfusing for 80-90 sec high K^+ solution containing the following (in mM): 90.5 NaCl, 40 KCl, 0.6 $MgCl_2$, 2.0 $CaCl_2$, 1.25 NaH_2PO_4, 26 $NaHCO_3$, and 10 D-glucose. SD could be reliably induced in 100% of slices by the application of high K^+ ACSF at a speed of 3 ml/min. The 0-Ca^{2+} ACSF contains (in mM): 126 NaCl, 2.5 KCl, 1.5 $MgCl_2$, 2.0 EGTA, 1.25 NaH_2PO_4, 26 $NaHCO_3$, and 10 D-glucose, pH 7.35; and the 0-Ca^{2+}/high K^+ solution contains (in mM): 88.5 NaCl, 40 KCl, 1.5 $MgCl_2$, 2.0 EGTA, 1.25 NaH_2PO_4, 26 $NaHCO_3$, and 10 D-glucose, pH 7.35.

3.2.3. Recording SD propagation

The IOS was monitored to identify the onset and propagation of SD as reported in our previous studies (Basarsky et al., 1998) (Figure 3.1). IOS data was collected from the transmitted light of the brain slices and the transient of IOS represented SD. The intrinsic optical imaging system was composed of a CCD camera (DAGE-MTI) connected to a DT3155 frame grabber (Data Translation) controlled by Imaging Workbench 5.0 software (INDEC). The illumination source was a standard Zeiss tungsten bulb whose output was directed through a 750DF20 filter.

Normalized IOS was defined as $\Delta T = (T_1 - T_0)/T_0$, where T_1 and T_0 are transmitted light intensity of the small region close to the recording site at a certain time point and at the beginning, respectively. IOS changes (Figure 3.1g, top trace) occurred simultaneously with the extracellular DC-potential shifts associated with SD (bottom trace). In all the experiments the IOSs were recorded simultaneously with real-time glutamate measurement to indicate the occurrence of SD.

3.2.4. Glutamate measurement

Real-time glutamate concentration changes were detected by enzyme-based microelectrode arrays (MEA) coated with glutamate oxidase (GluOx). Preparation of the ceramic-based MEA for recording has been extensively described in (Burmeister et al., 2002; Rutherford et al., 2007). Briefly, the platinum recording sites were dip coated with Nafion® and recording site 1 (out of 4 total sites) was coated with GluOx. The GluOx layer caused the enzymatic break-down of glutamate to α-ketoglutarate and H_2O_2. A potential of +0.7 V was applied to the MEA to oxidize H_2O_2 and generate electrons. The resulting current was amplified and recorded by a FAST recording system (Quanteon LLC, Lexington KY). Microelectrode recording sites 2 to 4 were used as self-referencing sites. When the currents from self-referencing sites were subtracted from site 1, the resulting signal represented glutamate measures. The MEA was calibrated with 20, 40 and 60 μM of glutamate solutions each day before experiments to calculate the slope (nA/μM) and R^2. To measure the extracellular glutamate changes, the tip of the MEA was positioned in the layer II/IV of the cortex with the GluOx coating site gently touching the surface of the brain slice. The final change of glutamate concentration was calculated as: Glutamate Concentration (μM) = current (nA) / slope (nA/μM). The change of glutamate concentration was calculated by the peak glutamate concentration during SD minus the baseline glutamate

concentration. The baseline concentration was calculated by the averaged glutamate concentration during the 2 minutes before high K^+ application. Because MEA recording could not be combined with other electrophysiology recordings, all the glutamate measurement experiments were performed with simultaneous IOS imaging to indicate the occurrence of SD onset.

3.2.5. Electrophysiology

Field EPSPs (fEPSPs) were evoked by stimulation of the Schaffer collateral pathway of hippocampus and recorded from stratum radiatum using a bipolar tungsten-stimulating electrode. Glass micropipettes filled with ACSF (resistance, 1–3MΩ) were used to measure CA1 fEPSPs in stratum radiatum. fEPSP signals were amplified 1000 times with an AC amplifier, bandpass filtered at 1000 Hz, digitized at 10 kHz using a Digidata 1440A, and transferred to a computer for analysis. fEPSPs were evoked every 30 s (0.03 Hz) and data were analyzed using Clampfit 10.0. Sample traces were the average of five sweeps from a recording that was included in the plot of the mean normalized fEPSP slope.

SD-related extracellular DC potentials were recorded from the stratum radiatum of hippocampus. The DC potential changes were recorded with one recording glass electrode within the slice and the other reference glass electrode in the bath. The potential changes were calculated by the difference of the potentials recorded from the two electrodes. DC-coupled field potentials were recorded with glass micropipettes filled with ACSF (resistance, 1–3MΩ) and were monitored with current-clamp mode of MultiClamp 700B amplifier, acquired via a Digidata 1440A. Data were sampled at 10 kHz, and most were low-pass filtered at 1 kHz. The traces of DC potential

changes were obtained by subtracting the potential of the reference channel from the potential of the recording channel.

3.2.6. Drugs

Alomone labs supplied TTX, applied continuously with 5 min incubation. Bioblocks supplied (R*,S*)-(2,8-Bis-trifluoromethyl-quinolin-4-yl)-piperidin-2-yl-methanol hydrochloride (mefloquine), applied continuously with 10 min incubation. Cedarlane Labs supplied CNQX; applied continuously with 20 min incubation; bafilomycin A1, applied with 3-5 hours incubation. Sigma supplied cadmium chloride, applied continuously with 5 min incubation; sulfasalazine, applied continuously with 10 min incubation; carbenoxolone, applied continuously with 10 min incubation; N-Methyl-D-aspartic acid (NMDA) and glycine, applied for 2-3 min or puffed from a glass pipette; (+)-cis-Diltiazem hydrochloride (diltiazem), applied continuously with 10 min incubation. Tocris supplied DL-2-Amino-5-phosphonopentanoic acid (DL-APV), applied continuously with 20 min incubation; DL-threo-b-Benzyloxyaspartic acid (DL-TBOA), applied continuously with 10 min incubation; CGP-37157 applied continuously with 3-5 hours incubation.

3.2.7. Data analysis

In all cases one-way ANOVA was used for statistical comparisons, with $p < 0.05$ considered significant. Values are reported as the mean ± SEM.

3.3. Results

3.3.1. Glutamate is released in SD without AP and VGCC

We first determined whether glutamate release still occurred from brain tissue during SD when synaptic transmission was blocked. Perfusing high external K^+ solution consistently triggered an SD in normal solutions that was measured as an extracellular DC potential shift of approximately 4 mV and a correlated propagating IOS transient consistent with previous reports (Basarsky et al., 1998; Anderson and Andrew, 2002) (Figure 3.1). Using an enzyme based glutamate electrode positioned within the brain slice (Rutherford et al., 2007) we detected a significant increase in extracellular glutamate during SD, approximately 50 to 100 seconds in duration (peak during SD, 93.2±10.2 μM, n=7). In response to the SD wave, this increase of extracellular glutamate occurred temporally coincident with propagation of the IOS component and reached a peak in about 5-10 seconds (Figure 3.1g). When synaptic transmission was completely blocked by tetrodotoxin (TTX, 1 μM, to block action potentials) and Cd^{2+} (30 μM, to inhibit high threshold VGCCs), no evoked field excitatory synaptic potentials (fEPSP) were observed (n=3, Figure 3.2a, b and Figure 3.3), yet high K^+ still evoked a robust propagating SD wave of similar amplitude to control (4.39±0.57 mV, n=6 in control versus 4.20±0.43 mV, n=5 in TTX and Cd^{2+}, $p>0.05$, Figure 3.2c, d). Under these conditions we still observed a dramatic glutamate increase during SD (52.4±6.3 μM in TTX and Cd^{2+}, n=8, Figure 3.2e, f). To be certain we had eliminated calcium entry via all VGCCs including T-type, we used a higher dose of Cd^{2+} (200 μM) and included Ni^{2+} (300 μM) (Huguenard, 1996; Tai et al., 2006). Under these conditions, SD still occurred and the associated glutamate release was not affected (40.2±8.1 μM, n=4, $p>0.05$ compared to 30 μM Cd^{2+} and TTX, Figure 3.2f). These data demonstrate that a large and

Figure 3.1. IOS changes are coincident with extracellular potential changes and glutamate transients during SD. (a) The brightfield image of a cortical slice before induction of SD. (b)-(f) Time series of the IOS difference signal from the same cortical brain slice during the initiation and spread of SD. The propagation of SD waveform was shown by the change of IOS (at indicated time points (min:sec)) after high K^+ perfusion. The asterisk shows the position of the glutamate enzyme multielectrode array recording site. (g) The IOS changes during SD (top trace) were temporally correlated with both glutamate efflux transients (middle trace) and the extracellular potential shifts (bottom trace). The arrow indicates the time point when high K^+ was washed out.

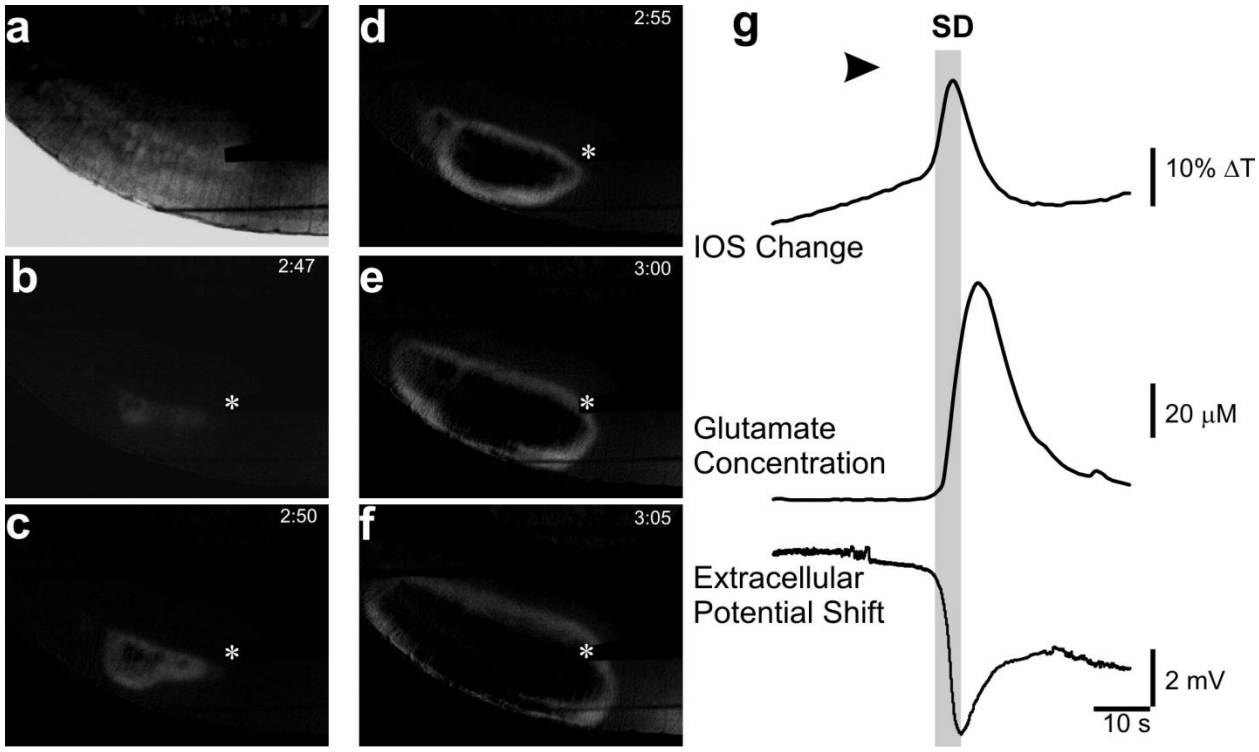
a
b
2:47
c
2:50
d
2:55
e
3:00
f
3:05
g
SD
10% ΔT
IOS Change
20 μM
Glutamate
Concentration
Extracellular
Potential Shift
2 mV
10 s

Figure 3.2. SD-associated glutamate release is independent of action potentials and VGCCs. (**a**) Evoked fEPSPs were blocked by TTX and Cd^{2+}. (**b**) Quantification of evoked fEPSPs blocked by TTX and Cd^{2+}. (**c**) Top traces show high K^+ application (indicated by the gray bar) triggered SD as indicated by the extracellular potential shift. Expanded traces demonstrate that the SD extracellular waveforms were not affected by TTX and Cd^{2+}. The propagation of SD was apparent in the spreading IOS signal (Fig.1) (**d**) Quantification of SD-related potential shift in control and with TTX and Cd^{2+}. (**e**) High K^+ evoked-propagating SDs were correlated with a large efflux of glutamate that occurred when the SD waveform propagated to the site of the glutamate electrode (timing indicated by dotted line). TTX and Cd^{2+} only partially inhibited the glutamate release. (**f**) Quantification of SD-related glutamate release. High doses of Cd^{2+} and Ni^{2+} did not additionally inhibit the glutamate concentration. In all figures, experimental values are the mean ± s.e.m. Double asterisk, $P < 0.01$.

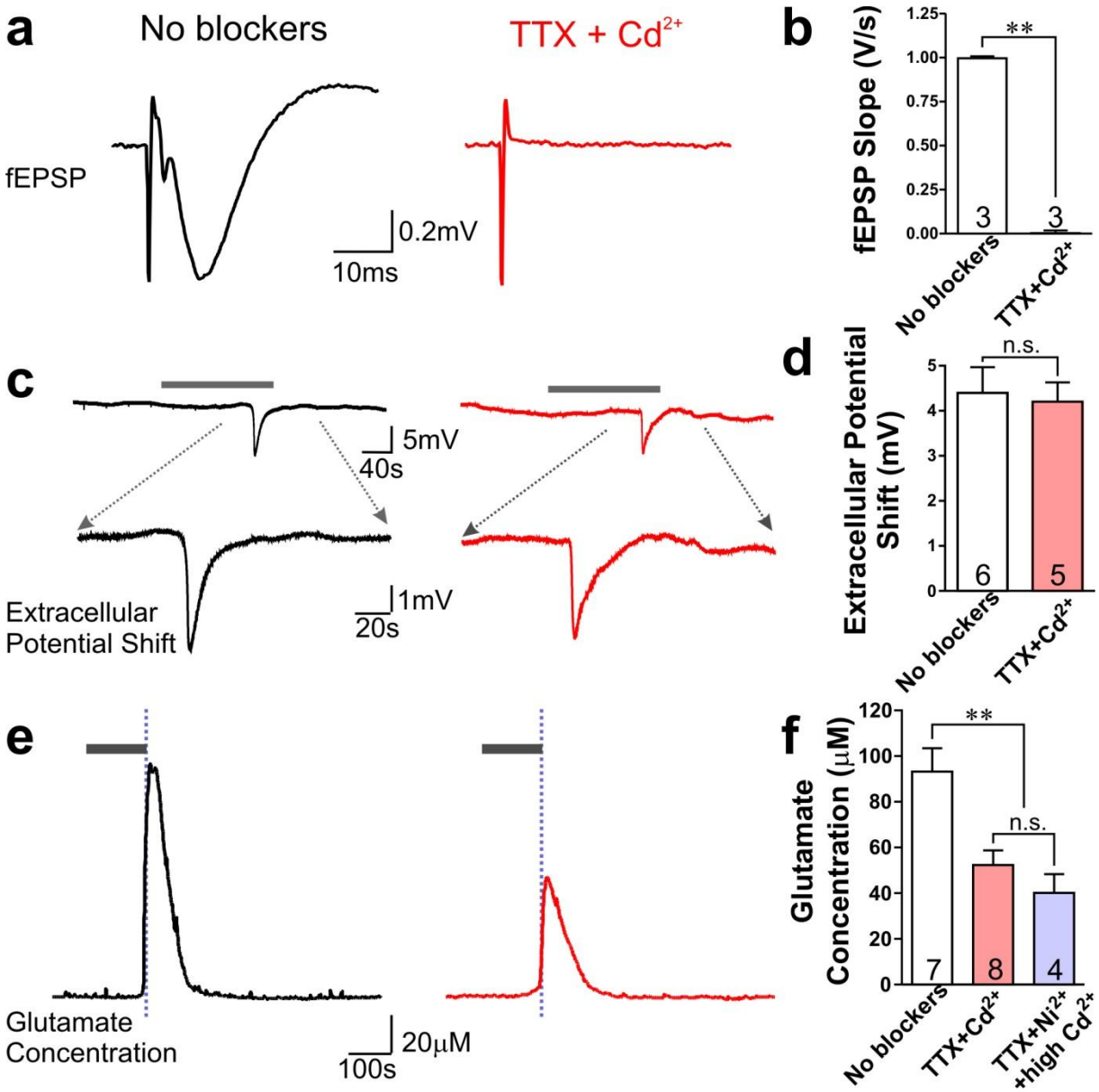
a
No blockers
TTX + Cd2+
fEPSP
0.2mV
10ms
b
fEPSP Slope (V/s)
1.25
1.00
0.75
0.50
0.25
0.00
**
3
3
No blockers
TTX+Cd2+
c
5mV
40s
Extracellular
Potential Shift
1mV
20s
d
Extracellular Potential Shift (mV)
n.s.
5
4
3
2
1
0
6
5
No blockers
TTX+Cd2+
e
Glutamate
Concentration
20μM
100s
f
Glutamate Concentration (μM)
120
100
80
60
40
20
0
**
n.s.
7
8
4
No blockers
TTX+Cd2+
TTX+Ni2+
+high Cd2+

Figure 3.3. TTX and Cd^{2+} completely block synaptic transmission in hippocampal slices. The fEPSP was abolished by Cd^{2+} (30 μM, red trace) compared with control (black trace); additional application of TTX (1 μM) abolished the presynaptic volley (green trace) that indicates the action potentials on presynaptic fibers (n=3).

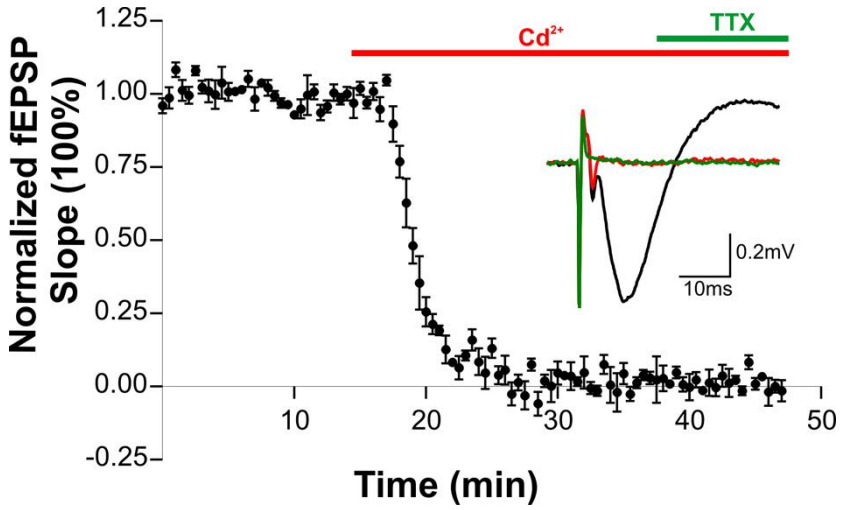
Normalized fEPSP Slope (100%)
1.25
1.00
0.75
0.50
0.25
0.00
-0.25
10
20
30
40
50
Time (min)
Cd2+
TTX
0.2mV
10ms

transient spike of glutamate release occurs during SD, which is not the result of action potentials or calcium entry through VGCCs.

3.3.2. SD glutamate is released by vesicular exocytosis

We next examined whether the mechanism underlying the increase in extracellular glutamate observed during SD was due to the exocytosis of glutamate-filled vesicles, or due to other non-vesicular mechanisms including glutamate transporters (Rossi et al., 2000), cystine-glutamate exchanger (Warr et al., 1999), pannexin (Thompson et al., 2006) or connexin hemichannels (Ye et al., 2003). We tested each of the possibilities in the presence of TTX and Cd^{2+} in order to isolate the novel release mechanism during SD which did not involve Na^{+} dependent action potentials or VGCCs. To test vesicular exocytosis we pre-treated the slices with bafilomycin A1, a potent and specific inhibitor of vacuolar H^{+}-ATPase (V-ATPase) that inhibits vesicular glutamate release by preventing glutamate transport into synaptic vesicles (Zhou et al., 2000). We first observed that fEPSPs were almost totally blocked by incubating slices in bafilomycin (10 μM) for >3 hr (Figure 3.4) then TTX and Cd^{2+} were applied. Bafilomycin greatly inhibited both SD glutamate release (5.2±0.6 μM, n=6, $p<0.001$, Figure 3.5a, c) and the extracellular potential shift (0.04±0.04 mV, n=9, $p<0.001$, Figure 3.5b, d). This indicates that glutamate is released during SD by a mechanism that still requires vesicular exocytosis. In contrast, none of the inhibitors of the other potential sources of glutamate release had any significant effect on SD evoked glutamate release (Figure 3.5e). Inhibiting glutamate transporters with TBOA (30 μM), which also inhibits reversed transport (Rossi et al., 2000), had no effect on glutamate transients during SD (45.9±11.2 μM, n=5, $p>0.05$). Blocking export of glutamate out of cells by inhibiting the cystine-glutamate exchanger with sulfasalazine (250 μM) (Lo et al., 2008) also did not

Figure 3.4. Input-output relationship of fEPSP after incubation of bafilomycin. Input-output relationship of fEPSP in control slices (black, n=6) and bafilomycin-treated slices (red, n=9) shows bafilomycin (10 μM) largely inhibits presynaptic transmitter release in hippocampal slices**.**

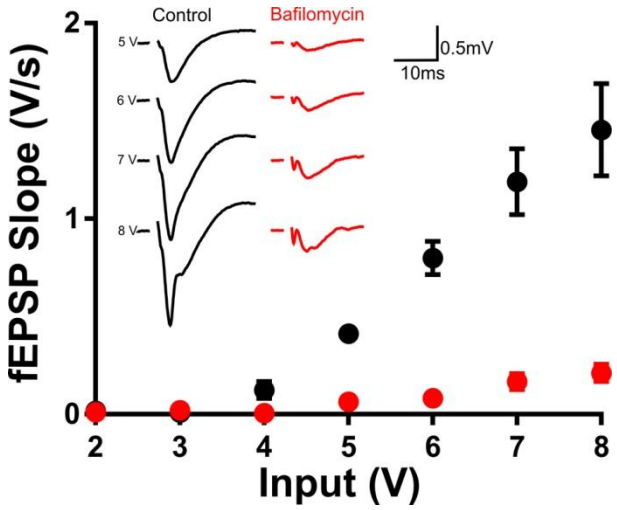
Control
Bafilomycin
5 V
6 V
7 V
8 V
0.5mV
10ms
fEPSP Slope (V/s)
Input (V)
0
1
2
2
3
4
5
6
7
8

Figure 3.5. Bafilomycin inhibits both the glutamate release and waveforms of SD showing that SD requires TTX and Cd^{2+}-insensitive vesicular release. Incubating slices in 10 μM bafilomycin (red traces) for sufficient time to inhibit synaptic transmission (Figure 3.4) blocked SD glutamate release in cortical slices (**a**) and the SD extracellular potential shifts in hippocampal slices (**b**) as compared to vehicle treated brain slices (black traces). Grey bars indicate the high K^+ application. Quantification of the glutamate release (**c**) and the extracellular potential shifts (**d**). (**e**) Quantification of glutamate release during SD showing, compared to control slices, no effect of TBOA, sulfasalazine, mefloquine or carbenoxolone. Double asterisk, $P < 0.01$.

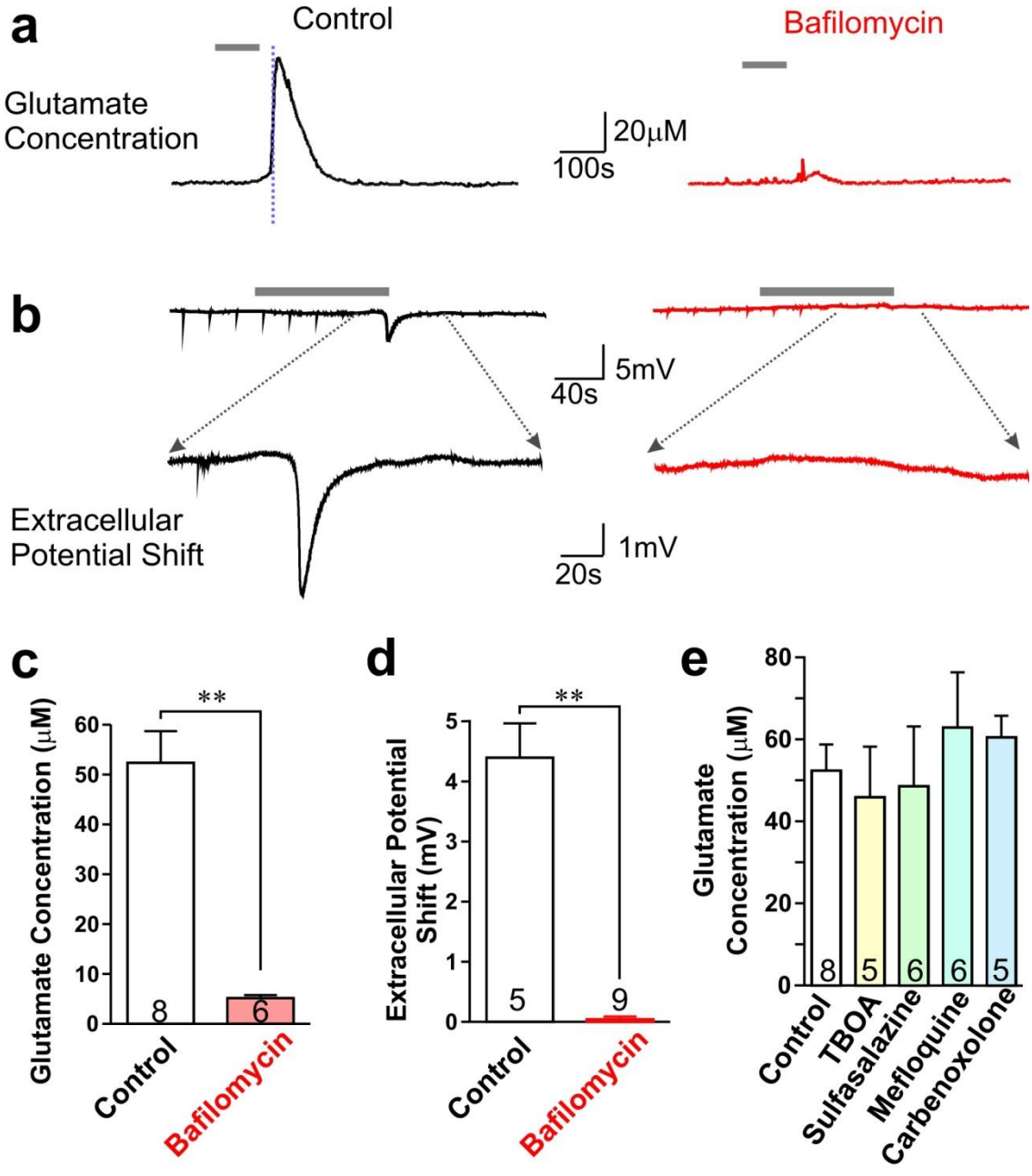
a
Control
Bafilomycin
Glutamate Concentration
20μM
100s
b
5mV
40s
Extracellular Potential Shift
1mV
20s
c
Glutamate Concentration (μM)
**
8
6
Control
Bafilomycin
d
Extracellular Potential Shift (mV)
**
5
9
Control
Bafilomycin
e
Glutamate Concentration (μM)
8
5
6
6
5
Control
TBOA
Sulfasalazine
Mefloquine
Carbenoxolone

reduce SD-associated glutamate release (48.5±14.6 μM, n=6, p>0.05). Finally, although connexin (Contreras et al., 2002; Retamal et al., 2007) and pannexin (Thompson et al., 2006) gap junction hemichannels allow permeation of glutamate during ischemia, we found that the pannexin and connexin hemichannel blockers mefloquine (Iglesias et al., 2008; Iglesias et al., 2009) (0.5 μM)(60.9±13.4 μM, n=6, p>0.05) and carbenoxolone (Bruzzone et al., 2005) (100 μM)(60.4±5.3 μM, n=5, p>0.05) failed to inhibit SD glutamate release. These data support only vesicular exocytosis as the source for glutamate release during SD.

3.3.3. SD glutamate release is dependent upon NMDAR

Exocytosis of synaptic vesicles at presynaptic sites requires elevation of cytosolic Ca^{2+} which, during normal synaptic transmission, results from calcium entry via VGCCs. Considering that our results to this point have shown that glutamate exocytosis during SD does not require VGCCs, we tested for alternative sources of calcium entry. NMDAR activation has been previously reported to be critical for SD propagation (Lauritzen, 1994). Recently, NMDARs have been localized to presynaptic terminals (Aoki et al., 1994; Jourdain et al., 2007), the activation of which can promote excitatory neurotransmitter release in the neocortex and hippocampus (Corlew et al., 2008). To test the hypothesis that the release of glutamate from presynaptic terminals occurs during SD as a result of activation of NMDARs, we pre-treated brain slices with the NMDAR antagonist APV (200 μM) (>15 minutes) and included APV in all the recording solutions. APV had little effect on evoked fEPSPs (85.7%, n=4, p>0.05). However, SD glutamate release was abolished by APV (2.5±0.4 μM, n=6, p<0.001, Figure 3.6b, d), and no propagating IOS signals or potential shifts were detected during high K^+ perfusion (Figure 3.6c, e). AMPA and kainate glutamate receptors are important for fast synaptic

Figure 3.6. SD glutamate release in TTX and Cd^{2+} requires activation of NMDARs. (**a**) CNQX, the AMPA/kainate receptor antagonist , but not APV, the NMDAR antagonist, abolished evoked fEPSPs. After TTX and Cd^{2+} were perfused to block action potentials and calcium channels, CNQX had no effect on SD glutamate release (**b**) or on the SD waveform (**c**) whereas APV blocked both the glutamate release and SD waveform. High K^+ application is indicated as the gray bar. Quantification of the SD glutamate release (**d**) and SD waveforms (**e**) in CNQX or APV. (**f**) SD-waveforms and SD glutamate release were blocked in a dose-dependent manner by raising $[Mg^{2+}]_o$. (**g**) Bath application of NMDA and glycine induced glutamate release in the presence of TTX and Cd^{2+} but this glutamate release was blocked by pre-treatment with bafilomycin. (**h**) Local application of NMDA induces a SD-like wave of IOS in the presence of TTX and Cd^{2+}. The left image shows the IOS of a cortical slice before NMDA application. The other images show SD propagation indicated by IOS signals (at indicated time points (min:sec)) after NMDA ejection at 0:00. Single asterisk, $P < 0.05$; double asterisk, $P < 0.01$.

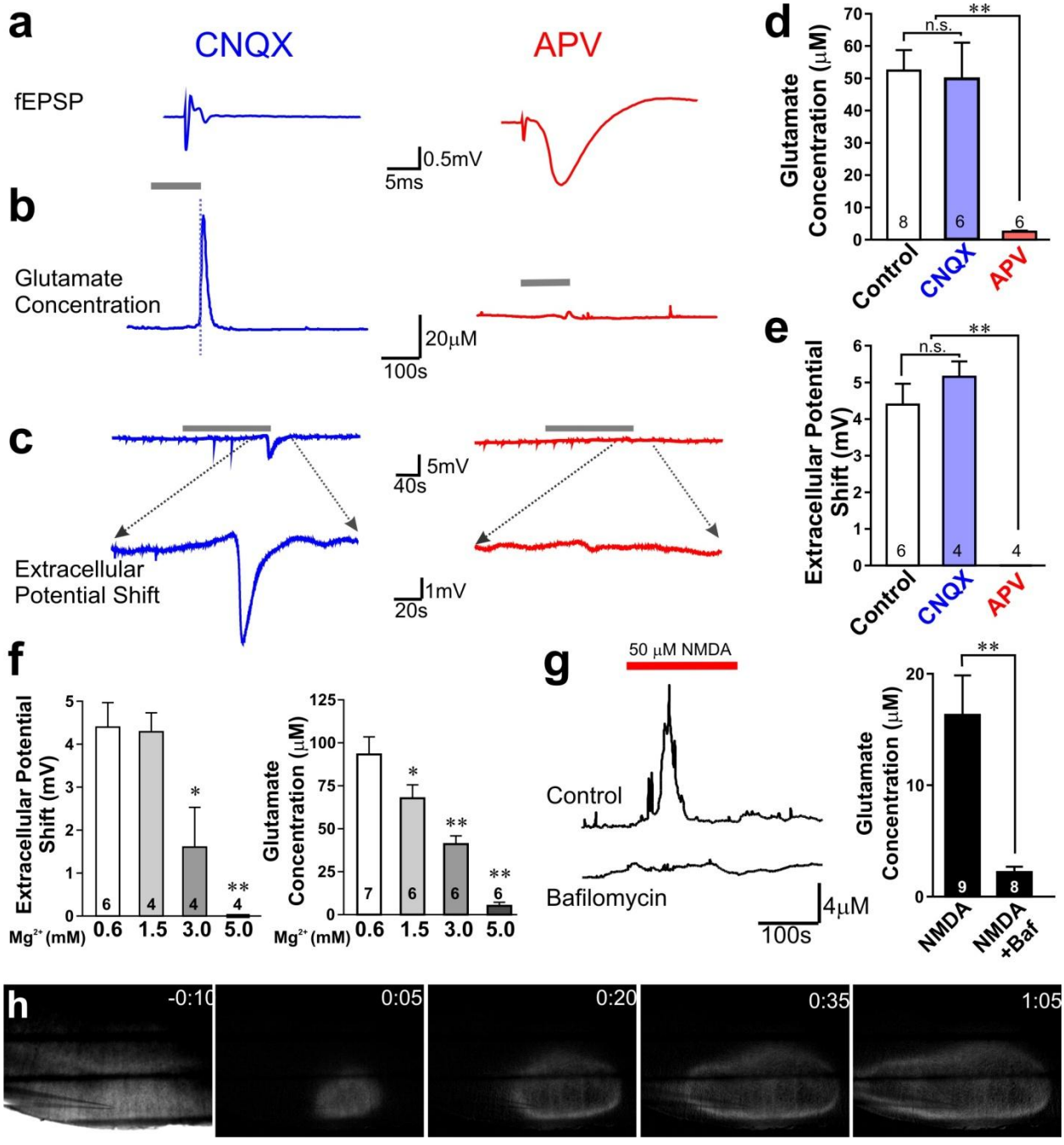
a
CNQX
APV
fEPSP
0.5mV
5ms
b
Glutamate
Concentration
20μM
100s
c
Extracellular
Potential Shift
5mV
40s
1mV
20s
d
Glutamate
Concentration (μM)
n.s.
**
Control
CNQX
APV
e
Extracellular Potential
Shift (mV)
n.s.
**
Control
CNQX
APV
f
Extracellular Potential
Shift (mV)
Mg2+ (mM) 0.6 1.5 3.0 5.0
Glutamate
Concentration (μM)
Mg2+ (mM) 0.6 1.5 3.0 5.0
g
50 μM NMDA
Control
Bafilomycin
4μM
100s
Glutamate
Concentration (μM)
**
NMDA
NMDA
+Baf
h
-0:10
0:05
0:20
0:35
1:05

transmission and may modulate presynaptic neurotransmitter release at some synapses (Pinheiro and Mulle, 2008). Therefore, we tested whether blockade of these glutamate receptors also prevented SD. The AMPA/kainate receptor antagonist CNQX (20 μM) completely inhibited evoked fEPSPs (1.7%, n=3, $p<0.001$, Figure 3.6a), but did not reduce either SD glutamate release (49.7±11.2 μM, n=6, $p>0.05$, Figure 3.6b, d) or SD field potential shifts (5.15±0.42 mV, n=4, $p>0.05$, Figure 3.6c, e). Therefore AMPA and kainate receptors are not involved in either the mechanism of SD propagation or in the glutamate release underlying SD. To further confirm the NMDAR-dependence of the glutamate release, we evoked SD in solutions containing different concentrations of Mg^{2+}, the voltage-dependent NMDAR channel blocker. Mg^{2+} will also differentiate between neuronal NMDARs that are sensitive to extracellular Mg^{2+} and astrocyte NMDARs that are Mg^{2+} insensitive at concentrations up to 10 mM (Lalo et al., 2006). Both SD potential shifts and SD glutamate release were inhibited by Mg^{2+} in a dose-dependent manner, showing complete block at 5 mM, (n=6, Figure 3.6f). These data indicate that NMDAR-dependent glutamate release from neurons but not astrocytes is critical for SD propagation.

3.3.4. Activation of NMDAR triggers glutamate release in the absence of AP and VGCC

If the exocytosis of glutamate-containing vesicles during SD is coupled to NMDAR opening, we hypothesized that NMDAR agonists should directly trigger glutamate release even when action potentials and VGCCs are blocked. Consistent with this idea, bath application of 50 μM of NMDA and 10 μM of glycine in the presence of TTX and Cd^{2+} induced significant glutamate release from brain slices (16.3±3.5 μM, n=9, Figure 3.6g). Pre-incubation of the slices with bafilomycin A1 abolished NMDA-induced glutamate release (2.2±0.5 μM, n=8, $p<0.01$)

indicating that the glutamate efflux was vesicular. Seeing that NMDAR activation causes glutamate release, and that NMDARs are themselves activated by glutamate, we hypothesized that regenerative NMDAR-dependent glutamate release could constitute a mechanism for SD wave propagation. For instance, if the rise in extracellular glutamate that occurred as a consequence of NMDAR activation could diffuse and activate NMDARs on adjacent synapses, the process could reinitiate thereby triggering a propagating wave. To test this idea we focally ejected NMDA from a glass pipette onto the surface of brain slices to rapidly activate NMDARs in a given region in the presence of TTX and Cd^{2+}. Notably, we observed a propagating IOS wave triggered initially at the injection site (Figure 3.6h), indicating that NMDAR activation is sufficient to evoke an SD-like wave by triggering regenerative glutamate release that is independent of VGCCs and action potentials.

3.3.5. SD glutamate release involves activation of NCXmito in the absence of Ca^{2+} entry

NMDARs are permeable to Ca^{2+} and thus Ca^{2+} entry through NMDAR might be a source for the elevation of cytosolic [Ca^{2+}] required for vesicular SD glutamate release. However in 0-Ca^{2+} external solutions in the presence of TTX and Cd^{2+} SD still occurred and glutamate release was only slightly decreased (37.3±6.7 μM, n=7, $p<0.05$ compared to control ACSF , Figure 3.7a, b and SD potential shift 6.87±0.77 mV, n=6, Figure 3.7c, d). These data indicate that Ca^{2+} influx through NMDARs is not a significant cause of glutamate release and suggest that release of Ca^{2+} from intracellular stores is likely important to evoke glutamate release during SD. Mitochondria are reservoirs for Ca^{2+} and are abundant in presynaptic terminals adjacent to synaptic vesicles at active zones (Rowland et al., 2000). The mitochondrial NCX_{mito} can export Ca^{2+} from the mitochondrial matrix when cytosolic Na^{+} increases thereby elevating cytosolic Ca^{2+} level (Castaldo et al., 2009) and inducing neurotransmitter release under some pathological conditions

Figure 3.7. SD glutamate release in 0 $[Ca^{2+}]_o$, TTX and Cd^{2+} is blocked by inhibitors of NCX_{mito}. (**a**) SD and the transient glutamate release still occurred when extracellular Ca^{2+} was removed (0 $[Ca^{2+}]_o$) in TTX and Cd^{2+} (control). Blocking NCX_{mito} with either DTZ or CGP significantly reduced SD glutamate release (**a**, **b**) and SD waveforms (**c**, **d**) as compared to control solution containing 0 $[Ca^{2+}]_o$, TTX and Cd^{2+}. (**e**, **f**) Bath application of NMDA in 0 $[Ca^{2+}]_o$, TTX and Cd^{2+} solution induced glutamate release, which was blocked by CGP.

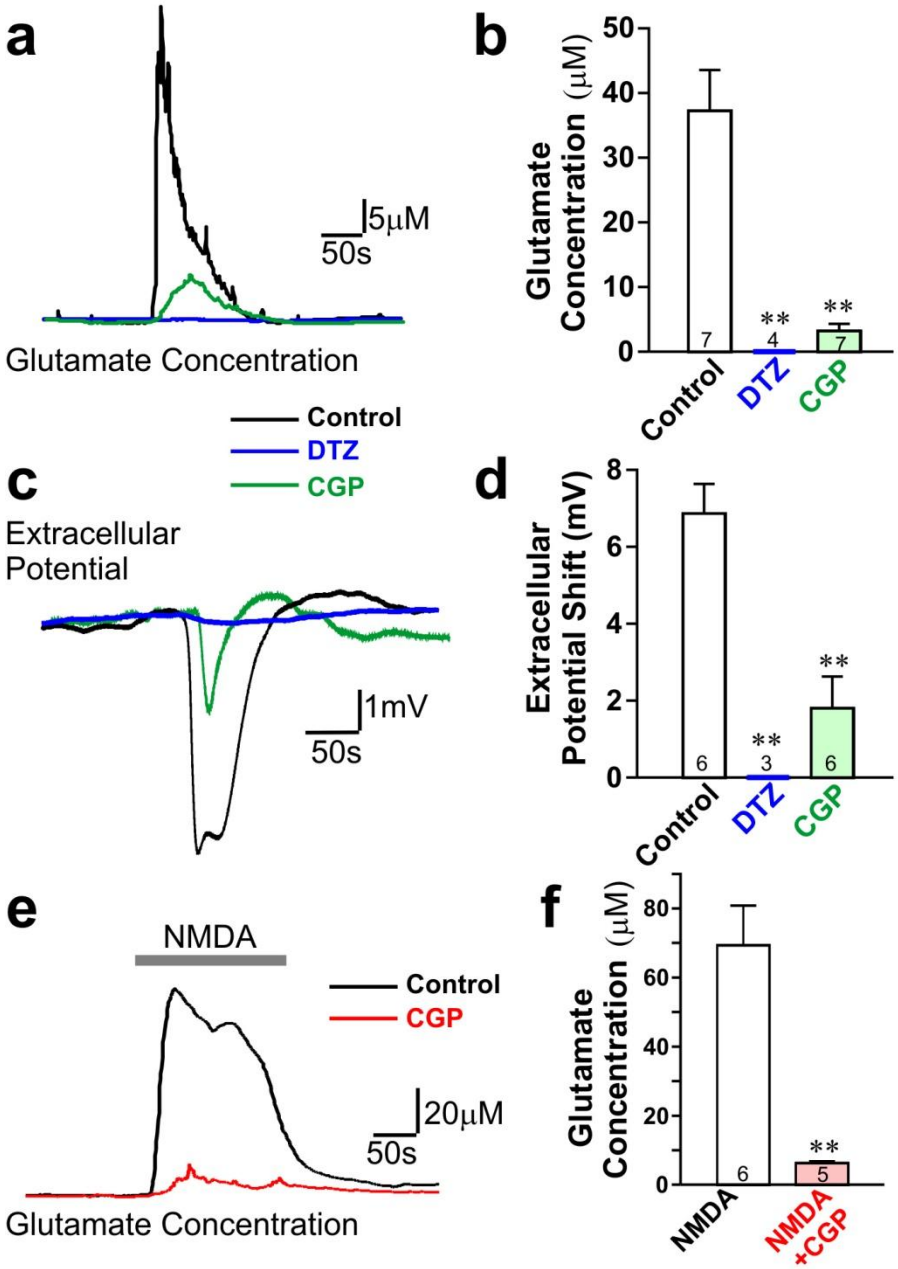
a
5μM
50s
Glutamate Concentration
Control
DTZ
CGP
b
Glutamate Concentration (μM)
50
40
30
20
10
0
7
**
4
**
7
Control
DTZ
CGP
c
Extracellular Potential
1mV
50s
d
Extracellular Potential Shift (mV)
8
6
4
2
0
6
**
3
**
6
Control
DTZ
CGP
e
NMDA
Control
CGP
20μM
50s
Glutamate Concentration
f
Glutamate Concentration (μM)
80
60
40
20
0
6
**
5
NMDA
NMDA +CGP

(Raiteri et al., 2007). Na^+ entry through NMDAR may lead to Ca^{2+} efflux from mitochondria via NCX_{mito}. Because the molecular identity of NCX_{mito} is still unknown and molecular manipulations of this protein are not yet possible, we investigated the involvement of NCX_{mito} by testing the NCX_{mito} blockers diltiazem (DTZ) and CGP-37157 (CGP) (Castaldo et al., 2009) in the presence of TTX, Cd^{2+} and 0 external Ca^{2+}. DTZ (500 μM) abolished both the SD glutamate release (0.0±0.0, n=4, $p<0.01$, Figure 3.7a, b) and the potential shifts (0.0±0.0, n=3, $p<0.01$, Figure 3.7c, d). Although DTZ also blocks L-type Ca^{2+} channels this should not be a factor because the solutions contained Cd^{2+} which inhibits these channels. Similarly, CGP-37157 (20 μM), inhibited both SD glutamate transients (6.2±0.5 μM, n=6, $p<0.05$) and SD potential shifts (2.08±0.63mV, n=8, $p<0.001$). These results suggest that Ca^{2+} efflux from NCX_{mito} as a result of high cytosolic Na^+ acts as a key step in triggering glutamate release during SD.

3.3.6. Activation of NMDAR induced glutamate release is dependent on NCX_{mito} activity

Finally, we examined whether NMDAR activation in the absence of Ca^{2+} entry could trigger glutamate release and whether it required NCX_{mito} activity. We bath applied NMDA (100 μM) and glycine (10 μM) with 0-Ca^{2+}ACSF containing TTX and Cd^{2+}. Under this condition, NMDA still triggered glutamate release from brain slices (69.4±11.4 μM, n=6, Figure 3.7e, f) and pre-incubation of the slices with CGP-37157 significantly inhibited the glutamate release evoked by NMDA (6.2±0.5 μM, n=5, $p<0.01$). These data suggest that sodium influx evoked by NMDAR activation can act via NCX_{mito} to release calcium from mitochondria in presynaptic terminals and thereby trigger vesicular release of glutamate.

Figure 3.8. Diagram of SD model involving NMDA-evoked glutamate release. In the present model, glutamate plays the key role in mediating the SD wave by activating presynaptic NMDARs. NMDARs are permeable to both Ca^{2+} and Na^{+}, which leads to two pathways to induce transmitter release. First, Ca^{2+} influx via NMDAR that are located at presynaptic sites may directly facilitate and/or trigger vesicle release. Second, Na^{+} entry via NMDAR increases cytosolic [Na^{+}], which activates NCX_{mito}. NCX_{mito} transports Na^{+} from the cytosol into the mitochondrial matrix exchanging against Ca^{2+}. The released Ca^{2+} from mitochondria can also evoke the release of glutamate-containing vesicles. The released glutamate further activates NMDAR on the same terminal to form a positive feedback. Glutamate can also activate postsynaptic NMDAR that causes the profound depolarization of SD, or can diffuse to adjacent terminals to evoke regenerative glutamate release by the same mechanism.

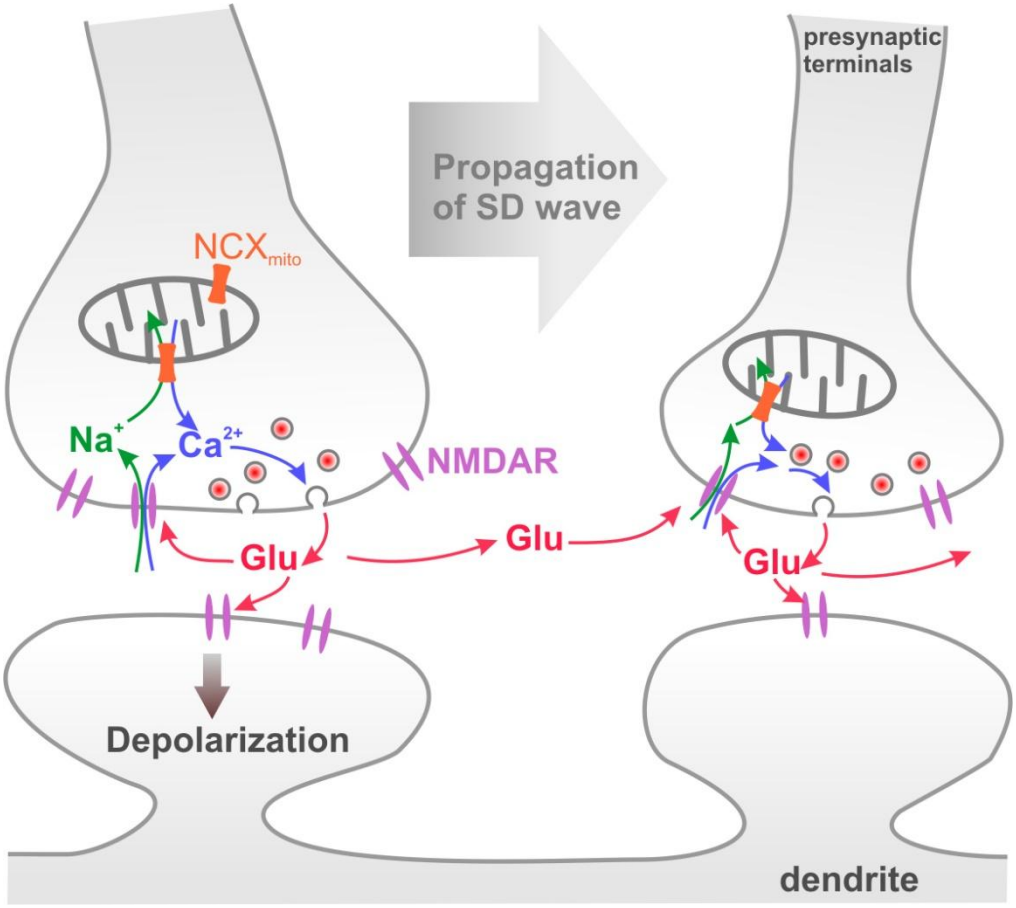
presynaptic terminals
Propagation of SD wave
NCX$_{mito}$
Na$^+$
Ca^{2+}
NMDAR
Glu
Glu
Glu
Depolarization
dendrite

3.4. Discussion

Here we show an unusual form of regenerative glutamate release that occurs during SD and is required for SD propagation. This mechanism is independent of action potentials and VGCCs. In contrast with classic presynaptic neurotransmitter release, glutamate release during SD requires opening of NMDARs likely on presynaptic sites (Figure 3.8). The activation of NMDARs induces presynaptic vesicular exocytosis by either Ca^{2+} influx via NMDARs or activation of NCX_{mito}. The released glutamate will in turn activate more presynaptic NMDARs on the same neuron or on adjacent neurons leading to further glutamate release. Our data suggests that it is this positive feedback that underlies the propagation of SD.

The conventional views postulate that SD is initiated by activating presynaptic VGCCs (in particular P/Q-type) and consequent releasing of glutamate from recurrent cortical pyramidal cell synapses; and activation of postsynaptic NMDAR is the important component of the positive feedback cycle that ignites SD (Pietrobon and Striessnig, 2003). This is supported by the findings that the mutant P/Q type channels expressed in patients with the familial hemiplegic migraine type 1 have a gain of function of increased Ca^{2+} current (Pietrobon, 2005). The knock-in mice model with the mutant P/Q channel exhibit enhanced action potential-evoked Ca^{2+} influx, increased probability of glutamate release and lower threshold for SD induction (van den Maagdenberg et al., 2004; Tottene et al., 2009). This suggests that the P/Q channels are important in initiating SD by facilitating glutamate release and thus increase the neuronal susceptibility. Our data show that TTX and Cd^{2+} do not prevent SD progression, but instead lead to a minor decrease of SD glutamate release once SD is elicited. This suggests that P/Q channel-associated glutamate release may contribute to the initiation, but not the propagation of SD. This is in line with previous concepts that SD is ignited when the cell excitability reaches a certain

threshold and that there may be different mechanisms to achieve this, however, the mechanism of SD propagation need not be identical (Somjen, 2001).

The assertion that the SD glutamate release requires NMDAR activity is consistent with previous studies that NMDAR antagonists inhibit both SD initiation and propagation (Gorelova et al., 1987; Hernandez-Caceres et al., 1987; Marrannes et al., 1988; Lauritzen and Hansen, 1992). Although NMDARs are more abundantly distributed at postsynaptic sites, our inability to block glutamate release by either inhibition of action potentials or blocking VGCCs argues against a direct postsynaptic action of NMDAR on presynaptic terminal release. Another possibility is that postsynaptic NMDARs trigger vesicular transmitter release from dendritic spines. Postsynaptic dendritic release of dense-core neuropeptides-containing vesicles has been shown in hypothalamic neurons (Ludwig and Pittman, 2003) and dendritic release of glutamate has been reported from mitral cells of the accessory olfactory bulb (Castro and Urban, 2009). This mechanism is unlikely to be responsible for the effects observed here, because dendritic synaptic vesicles and glutamate release have not been observed in the cortex or hippocampus as they have in the olfactory bulb (Schoppa and Urban, 2003). In the cortex the expression of NMDARs in axons and presynaptic terminals has been shown by numerous electron microscopy studies (Aoki et al., 1994; Liu et al., 1994; Farb et al., 1995; Corlew et al., 2007; Jourdain et al., 2007). Therefore in the cortex SD glutamate release is likely triggered by presynaptic NMDARs. Our findings that the direct application of NMDA evoked glutamate release and SD-like wave when action potentials and VGCCs were blocked suggest that the action of NMDAR on the glutamate release may be exerted presynaptically. This idea is consistent with physiological studies showing that presynaptic NMDARs can promote neurotransmitter release (Corlew et al., 2008).

Our results also demonstrate the mechanism by which SD can still propagate without Ca^{2+} in the extracellular fluid. Given that NMDAR are permeable to both Ca^{2+} and Na^{+}, our findings that either SD or NMDA application without extracellular Ca^{2+} could induce significant glutamate release suggest that Na^{+} influx via NMDAR might be responsible. Higher cytosolic [Na^{+}] can act via NCX_{mito} to release Ca^{2+} from mitochondria that are abundant within presynaptic terminals (Rowland et al., 2000). We propose that due to NCX_{mito}, mitochondria will extrude Ca^{2+} into the cytosol during sustained Na^{+} influx via NMDAR, and will trigger vesicle release (Castaldo et al., 2009). This is supported by our data that both SD- and NMDA-induced glutamate release were inhibited by NCX_{mito} blockers.

The principal pathological process associated with SD is migraine with aura (Pietrobon and Striessnig, 2003). However similar types of propagating depolarization are observed in human cortex in regions of stroke damage or trauma (Strong et al., 2002; Dreier et al., 2006; Fabricius et al., 2006). Understanding this unusual form of regenerative glutamate release may lead to new therapeutic targets for preventing migraines and neuronal damage in SD-related disorders.

3.5. References

Alle H, Geiger JR (2006) Combined analog and action potential coding in hippocampal mossy fibers. Science 311:1290-1293.

Anderson TR, Andrew RD (2002) Spreading depression: imaging and blockade in the rat neocortical brain slice. J Neurophysiol 88:2713-2725.

Aoki C, Venkatesan C, Go CG, Mong JA, Dawson TM (1994) Cellular and subcellular localization of NMDA-R1 subunit immunoreactivity in the visual cortex of adult and neonatal rats. J Neurosci 14:5202-5222.

Basarsky TA, Duffy SN, Andrew RD, MacVicar BA (1998) Imaging spreading depression and associated intracellular calcium waves in brain slices. J Neurosci 18:7189-7199.

Bender VA, Bender KJ, Brasier DJ, Feldman DE (2006) Two coincidence detectors for spike timing-dependent plasticity in somatosensory cortex. J Neurosci 26:4166-4177.

Bowyer SM, Aurora KS, Moran JE, Tepley N, Welch KM (2001) Magnetoencephalographic fields from patients with spontaneous and induced migraine aura. Annals of Neurology 50:582-587.

Brasier DJ, Feldman DE (2008) Synapse-specific expression of functional presynaptic NMDA receptors in rat somatosensory cortex. J Neurosci 28:2199-2211.

Bruzzone R, Barbe MT, Jakob NJ, Monyer H (2005) Pharmacological properties of homomeric and heteromeric pannexin hemichannels expressed in Xenopus oocytes. Journal of Neurochemistry 92:1033-1043.

Burmeister JJ, Pomerleau F, Palmer M, Day BK, Huettl P, Gerhardt GA (2002) Improved ceramic-based multisite microelectrode for rapid measurements of L-glutamate in the CNS. Journal of Neuroscience Methods 119:163-171.

Castaldo P, Cataldi M, Magi S, Lariccia V, Arcangeli S, Amoroso S (2009) Role of the mitochondrial sodium/calcium exchanger in neuronal physiology and in the pathogenesis of neurological diseases. Progress in Neurobiology 87:58-79.

Castro JB, Urban NN (2009) Subthreshold glutamate release from mitral cell dendrites. J Neurosci 29:7023-7030.

Contreras JE, Sanchez HA, Eugenin EA, Speidel D, Theis M, Willecke K, Bukauskas FF, Bennett MV, Saez JC (2002) Metabolic inhibition induces opening of unapposed connexin 43 gap junction hemichannels and reduces gap junctional communication in cortical astrocytes in culture. Proceedings of the National Academy of Sciences of the United States of America 99:495-500.

Corlew R, Brasier DJ, Feldman DE, Philpot BD (2008) Presynaptic NMDA receptors: newly appreciated roles in cortical synaptic function and plasticity. Neuroscientist 14:609-625.

Corlew R, Wang Y, Ghermazien H, Erisir A, Philpot BD (2007) Developmental switch in the contribution of presynaptic and postsynaptic NMDA receptors to long-term depression. J Neurosci 27:9835-9845.

Dreier JP, Woitzik J, Fabricius M, Bhatia R, Major S, Drenckhahn C, Lehmann TN, Sarrafzadeh A, Willumsen L, Hartings JA, Sakowitz OW, Seemann JH, Thieme A, Lauritzen M, Strong AJ (2006) Delayed ischaemic neurological deficits after subarachnoid haemorrhage are associated with clusters of spreading depolarizations. Brain 129:3224-3237.

Fabricius M, Jensen LH, Lauritzen M (1993) Microdialysis of interstitial amino acids during spreading depression and anoxic depolarization in rat neocortex. Brain Research 612:61-69.

Fabricius M, Fuhr S, Bhatia R, Boutelle M, Hashemi P, Strong AJ, Lauritzen M (2006) Cortical spreading depression and peri-infarct depolarization in acutely injured human cerebral cortex. Brain 129:778-790.

Farb CR, Aoki C, Ledoux JE (1995) Differential localization of NMDA and AMPA receptor subunits in the lateral and basal nuclei of the amygdala: a light and electron microscopic study. The Journal of Comparative Neurology 362:86-108.

Gorelova NA, Koroleva VI, Amemori T, Pavlik V, Bures J (1987) Ketamine blockade of cortical spreading depression in rats. Electroencephalography and Clinical Neurophysiology 66:440-447.

Hadjikhani N, Sanchez Del Rio M, Wu O, Schwartz D, Bakker D, Fischl B, Kwong KK, Cutrer FM, Rosen BR, Tootell RB, Sorensen AG, Moskowitz MA (2001) Mechanisms of migraine aura revealed by functional MRI in human visual cortex. Proceedings of the National Academy of Sciences of the United States of America 98:4687-4692.

Hernandez-Caceres J, Macias-Gonzalez R, Brozek G, Bures J (1987) Systemic ketamine blocks cortical spreading depression but does not delay the onset of terminal anoxic depolarization in rats. Brain Research 437:360-364.

Huguenard JR (1996) Low-threshold calcium currents in central nervous system neurons. Annual Review of Physiology 58:329-348.

Iglesias R, Dahl G, Qiu F, Spray DC, Scemes E (2009) Pannexin 1: the molecular substrate of astrocyte "hemichannels". J Neurosci 29:7092-7097.

Iglesias R, Locovei S, Roque A, Alberto AP, Dahl G, Spray DC, Scemes E (2008) P2X7 receptor-Pannexin1 complex: pharmacology and signaling. American Journal of Physiology 295:C752-760.

Jourdain P, Bergersen LH, Bhaukaurally K, Bezzi P, Santello M, Domercq M, Matute C, Tonello F, Gundersen V, Volterra A (2007) Glutamate exocytosis from astrocytes controls synaptic strength. Nature Neuroscience 10:331-339.

Lalo U, Pankratov Y, Kirchhoff F, North RA, Verkhratsky A (2006) NMDA receptors mediate neuron-to-glia signaling in mouse cortical astrocytes. J Neurosci 26:2673-2683.

Lauritzen M (1994) Pathophysiology of the migraine aura. The spreading depression theory. Brain 117 (Pt 1):199-210.

Lauritzen M, Hansen AJ (1992) The effect of glutamate receptor blockade on anoxic depolarization and cortical spreading depression. J Cereb Blood Flow Metab 12:223-229.

Lauritzen M, Rice ME, Okada Y, Nicholson C (1988) Quisqualate, kainate and NMDA can initiate spreading depression in the turtle cerebellum. Brain Research 475:317-327.

Leão AAP (1944) Spreading depression of activity in the cerebral cortex. J Neurophysiol 7:357-390.

Li YH, Han TZ (2007) Glycine binding sites of presynaptic NMDA receptors may tonically regulate glutamate release in the rat visual cortex. J Neurophysiol 97:817-823.

Liu H, Wang H, Sheng M, Jan LY, Jan YN, Basbaum AI (1994) Evidence for presynaptic N-methyl-D-aspartate autoreceptors in the spinal cord dorsal horn. Proceedings of the National Academy of Sciences of the United States of America 91:8383-8387.

Lo M, Wang YZ, Gout PW (2008) The x(c)- cystine/glutamate antiporter: a potential target for therapy of cancer and other diseases. Journal of Cellular Physiology 215:593-602.

Ludwig M, Pittman QJ (2003) Talking back: dendritic neurotransmitter release. Trends in neurosciences 26:255-261.

Marrannes R, Willems R, De Prins E, Wauquier A (1988) Evidence for a role of the N-methyl-D-aspartate (NMDA) receptor in cortical spreading depression in the rat. Brain Research 457:226-240.

Meinrenken CJ, Borst JG, Sakmann B (2002) Calcium secretion coupling at calyx of held governed by nonuniform channel-vesicle topography. J Neurosci 22:1648-1667.

Pietrobon D (2005) Function and dysfunction of synaptic calcium channels: insights from mouse models. Current opinion in Neurobiology 15:257-265.

Pietrobon D, Striessnig J (2003) Neurobiology of migraine. Nature Reviews Neuroscience 4:386-398.

Pinheiro PS, Mulle C (2008) Presynaptic glutamate receptors: physiological functions and mechanisms of action. Nature Reviews Neuroscience 9:423-436.

Raiteri L, Zappettini S, Milanese M, Fedele E, Raiteri M, Bonanno G (2007) Mechanisms of glutamate release elicited in rat cerebrocortical nerve endings by 'pathologically' elevated extraterminal K^+ concentrations. Journal of Neurochemistry 103:952-961.

Retamal MA, Schalper KA, Shoji KF, Bennett MV, Saez JC (2007) Opening of connexin 43 hemichannels is increased by lowering intracellular redox potential. Proceedings of the National Academy of Sciences of the United States of America 104:8322-8327.

Rossi DJ, Oshima T, Attwell D (2000) Glutamate release in severe brain ischaemia is mainly by reversed uptake. Nature 403:316-321.

Rowland KC, Irby NK, Spirou GA (2000) Specialized synapse-associated structures within the calyx of Held. J Neurosci 20:9135-9144.

Rutherford EC, Pomerleau F, Huettl P, Stromberg I, Gerhardt GA (2007) Chronic second-by-second measures of L-glutamate in the central nervous system of freely moving rats. Journal of Neurochemistry 102:712-722.

Schoppa NE, Urban NN (2003) Dendritic processing within olfactory bulb circuits. Trends in Neurosciences 26:501-506.

Shu Y, Hasenstaub A, Duque A, Yu Y, McCormick DA (2006) Modulation of intracortical synaptic potentials by presynaptic somatic membrane potential. Nature 441:761-765.

Siegel SJ, Brose N, Janssen WG, Gasic GP, Jahn R, Heinemann SF, Morrison JH (1994) Regional, cellular, and ultrastructural distribution of N-methyl-D-aspartate receptor subunit 1 in monkey hippocampus. Proceedings of the National Academy of Sciences of the United States of America 91:564-568.

Sjostrom PJ, Turrigiano GG, Nelson SB (2003) Neocortical LTD via coincident activation of presynaptic NMDA and cannabinoid receptors. Neuron 39:641-654.

Somjen GG (2001) Mechanisms of spreading depression and hypoxic spreading depression-like depolarization. Physiological Reviews 81:1065-1096.

Strong AJ, Fabricius M, Boutelle MG, Hibbins SJ, Hopwood SE, Jones R, Parkin MC, Lauritzen M (2002) Spreading and synchronous depressions of cortical activity in acutely injured human brain. Stroke 33:2738-2743.

Tai C, Kuzmiski JB, MacVicar BA (2006) Muscarinic enhancement of R-type calcium currents in hippocampal CA1 pyramidal neurons. J Neurosci 26:6249-6258.

Thompson RJ, Zhou N, MacVicar BA (2006) Ischemia opens neuronal gap junction hemichannels. Science 312:924-927.

Tottene A, Conti R, Fabbro A, Vecchia D, Shapovalova M, Santello M, van den Maagdenberg AM, Ferrari MD, Pietrobon D (2009) Enhanced excitatory transmission at cortical synapses as the basis for facilitated spreading depression in Ca(v)2.1 knockin migraine mice. Neuron 61:762-773.

van den Maagdenberg AM, Pietrobon D, Pizzorusso T, Kaja S, Broos LA, Cesetti T, van de Ven RC, Tottene A, van der Kaa J, Plomp JJ, Frants RR, Ferrari MD (2004) A Cacna1a knockin migraine mouse model with increased susceptibility to cortical spreading depression. Neuron 41:701-710.

Van Harreveld A (1959) Compounds in brain extracts causing spreading depression of cerebral cortical activity and contraction of crustacean muscle. Journal of Neurochemistry 3:300-315.

Warr O, Takahashi M, Attwell D (1999) Modulation of extracellular glutamate concentration in rat brain slices by cystine-glutamate exchange. The Journal of Physiology 514 (Pt 3):783-793.

Ye ZC, Wyeth MS, Baltan-Tekkok S, Ransom BR (2003) Functional hemichannels in astrocytes: a novel mechanism of glutamate release. J Neurosci 23:3588-3596.

Zhou Q, Petersen CC, Nicoll RA (2000) Effects of reduced vesicular filling on synaptic transmission in rat hippocampal neurones. The Journal of Physiology 525 Pt 1:195-206.

4. CONCLUDING CHAPTER

4.1. Summary of Findings

This present study is focused on the cellular mechanisms that promote SD progression and SD-associated pathophysiological responses. The goal of this research was to examine changes in cell volumes, intracellular pH and mitochondrial membrane potentials and to compare the contribution of neurons versus astrocytes to these responses. This research also aimed to examine the role of glutamate signalling in mediating SD propagation and the novel mechanisms underlying glutamate release during SD. We have used a combination of techniques including imaging, electrophysiology and amperometric measurement to investigate these objectives in the SD model that is induced by elevation of extracellular K^+ in brain slices. Our experiments have led to several interesting findings that are summarized below:

1. Neurons exhibit transient volume increase, transient intracellular acidosis and transient mitochondrial depolarization, and all of these neuronal responses occur at the onset of SD.
2. Astrocytes show volume increases, intracellular alkalinization and mitochondrial depolarization when extracellular K^+ is increased. However, they do not display any additional changes when SD occurs.
3. Glutamate release accompanies SD and is independent of action potentials and Ca^{2+} influx via VGCCs. Instead, glutamate is released during SD from presynaptic vesicular exocytosis that depends on NMDA receptor activation.
4. Both Ca^{2+} and Na^+ influxes via presynaptic NMDA receptors are important in triggering glutamate release during SD. When Ca^{2+} influx is blocked by removing extracellular Ca^{2+}, Na^+ flow through NMDA receptors can activate NCX_{mito}, which releases Ca^{2+} from mitochondrial matrix and thus triggers vesicular glutamate release.

These results suggest that neurons are the primary contributor to the SD-associated pathophysiological changes, including cell swelling, cellular pH changes and mitochondrial responses. These changes in neurons are reversible, suggesting that a single SD episode alone in normal tissue does not induce prolonged cell damage. In contrast, astrocytes exhibit changes mainly in response to raised extracellular K^+ concentration, which is an accompanying but not necessarily the causal event of SD. Therefore, astrocytes play a more passive role compared with neurons in the SD-induced responses.

Our studies also suggest that release of glutamate and activation of NMDAR is crucial for SD propagation. Interestingly, in contrast to classical transmitter release that is triggered by action potential-evoked VGCC activation, SD is dependent upon a novel mechanism of regenerative glutamate release. Activation of NMDARs that are most likely expressed at presynaptic sites seems to be the key step, as Ca^{2+} influx via presynaptic NMDARs may directly trigger glutamate release. The Na^+ influx via NMDARs is also critical in the whole process, since Na^+ overload will activate NCX_{mito} that exports Ca^{2+} against Na^+ into the cytosol, and thus will induce glutamate release. Finally, the released glutamate can activate more NMDARs located on the same terminals, or can diffuse and activate NMDARs on adjacent pre- or post-synaptic sites to form a positive feedback. This form of regenerative glutamate release will spread out and cause profound depolarization at the wave front, which manifests as the propagation of SD.

4.2. Mechanisms of SD Initiation

As mentioned in chapter 1, SD can be initiated by different stimuli, like electrical stimulation, mechanical stimulation and focal KCl application. Electrical stimulation is known to trigger neuronal responses by affecting the voltage gradient across the cell membranes, which normally

induce intensive neuronal spikes. The enhanced neuronal firing will induce both transmitter release and K^+ efflux into extracellular space. Mechanical stimuli are known to induce intracellular Ca^{2+} responses in epithelial and glial cells (Sanderson et al., 1990; Charles et al., 1991). Traumatic mechanical insult will cause structural and functional breakdown of cell membranes (Singleton and Povlishock, 2004; Whalen et al., 2008), which leads to acute Ca^{2+} influx into and glutamate release from the injured cells (Park et al., 2008). Focal application of high K^+ will induce intense action potential firing, facilitate neurotransmitter release and enhance postsynaptic currents. High concentration of $[K^+]_o$ can also reverse the action of glutamate transporters, leading to impaired function of clearance of extracellular glutamate. Therefore, the common consequences following all these stimuli are that increased neuronal excitability causes more release of glutamate and/or K^+.

In the present study, we induced SD by bath perfusion of extracellular solution containing 40 mM of KCl onto brain slices. This protocol can reliably trigger SD, even when extracellular Ca^{2+} is removed. Elevation of $[K^+]_o$ from 2.5 to 40 mM will cause neuronal membrane potential to depolarize from ~73 mV to ~ 37 mV, according to the Goldman-Hodgkin-Katz equation:

$$V_m = \frac{RT}{F} \ln\left(\frac{p_K[K]_o + p_{Na}[Na]_o + p_{Cl}[Cl]_i}{p_K[K]_i + p_{Na}[Na]_i + p_{Cl}[Cl]_o} \right)$$

Where T is 303 °K (30 °C + 273.15); pK : pNa : pCl = 1 : 0.05 : 0.45; the intracellular concentrations of K^+, Na^+ and Cl^- are 140 mM, 7 mM and 7 mM respectively. The membrane potential of glial cells is more dependent upon the transmembrane K^+ concentration gradient. It has been reported that cortical glial cells can depolarize from ~ 90 mV to ~35 mV when $[K^+]_o$ is raised to 40 mM (Pape and Katzman, 1972; Ransom and Goldring, 1973).

Therefore, in our experimental model, perfusion of high K^+ will cause neuronal hyperexcitability universally in the whole brain slice. By moving membrane potentials of neurons closer to the firing threshold, this application will greatly increase the release and reduce the uptake of extracellular glutamate. It is reasonable to postulate that when the enhanced glutamate release at some synapses of a small area first reach the threshold, it is very likely to induce a SD wave from this site and this wave can easily spread out to adjacent neurons due to the increased excitability. Blocking Na^+-dependent spikes by TTX does not impact SD, probably because the high K^+-induced depolarization alone is strong enough to open presynaptic VGCCs (Bloedel et al., 1966).

In summary, the elevated extracellular K^+ and glutamate are important in facilitating SD generation, as they appear to be the initial cellular consequences following all the simulation protocols of SD mentioned above. Nevertheless, SD is considered to be a complex chain of tightly bound events (Marshall, 1959). It still remains unclear what is the genuine factor that directly controls the "switch" of the SD ignition.

4.3. Mechanisms of SD Propagation

We postulate that propagation of SD is mediated by several positive feedback pathways, in all of which glutamate is the key step (Figure 4.1). With conventional views, glutamate activates postsynaptic NMDAR and triggers action potential-evoked presynaptic Ca^{2+} influx, causing regenerative glutamate release by an action potential-dependent inter-neuronal communication. Other mechanisms have also been reported to be involved in the mechanism of glutamate release during SD. For instance, cell swelling during ouabain-induced SD evokes activation of volume-sensitive organic anion channels (VSOAC) that allows efflux of glutamate from astrocytes, but

Figure 4.1. Conceptual diagram of positive feedback involving glutamate release during SD progression. In the present model, most types of stimuli ultimately induce glutamate release at the stimulation site. The initial released glutamate activates several interactive pathways that all contribute to the positive feedback. In the conventional model, glutamate activates postsynaptic NMDARs and evokes further glutamate release via action potential-triggered VGCC activation. In our model, glutamate additionally activates presynaptic NMDARs that can either facilitate neuronal firing and VGCC opening, or directly contributes to glutamate release by its permeability to Ca^{2+} influx. Na^{+} influx via NMDARs activates NCX_{mito}, causing glutamate release, too. All the pathways ultimately induce more glutamate release at the same site or at adjacent synapse, causing the propagation of SD wave.

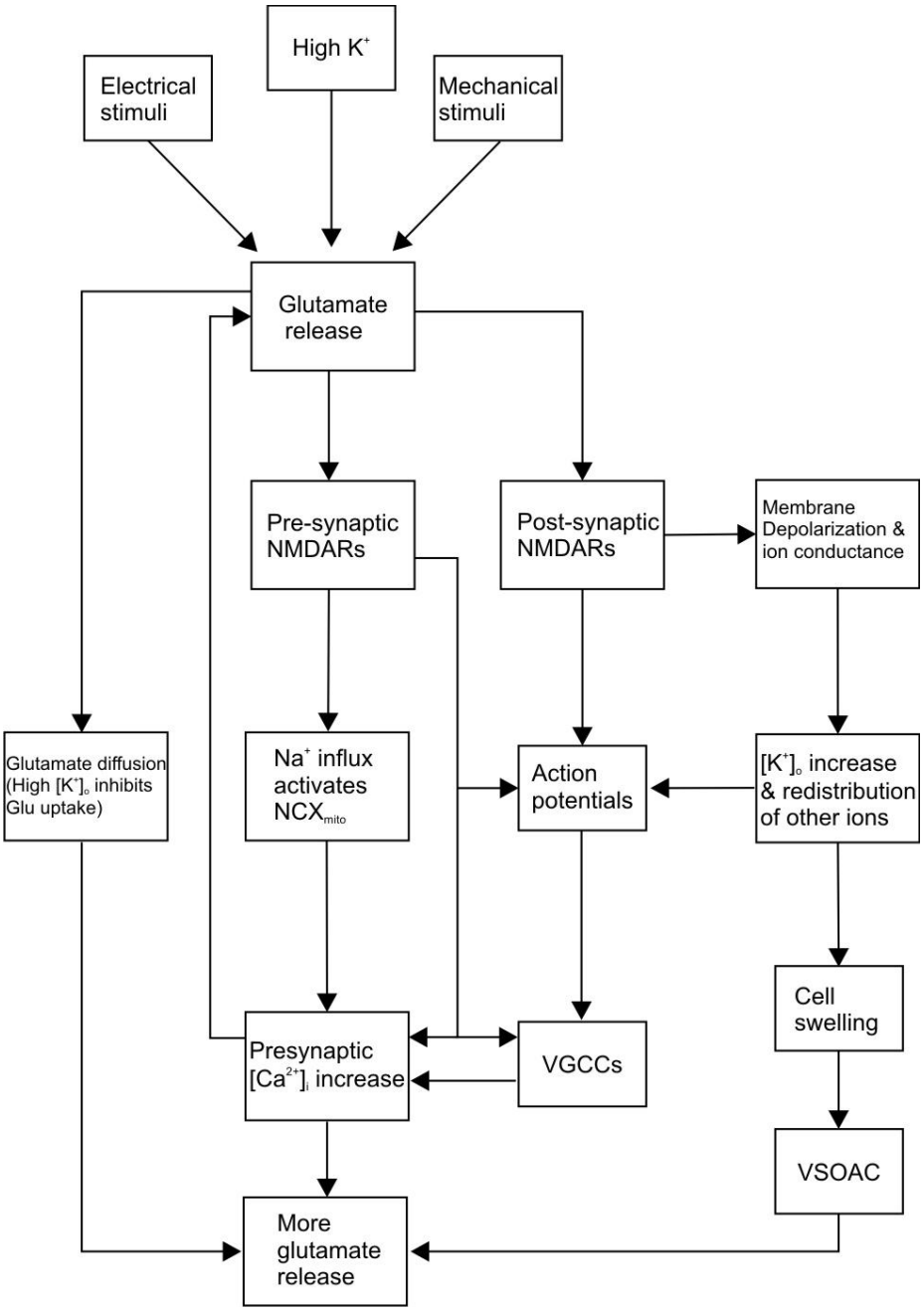
High K^+
Electrical stimuli
Mechanical stimuli
Glutamate release
Pre-synaptic NMDARs
Post-synaptic NMDARs
Membrane Depolarization & ion conductance
Glutamate diffusion (High $[K^+]_o$ inhibits Glu uptake)
Na^+ influx activates NCX_{mito}
Action potentials
$[K^+]_o$ increase & redistribution of other ions
Cell swelling
Presynaptic $[Ca^{2+}]_i$ increase
VGCCs
VSOAC
More glutamate release

this pathway is not necessarily required for the SD propagation (Basarsky et al., 1999). Our present model provides a novel pathway of regenerative glutamate release, in which activation of presynaptic NMDARs is a crucial factor. This model also explains the mechanism of SD propagation when both Na^+ and Ca^{2+} spikes are blocked.

4.3.1. Contribution of astrocytes

Astrocytes are highly permeable to K^+ and function as the main regulatory system of extracellular K^+ homeostasis. Under physiological conditions, astrocytes can remove K^+ from the extracellular space by several mechanisms, including (1) inwardly rectifying K^+ channels, (2) Na^+, K^+ ATPase, (3) Na^+, K^+, Cl^- cotransporters, and (4) spatial K^+ buffering via gap junctions (Kofuji and Newman, 2004; Olsen and Sontheimer, 2008). Astrocytes are also an important site of glutamate uptake as they express EAAT1 and EAAT2 types of glutamate transporters. Studies have shown that astrocyte glutamate transporters are activated by synaptically released glutamate and are important for limiting glutamate spillover from the synaptic cleft (Wang and Bordey, 2008). Thus, it is reasonable to postulate that astrocytes play a protective role in SD by regulating $[K^+]_o$ and buffering excitatory amino acids. This hypothesis is supported by the study showing that the metabolic glial toxin fluorocitrate does not inhibit SD, but instead facilitates SD by increasing its propagation rate and duration (Largo et al., 1997). Consistently, our studies suggest the lack of a direct relationship between astrocytes and the cellular responses associated with the large ion current of SD. The passive responses of astrocytes to elevated $[K^+]_o$ might contribute to the protective function against SD.

4.3.2. Contribution of potassium

K^+ is believed to play an important role in forming the positive feedback loop by facilitating neuronal excitability in several processes. First, elevated $[K^+]_o$ will directly depolarize

membrane potentials, thus causing intense neuronal firing and activation of VGCCs (section 4.1). Second, the K^+-induced depolarization can also remove Mg^{2+} blockade of NMDARs (Nowak et al., 1984) and thus facilitate their opening at both pre- and post-synaptic sites. Third, glutamate transporters will act in reverse mode to release glutamate when $[K^+]_o$ is increased and membrane is depolarized (Barbour et al., 1988; Szatkowski et al., 1990). This reversed action will prevent the clearance of glutamate from extracellular space, which may enable glutamate to diffuse to a much greater distance to reach adjacent synapses. Finally, increased $[K^+]_o$-induced astrocytic swelling activates VSOAC, which are permeant to Cl^- and organic anions, including glutamate (Lascola and Kraig, 1996; Okada et al., 2009). However, previous work has shown that blocking VSOAC suppresses, but does not completely abolish ouabain-induced SD (Basarsky et al., 1999). Because ouabain-induced SD is more relevant to hypoxic/ischemic depolarization over normal SD (Balestrino et al., 1999), the role of VSOAC in high K^+-induced SD still remains to be determined.

4.3.3. Pre- and post-synaptic NMDARs

Our studies indicate that NMDAR-induced vesicular glutamate release, which is independent of Na^+ and Ca^{2+} currents, underlies the mechanism of SD propagation. Although activation of presynaptic NMDARs is the simplest explanation for our finding, specific pharmacological or molecular approaches are still required to differentiate the role of pre- versus post-synaptic NMDARs in SD. Previous pharmacological studies have suggested that presynaptic NMDARs preferentially retain NR2B rather than NM2A subunits (Woodhall et al., 2001; Sjostrom et al., 2003; Yang et al., 2006; Brasier and Feldman, 2008). If the predominant expression of NR2B at presynaptic sites can be confirmed by anatomical studies, specific pharmacological methods can be employed to examine the relative contribution of presynaptic NMDARs to SD. Moreover, it will be interesting to study the mechanisms of how presynaptic NMDARs interact with

scaffolding proteins (O'Brien et al., 1998; Fujita and Kurachi, 2000), which might be different from the postsynaptic mechanisms and might shed light onto the methods of molecular manipulating loci-specific NMDARs in the future.

4.3.4. Mitochondrial Na^+/Ca^{2+} exchanger

The molecular structure of NCX_{mito} was unknown until a recent report in which a mitochondrial Na^+/Ca^{2+} exchanger termed NCLX was identified (Palty et al., 2004). NCLX has been recently confirmed as the long-sought NCX_{mito} since they share very similar biological and pharmacological characteristics (Palty et al., 2010). The newly developed antibodies and siRNA of NCX_{mito} will provide us with more specific approaches to test the contribution of NCX_{mito} to SD. It will also be interesting to test how our present mechanism of SD contributes to PID following ischemia by using the NCX_{mito} siRNA in the *in vivo* animal models.

4.4. Future Directions

We have used enzyme-based glutamate recordings to show the massive glutamate release during SD. However, there are several limitations to this technique. First, this method cannot measure glutamate release at the single cell level. Each recording site covers an area of about 0.01 mm^2 (~0.2mm×~0.05 mm, see Figure 4.2), so the glutamate concentration changes are resulted from tens to hundreds cells. Second, it is difficult to determine whether the longer time course of glutamate release compared with IOS changes is due to persistent release or to impaired clearance mechanisms. Finally, this method cannot be combined with other electrophysiological recordings. Therefore, other approaches with better spatial resolution should be applied in the future studies. For example, FM1-43 selectively stains secretory membrane structures and is

Figure 4.2. Schematic drawing of the enzyme-based glutamate sensor tip.

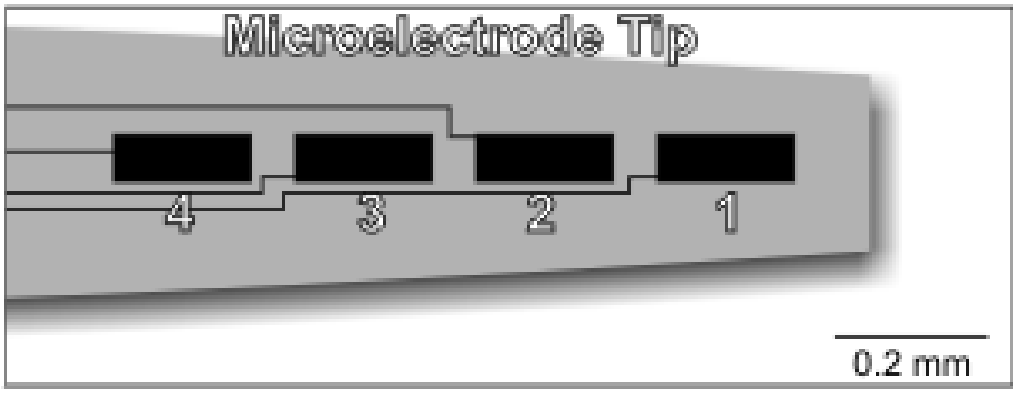

The microelectrode array consists of four ~200 × ~50 micron Pt recording sites. All four recording sites are coated with Nafion®. Only site 1 is additionally coated with glutamate oxidase.

widely used in studying synaptic vesicle recycling (Brumback et al., 2004). This method will provide the advantage of monitoring the time course and the locations of vesicular exocytosis during SD. In addition, glutamate optical sensors have been recently developed to image extracellular glutamate dynamics with excellent spatiotemporal resolution (Okubo et al.). The glutamate sensor changes its fluorescence intensity upon binding of glutamate, and it shows high affinity and selectivity to glutamate. This imaging technique has been used in both brain slices and *in vivo* animals. It will be very interesting to combine glutamate optical imaging with electrophysiological recordings to test the spatial distribution of glutamate transients during SD.

The biophysical property of ischemic depolarization is known to be very similar to SD. It is interesting to test the time course and the amplitude of glutamate release following ischemic insults. It has been reported that ischemic depolarization is insensitive to NMDAR blockers (Hernandez-Caceres et al., 1987), suggesting that glutamate release following ischemia may depend on non-NMDA glutamate receptors or other Ca^{2+} permeable channels. Na^{+} overload is thought to be an important cause to initiate damage processes, but its direct consequences have not been identified yet (Lipton, 1999). It is reasonable to hypothesize that Na^{+} overload during ischemia activates NCX_{mito} to increase cytosolic Ca^{2+}, leading to glutamate release and cell death.

SD is known to occur in several neurological disorders, including migraine with aura, stroke and brain trauma. An important question is whether these neurological conditions involve the same mechanisms as we tested in brain slices. This could be tested using *in vivo* animal models like *in vivo* SD initiation models, focal ischemic models (Back et al., 1996), or traumatic brain injury models (Nilsson et al., 1993). Both DC-coupled extracellular potential shifts and extracellular glutamate changes can be tested in the *in vivo* brain. The NCX_{mito} blocker diltiazem has been used as an effective preventive medication for migraine, but its pharmacological mechanism is

still unknown (Grossman and Messerli, 2004). It will be interesting to test the effect of NCX_{mito} blockers on blocking SD as well as preventing the consequent tissue damage in these *in vivo* models.

4.5. References

Back T, Ginsberg MD, Dietrich WD, Watson BD (1996) Induction of spreading depression in the ischemic hemisphere following experimental middle cerebral artery occlusion: effect on infarct morphology. J Cereb Blood Flow Metab 16:202-213.

Balestrino M, Young J, Aitken P (1999) Block of Na^+, K^+ATPase with ouabain induces spreading depression-like depolarization in hippocampal slices. Brain Research 838:37-44.

Barbour B, Brew H, Attwell D (1988) Electrogenic glutamate uptake in glial cells is activated by intracellular potassium. Nature 335:433-435.

Basarsky TA, Feighan D, MacVicar BA (1999) Glutamate release through volume-activated channels during spreading depression. J Neurosci 19:6439-6445.

Bloedel J, Gage PW, Llinas R, Quastel DM (1966) Transmitter release at the squid giant synapse in the presence of tetrodotoxin. Nature 212:49-50.

Brasier DJ, Feldman DE (2008) Synapse-specific expression of functional presynaptic NMDA receptors in rat somatosensory cortex. J Neurosci 28:2199-2211.

Brumback AC, Lieber JL, Angleson JK, Betz WJ (2004) Using FM1-43 to study neuropeptide granule dynamics and exocytosis. Methods 33:287-294.

Charles AC, Merrill JE, Dirksen ER, Sanderson MJ (1991) Intercellular signaling in glial cells: calcium waves and oscillations in response to mechanical stimulation and glutamate. Neuron 6:983-992.

Fujita A, Kurachi Y (2000) SAP family proteins. Biochem Biophys Res Commun 269:1-6.

Grossman E, Messerli FH (2004) Calcium antagonists. Prog Cardiovasc Dis 47:34-57.

Hernandez-Caceres J, Macias-Gonzalez R, Brozek G, Bures J (1987) Systemic ketamine blocks cortical spreading depression but does not delay the onset of terminal anoxic depolarization in rats. Brain research 437:360-364.

Jiang D, Zhao L, Clapham DE (2009) Genome-wide RNAi screen identifies Letm1 as a mitochondrial Ca^{2+}/H^+ antiporter. Science 326:144-147.

Kofuji P, Newman EA (2004) Potassium buffering in the central nervous system. Neuroscience 129:1045-1056.

Largo C, Ibarz JM, Herreras O (1997) Effects of the gliotoxin fluorocitrate on spreading depression and glial membrane potential in rat brain in situ. Journal of Neurophysiology 78:295-307.

Lascola CD, Kraig RP (1996) Whole-cell chloride currents in rat astrocytes accompany changes in cell morphology. J Neurosci 16:2532-2545.

Lipton P (1999) Ischemic cell death in brain neurons. Physiol Rev 79:1431-1568.

Marshall WH (1959) Spreading cortical depression of Leão. Physiol Rev 39:239-279.

Nilsson P, Hillered L, Olsson Y, Sheardown MJ, Hansen AJ (1993) Regional changes in interstitial K^+ and Ca^{2+} levels following cortical compression contusion trauma in rats. J Cereb Blood Flow Metab 13:183-192.

Nowak L, Bregestovski P, Ascher P, Herbet A, Prochiantz A (1984) Magnesium gates glutamate-activated channels in mouse central neurones. Nature 307:462-465.

O'Brien RJ, Lau LF, Huganir RL (1998) Molecular mechanisms of glutamate receptor clustering at excitatory synapses. Curr Opin Neurobiol 8:364-369.

Okada Y, Sato K, Numata T (2009) Pathophysiology and puzzles of the volume-sensitive outwardly rectifying anion channel. J Physiol. doi: 10.1113/jphysiol.2008.165076

Okubo Y, Sekiya H, Namiki S, Sakamoto H, Iinuma S, Yamasaki M, Watanabe M, Hirose K, Iino M (2010) Imaging extrasynaptic glutamate dynamics in the brain. Proceedings of the National Academy of Sciences of the United States of America 107:6526-6531.

Olsen ML, Sontheimer H (2008) Functional implications for Kir4.1 channels in glial biology: from K+ buffering to cell differentiation. Journal of Neurochemistry 107:589-601.

Palty R, Ohana E, Hershfinkel M, Volokita M, Elgazar V, Beharier O, Silverman WF, Argaman M, Sekler I (2004) Lithium-calcium exchange is mediated by a distinct potassium-independent sodium-calcium exchanger. J Biol Chem 279:25234-25240.

Palty R, Silverman WF, Hershfinkel M, Caporale T, Sensi SL, Parnis J, Nolte C, Fishman D, Shoshan-Barmatz V, Herrmann S, Khananshvili D, Sekler I (2010) NCLX is an essential component of mitochondrial Na^+/Ca^{2+} exchange. Proceedings of the National Academy of Sciences of the United States of America 107:436-441.

Pape LG, Katzman R (1972) Response of glia in cat sensorimotor cortex to increased extracellular potassium. Brain Research 38:71-92.

Park E, Bell JD, Baker AJ (2008) Traumatic brain injury: can the consequences be stopped? CMAJ 178:1163-1170.

Ransom BR, Goldring S (1973) Ionic determinants of membrane potential of cells presumed to be glia in cerebral cortex of cat. Journal of Neurophysiology 36:855-868.

Sanderson MJ, Charles AC, Dirksen ER (1990) Mechanical stimulation and intercellular communication increases intracellular Ca^{2+} in epithelial cells. Cell Regul 1:585-596.

Singleton RH, Povlishock JT (2004) Identification and characterization of heterogeneous neuronal injury and death in regions of diffuse brain injury: evidence for multiple independent injury phenotypes. J Neurosci 24:3543-3553.

Sjostrom PJ, Turrigiano GG, Nelson SB (2003) Neocortical LTD via coincident activation of presynaptic NMDA and cannabinoid receptors. Neuron 39:641-654.

Szatkowski M, Barbour B, Attwell D (1990) Non-vesicular release of glutamate from glial cells by reversed electrogenic glutamate uptake. Nature 348:443-446.

Wang DD, Bordey A (2008) The astrocyte odyssey. Prog Neurobiol 86:342-367.

Whalen MJ, Dalkara T, You Z, Qiu J, Bermpohl D, Mehta N, Suter B, Bhide PG, Lo EH, Ericsson M, Moskowitz MA (2008) Acute plasmalemma permeability and protracted clearance of injured cells after controlled cortical impact in mice. J Cereb Blood Flow Metab 28:490-505.

Woodhall G, Evans DI, Cunningham MO, Jones RS (2001) NR2B-containing NMDA autoreceptors at synapses on entorhinal cortical neurons. Journal of Neurophysiology 86:1644-1651.

Yang J, Woodhall GL, Jones RS (2006) Tonic facilitation of glutamate release by presynaptic NR2B-containing NMDA receptors is increased in the entorhinal cortex of chronically epileptic rats. J Neurosci 26:406-410.

APPENDIX: ETHICS BOARD CERTIFICATES

THE UNIVERSITY OF BRITISH COLUMBIA

ANIMAL CARE CERTIFICATE

Application Number: A06-0429

Investigator or Course Director: Brian MacVicar

Department: Psychiatry

Animals:

Rats Sprague-Dawley 920
Mice Sacytm1Lex/Sacytm1Lex 20
Mice CX3Cr1/EGFP 50
Mice Thy1/YFP 50

Start Date: **August 17, 2006** **Approval Date:** **February 12, 2010**

Funding Sources:

Funding Agency: Michael Smith Foundation for Health Research
Funding Title: Signalings pathway underlying spreading depression and ischemic depolarization

Funding Agency: Heart and Stroke Foundation of British Columbia and Yukon
Funding Title: Cellular mechanisms underlying ischemia induced neuronal necrosis

Funding Agency: Heart and Stroke Foundation of Canada
Funding Title: Microglia Cells limit the spread of neurotrauma in stroke model

Funding Agency: Alberta Innovates - Health Solutions
Funding Title: Neuronal astrocyte interactions underlie cerebral vasculature control

Funding Agency: Canadian Stroke Network (CSN) - Networks of Centres of Excellence (NCE)
Funding Title: Targeting cell death cascades in the neuro vascular-inflammatory unit

Funding Agency: Heart and Stroke Foundation of Canada
Funding Title: R-type VGCCs and TRP channels contribute to stroke-induced neuronal death

Funding Agency: Canadian Institutes of Health Research (CIHR)
Funding Title: Development of molecular mechanisms underlying neuron-astrocyte control of cerebral blood flow

Funding Agency: Heart and Stroke Foundation of Canada
Funding Title: Signaling pathways underlying spreading depression and Ischemic Depolarization

Funding Agency: Canadian Institutes of Health Research (CIHR)
Funding Title: Synaptic and nonsynaptic modulation of neuronal excitability

Funding Agency: Leducq Foundation
Funding Title: Mechanisms matching the brian's vascular energy supply to neural activity, and their failure in dise...

Funding Agency: Canadian Institutes of Health Research (CIHR)
Funding Title: NEURO Research program

Funding Agency: Heart and Stroke Foundation of Canada
Funding Title: A novel pathway in astrocytes providing a neuronal energy substrate during ischemic conditions

Funding Agency: Michael Smith Foundation for Health Research
Funding Title: Synaptic and non-synaptic modulation of neuronal excitability

Funding Agency:	Canadian Institutes of Health Research (CIHR)
Funding Title:	Synaptic function and plasticity
Funding Agency:	UBC Faculty of Medicine
Funding Title:	Start Up Funding
Funding Agency:	Networks of Centres of Excellence (NCE)
Funding Title:	CSN project #9: Molecular mechanisms of neuronal injury: Development of a therapeutic strategy for stroke-induced damage
Funding Agency:	Networks of Centres of Excellence (NCE)
Funding Title:	Theme III Admin. Support - Molecular mechanisms of neuronal injury: Development of a therapeutic strategy for stroke-induced damage
Funding Agency:	Canadian Stroke Network (CSN) - Networks of Centres of Excellence (NCE)
Funding Title:	Neuroprotection: Preventing cell death and neuronal damage from stroke
Funding Agency:	Michael Smith Foundation for Health Research
Funding Title:	Synaptic and non-synaptic modulation of neuronal excitability
Funding Agency:	Michael Smith Foundation for Health Research
Funding Title:	Neuronal astrocyte interactions underlie cerebral vasculature control
Funding Agency:	Canadian Institutes of Health Research (CIHR)
Funding Title:	Calcium signaling in astrocytes
Funding Agency:	Canadian Institutes of Health Research (CIHR)
Funding Title:	Synaptic and non-synaptic mechanisms in controlling neuronal excitability
Funding Agency:	Michael Smith Foundation for Health Research
Funding Title:	Synaptic and non-synaptic modulation of neuronal excitability

Funding Agency:	Canadian Institutes of Health Research (CIHR)
Funding Title:	Synaptic function and plasticity
Funding Agency:	Networks of Centres of Excellence (NCE)
Funding Title:	CSN Project #9: Molecular mechanisms of neuronal injury: Development of a therapeutic strategy for stroke-induced damage
Funding Agency:	UBC Start Up Funds
Funding Title:	Synaptic and non-synaptic modulation of neuronal excitability
Unfunded title:	N/A

The Animal Care Committee has examined and approved the use of animals for the above experimental project.

This certificate is valid for one year from the above start or approval date (whichever is later) provided there is no change in the experimental procedures. Annual review is required by the CCAC and some granting agencies.

A copy of this certificate must be displayed in your animal facility.

Office of Research Services and Administration
102, 6190 Agronomy Road, Vancouver, BC V6T 1Z3
Phone: 604-827-5111 Fax: 604-822-5093

THE UNIVERSITY OF BRITISH COLUMBIA

ANIMAL CARE CERTIFICATE
BREEDING PROGRAMS

Application Number: A06-0448

Investigator or Course Director: Brian MacVicar

Department: Psychiatry

Animals:

Mice C57BL/6 24
Mice Balb/c 24
Mice Thy1/YFP 120
Mice CX3CR1/EGFP 120

Approval Date: March 26, 2009

Funding Sources:

Funding Agency:	Canadian Institutes of Health Research (CIHR)
Funding Title:	Calcium signalling in astrocytes
Funding Agency:	Heart and Stroke Foundation of British Columbia and Yukon
Funding Title:	Cellular mechanisms underlying ischemia induced neuronal necrosis
Funding Agency:	Canadian Institutes of Health Research (CIHR)

Funding Title:	Development of molecular mechanisms underlying neuron-astrocyte control of cerebral blood flow
Funding Agency:	Canadian Institutes of Health Research (CIHR)
Funding Title:	Identification of ischemia-sensitive cation channels in hippocampal neurons
Funding Agency:	Canadian Institutes of Health Research (CIHR)
Funding Title:	NEURO Research program
Funding Agency:	Canadian Institutes of Health Research (CIHR)
Funding Title:	Synaptic and nonsynaptic modulation of neuronal excitability
Funding Agency:	Heart and Stroke Foundation of Canada
Funding Title:	Gap Junctional Hemichannels in Astrocytes: Regulation in Normal and Injured CNS
Funding Agency:	Canadian Institutes of Health Research (CIHR)
Funding Title:	Synaptic function and plasticity
Funding Agency:	Canadian Institutes of Health Research (CIHR)
Funding Title:	Synaptic and non-synaptic mechanisms in controlling neuronal excitability
Funding Agency:	Canadian Institutes of Health Research (CIHR)
Funding Title:	Calcium signaling in astrocytes
Funding Agency:	Canadian Institutes of Health Research (CIHR)
Funding Title:	Synaptic function and plasticity
Unfunded title:	N/A

The Animal Care Committee has examined and approved the use of animals for the above breeding

program.

This certificate is valid for one year from the above approval date provided there is no change in the experimental procedures. Annual review is required by the CCAC and some granting agencies.

A copy of this certificate must be displayed in your animal facility.

Office of Research Services and Administration
102, 6190 Agronomy Road, Vancouver, BC V6T 1Z3
Phone: 604-827-5111 Fax: 604-822-5093